Contents

Comparative analysis of siro yarn properties spun on ring and pneumatic compact spinning systems

M. FURQAN KHURSHID SARMAD ASLAM USMAN ALI
AMIR ABBAS TALHA ALI HAMDANI FIAZ HUSSAIN

REZUMAT – ABSTRACT

Analiza comparativă a proprietăților firelor Siro cu filare compactă pneumatica și cu inele

Scopul acestui studiu este de a investiga influența sistemului de filare compactă pneumatică (Rieter® K-44) asupra proprietăților firelor filate Siro cu densități liniare grosiere, medii și fine. În acest scop, firele filate Siro au fost filate pe sistemul de filare cu inele (RS) și filare compactă cu trei densități liniare (grosieră, medie și fină) din bumbac Pakistan. Au fost testați și analizați parametrii de calitate, cum ar fi: neregularitățile de masă (U%, CVm%, CV10m), indicele de imperfecțiune (IPI), pilozitatea și comportamentul la tracțiune al firelor filate siro și al firelor filate compacte. Rezultatele au arătat că firele Siro cu filare compactă au avut o variație mai mică a masei, o valoare IPI scăzută, pilozitate mai redusă și caracteristici de rezistență la tracțiune mai mari în comparație cu firele Siro filate cu inele. De asemenea, proprietățile firului compact Siro cu densitatea liniară grosieră, medie și fină au demonstrat că sistemul de filare compactă K-44 îmbunătățește proprietățile firelor Siro, indiferent de intervalul de densitate liniară.

Cuvinte-cheie: fir Siro, fir compact Siro (K-44), parametri de calitate, densitate liniară

Comparative analysis of siro yarn properties spun on ring and pneumatic compact spinning systems

The aim of the present work is to investigate the influence of pneumatic compact spinning system (Rieter® K-44) on siro yarn properties with coarse, medium and fine linear densities of yarn. For this purpose, siro yarns were spun on Ring (RS) and pneumatic compact spinning system (CS) with three linear densities (coarse, medium and fine) from Pakistani cotton. The quality parameters such as mass irregularity (U%, CVm%, CV10m), imperfection index (IPI), hairiness and tensile behavior of ring spun siro and compact spun siro yarns were tested and analyzed. The results revealed that compact spun siro yarn had less mass variation, low IPI value, less hairiness and high tensile properties as compared to ring siro yarn. It is also concluded from the properties of coarse, medium and fine siro compact yarn that K-44 compact spinning system improves siro yarn properties irrespective of the linear density range.

Keywords: siro yarn, compact siro yarn (K-44), quality parameters, linear density

INTRODUCTION

There are various spinning techniques to spun textile yarns. Every spinning technique has produced different yarn structures with different yarn properties. Ring is the leading spinning technique that spun yarn with improved properties in spite of its limitations. These limitations are traveler speed, balloon tension, spindle speed and spinning triangle. These limitations are responsible for less production and hairy yarn structure. Many researchers focused to improve ring yarn properties and structure by overcoming these limitations [1–5].

In the early of 1980s, Commonwealth Scientific International Research Organization (CSIRO) introduces siro yarn with superior yarn properties. CSIRO prepared siro yarn by introducing two parallel rovings with a predetermined spacing in the drafted zone of conventional ring spinning system. Then, rovings were twisted together to form a two ply structure with improved yarn structure and characteristics [6–9]. Siro yarn has improved structure with remarkable physical properties such as high evenness, low CV %, less Imperfection and low hairiness and mechanical properties such as high tenacity, more extension, higher work of rupture and more breaking strength as compared to conventional ring spun yarn, two ply yarn, vortex spun yarn, open end spun yarn and solo spun. Fabrics made from siro yarn also have superior abrasion resistance, high wrinkle resistance, low pilling tendency, high bursting strength and improved fastness properties (wash, rub and perspiration) as compared to conventional ring spun yarn. Siro yarn is cost effective as compared to folded (two ply) yarn and there is no need to sizing in the weaving process as well [6–20].

In the start of 1990s, Dr. Fehrer developed compact spinning by eliminating spinning triangle in conventional ring spinning. In compact spinning, fibers assembly is condensed in the spinning triangle zone pneumatically, magnetically and/or mechanically [5, 21]. Compact spinning developed a compact yarn structure with excellent yarn properties such as increased uniformity, less imperfections, low hairiness and superior yarn strength. Fabric made from compact yarn has improved tensile strength, low pilling and high abrasion resistance [1–5, 22–27]. It has been established to large extent that the improved siro and compact yarn properties are related to change of structure such as higher mean fiber position, high migration factor, and more integrated

structure as compared to ring yarn structure [11–12, 15–17]. Many researchers focused to compare siro yarn properties or structure with properties of others yarns e.g. solo yarn, siro solo, vortex yarn, OE yarn and/or ring spun yarn [8–20].

The aim of the present work is to investigate the influence of pneumatic compact spinning system (K-44) on siro yarn properties with course, medium and fine yarn linear densities. The selection of wide range of linear densities is to determine whether the compacting efficiency of the system is affected by handling more number of fibers in the drafting section. To the best of author's knowledge, ring spun siro and compact (K-44) spun siro yarn is being compared first time in this study with course, medium and fine yarn linear densities.

EXPERIMENTAL WORK

Materials and method

The Pakistani cotton was used as raw material to spun siro yarn. Cotton were tested under standard atmospheric conditions (20±2 °C and 65% RH) on High Volume Instrument (HVI) and average results are tabulated in the table 1.

A standard spinning setup was used to spun siro yarn on ring and compact spinning systems. For this purpose, conditioned cotton was opened and cleaned in the blow room section. The blow room machinery (Rieter) consists of UniFloc (A-11), UniClean (B-11), UniMix (B-70) and UniFlex (B-60). Furthermore, chute feed cotton was further processed on card

Table 1

COTTON FIBRE PROPERTIES	
Fibre properties	**Values± SD %**
Spinning Consistency Index	110 ± 6.55
Fineness (mtex)	177 ± 2.1
Maturity Index	0.88 ± 0.06
Length (mm)	28.2 ± 0.9
Uniformity Index	83.3 ± 1.2
Short Fiber Index	9.13 ± 0.5
Strength (cN/tex)	30 ± 0.8
Elongation (%)	4.9 ± 5.6
Moisture (%)	8.26 ± 0.4
Reflectance (Rd)	72.3 ± 0.6
Yellowness (+b)	8.7 ± 0.04

machine (C-51), drawing breaker (SB-2), drawing finisher (RSB D-35) and simplex (FL-100). For the purpose of comparative analysis, all rovings were prepared on same simplex machines and all technological and kinematical parameters were kept constant as shown in the table 2.

Three linear densities of yarns (60tex, 30tex and 12tex) were selected to spun siro and compact siro yarn. Each siro yarn samples were spun on same ring and K-44 compact spinning machines with similar technological and kinematical parameters as shown in the table 2. Quality parameters such as mass irregularity (U%, CVm%, CV10m), imperfection

Table 2

TECHNOLOGICAL AND KINEMATICAL PARAMETERS OF RING AND COMPACT SIRO YARN			
Parameters	**Yarn Linear Density (tex)**		
	60tex	**30tex**	**12tex**
Delivered weight per yard of Card (grains)	110	110	70
Card Delivery rate (m/min)	228	228	160
Card Dropping %	4.5	4.5	3.2
Card Fly %	7.8	7.8	3
Breaker Doubling	5	5	6
Delivered weight per yard at Breaker	80	80	70
Breaker Delivery Rate(m/min)	374	374	380
Finisher Doubling	6	6	6
Delivered weight per yard at Finisher (grains)	75	75	60
Finisher Delivery Rate(m/min)	459	459	350
Flyer Speed (rpm)	980	980	900
Twist per meter at Roving	48	50	69
Break Draft at Roving	1.3	1.19	1.3
Roving Linear Density (tex)	881,881	514,514	348,348
Spindle Speed (rpm)	11800	13000	18000
Yarn Twist per Meter	498	676	1230
Back Draft at ring	1.36	1.29	1.35
Spacer (SKF Company)	Violet	Violet	Red
Ring Diameter (mm)	42	38	35

Table 2

PHYSICAL PROPERTIES OF SIRO YARN ± CV %								
Sr.	Linear Density	Spinning system	Siro Yarn Properties ± CV %					
			U	CVm	CV10m	H	IPI	CLSP
01	60	CS	8.74 ± 1.08	11.1 ± 0.9	1.89 ± 14.07	7.54 ± 1.2	21 ± 19.3	2868 ± 2.25
02		RS	9.45 ± 1.41	12 ± 1.51	2.07 ± 16.65	8.51 ± 1.6	33 ± 19.9	2601 ± 2.73
03	30	CS	9.8 ± 1.1	12.3 ± 1.2	2.01 ± 11.2	6.8 ± 0.8	121 ± 11	2680 ± 2.5
04		RS	10.53 ± 1.61	13.4 ± 1.71	2.19 ± 13.64	7.4 ± 1.8	154 ± 13.4	2450 ± 3.45
05	12	CS	11.4 ± 0.8	14.3 ± 0.85	3.7 ± 9.25	3.8 ± 1.6	352 ± 9.5	2910 ± 2.64
06		RS	12.57 ± 1.38	15.7 ± 1.41	4.08 ± 15.42	4.3 ± 2.2	557 ± 9.9	2640 ± 3.64

Index (IPI) and hairiness were measured with Uster Tester-4. The yarn linear density was measured by auto sorter and lea strength of yarn was measured on Tensile Tester machine (mesdan tensile tester) under standard atmospheric conditions (20±2 °C and 65% RH). The nominal linear density and lea strength is used for the measurement of CLSP.

RESULTS AND DISCUSSION

The results of measurements of yarn irregularity, imperfection index, hairiness and tensile behavior of ring siro and compact siro yarn with linear densities of 60tex, 30tex and 12tex are given in table 3.

Comparison of yarn irregularity

Yarn irregularity is defined as the variation in weight per unit length of the yarn or as the variation in thickness of the yarn. Uster Tester measures the thickness variation of a yarn by measuring capacitance. Yarn irregularity is measured by Uster Tester in terms of U% and coefficient of variation of irregularity in terms of CVm, CV3m, CV10m and DR 1.5 m% [28, 29]. Yarn irregularity (U%) and coefficient of variation of irregularity (CVm) of ring and compact siro yarn with different linear densities are shown in the figure 1 and figure 2. The irregularity of compact siro yarn with 60tex, 30tex and12tex has improved by 7.5%, 6% and 9% respectively as compared to ring siro yarn.

The Coefficient of variation of irregularity (CV10 m %) of compact siro yarn with linear density of 60tex, 30tex, 12tex is 8.5%, 8%, 9% better than ring siro yarn. These improvements in yarn irregularity and

coefficient of variation of irregularity in compact siro yarn are due to improvement in the structure. The structure of siro compact yarn has more integrated and smoother as compared to ring siro yarn. It may be due to the low hairiness value as compared to ring siro yarn [6, 11, 19].

Comparison of imperfection index (IPI)

Yarn faults are classified into two main categories. These are seldom occurring yarn faults and frequent occurring yarn faults. Seldom occurring yarn faults are measured in 100 km of yarn length. While, frequent occurring yarn faults are measured in 1 km of yarn length. Frequent occurring yarn faults are thick places, thin places and neps. Imperfection index (IPI) is the sum of yarn Thin places (–50), Thick places (+50) and Neps (+200) per kilometer [1, 28, 29].

There is change in the values of thick places, thin places and neps of compact siro yarn of all linear densities as compared to ring spun siro yarn as shown in the figure 3. The compact siro yarn with linear densities of 60tex, 30tex and 12tex has 36%, 24% and 37% less IPI as compared to ring spun siro yarn. It is because of fibers are almost completely bound in the body that yields much smoother surface and consequently, yarn faults were decreased [6, 11, 19].

Comparison of yarn hairiness

In Uster Tester, hairiness is the ratio of the total length of protruding fibers (in centimeters) per centimeter of yarn [28, 29]. The hairiness of compact siro yarn of all linear densities as compared to ring spun siro yarn is shown in the figure 4. The siro yarn with
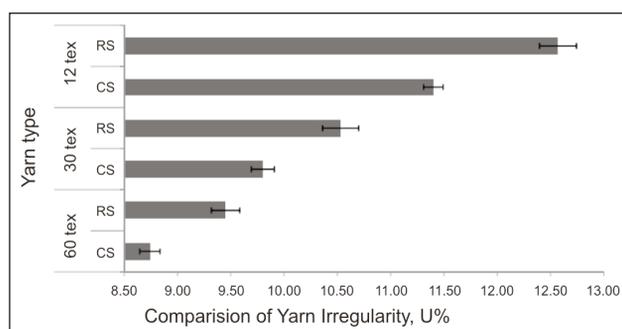
Fig. 1. Comparisons of yarn irregularity
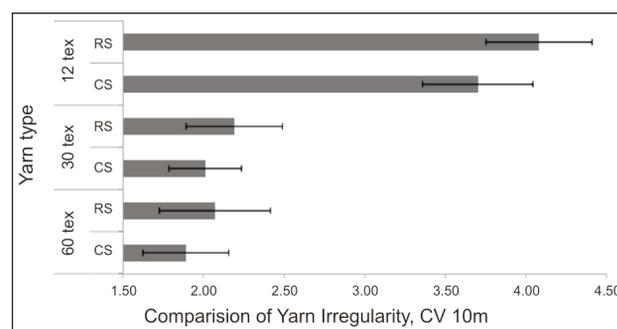
Fig. 2. Comparisons of Yarn Irregularity (CV10m)
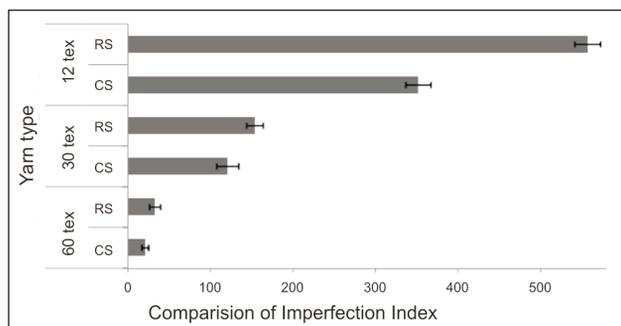
Fig. 3. Comparisons of yarn imperfection index
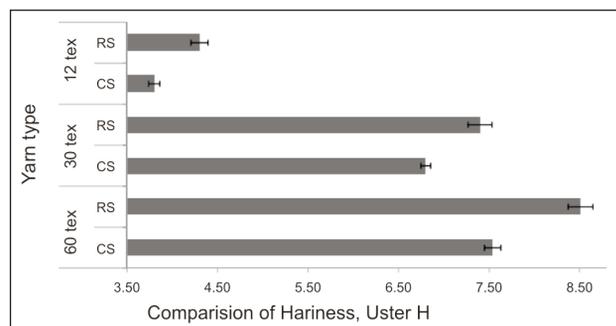
Fig. 4. Comparisons of yarn hairiness

linear density of 60tex, 30tex and 12tex spun on compact spinning has 11%, 8% and 12% less hairiness as compared to ring spun siro yarn respectively. Lower hairiness is an indicator of more compact structure. It shows that fibers are highly integrated in the body of compact siro yarn as compared to ring siro yarn [11, 15].

Comparison of tensile properties of yarn

The tensile properties of textile yarn are measured in various ways. These are breaking force, tenacity, rapture per kilometer (Rkm) and count lea strength product (CLSP). Breaking strength is a measure of steady force necessary to break the specimen and is given experimentally by the maximum load developed in a tensile test. The tenacity is defined as ratio of Force per unit Linear Density. Rupture per kilometer (Rkm) is defined as the theoretical length of a specimen of yarn whose own weight would exert a force to break the specimen of yarn. CLSP is defined as the product of nominal lea count and lea strength of a yarn [28, 30].

The CLSP of all compact siro yarns as compared to ring spun siro yarn is shown in the figure 5. CLSP of compact siro spun yarns with linear density of 60tex, 30tex and 12tex has 10%, 11% and 12% more strength than ring siro yarn respectively. It is because of number of factors. The compact siro yarn has more fiber migration, higher spinning in coefficient, improved percentage of straight fibers, low number of broken fibers and fever hairiness. The fiber migration parameters include mean fiber position, migration factor, packing density, migration index, root mean square deviation and amplitude of migration. These
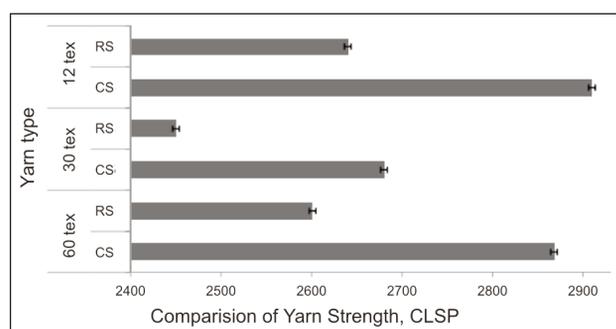
Fig. 5. Comparisons of yarn strength (CLSP)

higher migration parameters were also responsible for higher strength of compact spun siro yarn [6, 10–15, 19].

CONCLUSIONS

The siro yarn with course, medium and fine linear densities from Pakistani cotton were spun on pneumatic compact (K-44) and ring spinning systems. The physical and mechanical properties of these yarns were tested and analyzed. The results revealed that siro yarn spun on pneumatic compact (K-44) spinning system has remarkable properties as compared to ring spun siro yarn. It has excellent yarn evenness, low imperfection Index and very low yarn hairiness with improved tensile properties. It is also depicted from the results of course, medium and fine siro compact yarn that compacting efficiency of K-44 compact spinning system (K-44) has not affected by handling two roving (double number of fibers)in its drafting section.

BIBLIOGRAPHY

[1] Lawrence, C.A., *Fundamentals of Spun Yarn Technology*, In: New York, Washington D.C.: CRC Press, 2003.

[2] Fatma Göktepe, Demet Yilmaz, Özer Göktepe, *A comparison of compact yarn properties produced on different systems,* In: Textile Research Journal, vol. 76, no. 3, pp. 226–234, 2006.

[3] Ortlek, H.S.G., Kilic, G., Bilgin, S., *Comparative study on the properties of yarns produced by modified ring spinning,* In: Industria Textila, 2011. 62(3): pp. 129–133.

[4] Brunk, N., S. Schurr, *EliTe Compact Set: Versatile compact spinning system,* In: Industria Textila, 2004, 420, pp. 12–19.

[5] Nadeem, K., Asad, M., Chaudhry, M.A., Amanullah, M., Khurshid, M. Furqan, *Comparative analysis of cotton yarn properties spun on pneumatic compact spinning systems*, In: Fibres & Textiles in Eastern Europe, vol. 21, no. 5, pp. 30–34.

[6] Ali Kireccia Halil IbrahimIcoglua, *Investigation of the fastness properties and color values of cotton fabrics knitted from ring spun and Sirospun® yarns*, In: Journal of The Textile Institute, vol. 102, no. 2, pp. 114–119, 2011.

[7] Anbumanib, N., Subramaniamc, V., Gokarneshana, N., *Influence of strand spacing on the interfibre cohesion in siro yarns,* In: Journal of The Textile Institute, vol. 98, no. 3, pp. 289–292, 2007.

[8] Khan, Z.A., Wang, X.G., Shaikhzadeh Najar, S.*, The new Solo-Siro spun process for worsted yarns*, In: Journal of The Textile Institute, vol. 97, no. 3, pp. 205–210, 2006.

[9] Sun, M.N., Cheng, K.P.S., *Effect of Strand Spacing and Twist Multiplier on Cotton Sirospun Yarn,* In: Textile Research Journal, vol. 68, no. 7, pp. 520-527, July 1998.

[10] Jamal Shahrabib, Shahrokh Asadib, Esmaeil Hadavandib, Majid Safar Joharia Parham Soltania, *A study on siro, solo, compact, and conventional ring-spun yarns. Part III: modeling fiber migration using modular adaptive neuro-fuzzy inference system,* In: Journal of The Textile Institute, vol. 104, no. 7, pp. 755–765, 2013.

[11] Joharia, M.S., Soltani, P., *A study on siro-, solo-,compact-, and conventional ring-spun yarns. Part II: yarn strength with relation to physical and structural properties of yarns*, In: Journal of The Textile Institute, vol. 103, pp. 921–930, 2012.

[12] Joharia, M.S., Soltani, P., *A study on siro-, solo-, compact-, and conventional ring-spun yarns. Part I: structural and migratory properties of the yarns*, In: Journal of The Textile Institute, vol. 103, no. 6, pp. 622–628, 2012.

[13] Demet Yilmaz, *A comparison of compact-jet, compact, and conventional ring-spun yarns*, In: Textile Research Journal, vol. 81, no. 5, pp. 459–470, March 2011.

[14] Banu Uygun Nergis Yeşim Beceren, *Comparison of the effects of cotton yarns produced by new, modified and conventional spinning systems on yarn and knitted fabric performance,* In: Textile Research Journal, vol. 78, no. 4, pp. 297–303, April 2008.

[15] Johari, M.S., Soltani, P., *Effect of strand spacing and twist multiplier on structural and mechanical properties of Siro-spun yarns*, In: Fibers and Polymers, vol. 13, no. 1, pp. 110–117, 2012.

[16] Gaye Yolacan, Ozlem Bilget, Sinem Bilgin Huseyin Gazi Ortlek, *Effects of enzymatic treatment on the performance of knitted fabrics made from different yarn types*, In: Tekstil Ve Konfeksiyon, vol. 2, pp. 115–119, 2010.

[17] Johari, M.S., Soltani, P., *Effect of using the new solo-siro spun process on structural and mechanical properties of yarns*, In: Fibres & Textiles in Eastern Europe, vol. 21, no. 3, pp. 51–54, 2013.

[18] Arindam Basu, *Yarn Structure-properties relationship*, In: Indian Journal of Fibre and Science Research, vol. 34, pp. 287–294, September 2009.

[19] Pinar Çelik Emrah Temel, *A research on spinnability of 100% polyester and polyester – cotton blend sirospun yarns*, In: Tekstil Ve Konfeksiyon, vol. 1, pp. 23–29, 2010.

[20] Mozafari-Dana, R., Etrati, S.M., Shaikhzadeh Najar, S., Ghasemi, R., *Comparing the physical properties of produced sirospun and new hybrid solo-siro spun blend wool/polyester worsted yarns*, In: Fibres & Textiles in Eastern Europe, vol. 16, no. 1, pp. 24–27, 2008.

[21] Huseyin Kadoglu Sevda Altas*, Comparison of conventional ring, mechanical compact and pneumatic compact yarn spinning systems*, In: Journal of Engineered Fibers and Fabrics, vol. 7, no. 1, pp. 87–100, 2012.

[22] Hüseyin Kadoğlu Pinar Çelik, A *research on the compact spinning for long staple yarns*, In: Fibres & Textiles in Eastern Europe, vol. 12, no. 4, pp. 27–31, 2004.

[23] Altas, S., Kadoglu, H., *Comparative study on the properties of yarns produced by modified ring spinning,* In: Industira Textila, 2013. 64(2): pp. 65–68.

[24] Ishtiaque, S. M., Alagirusamy, R., Yoti Ranjan Dash, *Properties and processibility of compact yarns*, In: Indian Journal of Fibre & Textile Research, vol. 27, no. 4, pp. 362–368, 2002.

[25] M. Dean Ethridge Mourad Krifa*, Compact spinning effect on cotton yarn quality:interactions with fiber characteristics*, In: Textile Research Journal, vol. 76, no. 5, pp. 388–399, 2006.

[26] Kilic, G.B., Okur, A., *A comparison for the physical properties of cotton, modal and acrylic yarns spun in ring and OE-rotor spinning systems.* In: Industria Textila, 2016. 67(2): pp. 81–90.

[27] Danuta Cyniak, Jerzy Czekalski Tadeusz Jackowski*, Compact cotton yarn*, In: Fibres & Textiles in Eastern Europe, vol. 12, no. 4, pp. 22–26, 2004.

[28] Saville, B.P., *Physical testing of textiles*, In: New York, Washington, DC: CRC Press, 1999.

[29] Technical Manual of Uster Tester-4.

[30] Hearle, W.S., Morton, W.E., *Physical properties of textile fibres*. In: New York , Washington, D.C.: CRC Press, 2008.

Authors:

MUHAMMAD FURQAN KHURSHID [1]
SARMAD ASLAM [1]
USMAN ALI [1]
AMIR ABASS [1]
TALHA ALI HAMDANI [2]
FIAZ HUSSAIN [2]

[1]Department of Textile Engineering, Bahauddin Zakariya University, Multan 59060, Pakistan
[2]Faculty of Engineering &Technology, National Textile University, Faisalabad 37610, Pakistan

e-mail: engr.furqan@bzu.edu.pk, sarmad_aslam@hotmail.com, usman.ali@bzu.edu.pk,
amir.abbas@bzu.edu.pk, hamdani.talha@ntu.edu.pk, fiaz@ntu.edu.pk

Corresponding author:

MUHAMMAD FURQAN KHURSHID
engr.furqan@bzu.edu.pk

Preparation and properties of electrospun PAN/LA-SA composite phase change fibers

GUIZHEN KE   JIAFENG PEI   KUNDI ZHU

REZUMAT – ABSTRACT

Prepararea și proprietățile materialelor compozite PAN/LA-SA realizate prin electrofilare

Materialele cu schimbare de fază stabile ca formă pe bază de compozite PAN/binare eutectice LA-SA, în care LA-SA a servit ca material de schimbare de fază solid-lichid, iar PAN a acționat ca material de susținere, au fost fabricate cu succes prin electrofilare. Au fost studiate efectele cantității eutectice LA-SA asupra proprietăților de morfologie, structură și stocare a energiei termice a compozitelor PAN/LA-SA electrofilate. Imaginile cu microscop electronic (SEM) au arătat că compozitele PAN/LA-SA au o formare bună. Finețea fibelor a crescut odată cu creșterea conținutului eutectic LA-SA. Spectroscopia în infraroșu cu transformată Fourier (FTIR) a arătat că în materialul compozit PAN/LA-SA nu există legături chimice, iar interacțiunea principală dintre PAN și LA-SA a fost fizică. Analiza de calorimetrie prin scanare diferențială (DSC) a indicat că valorile entalpiei compozitelor cu schimbare de fază au crescut treptat odată cu creșterea cantității eutectice LA-SA, iar temperaturile de topire ale acestora au fost cuprinse între 33,3° C și 38,9°C. Analiza gravimetrică termică (TG) a arătat că materialul compozit cu schimbare de fază PAN/LA-SA are o stabilitate termică bună sub 100°C.

Cuvinte-cheie: electrofilare, LA-SA eutectic, PAN, compozite cu schimbare de fază

Preparation and properties of electrospun PAN/LA-SA composite phase change fibers

Form-stable phase change fibers based on LA-SA binary eutectic/PAN composite fibers in which LA-SA served as a solid-liquid phase change material and PAN acted as a supporting material were successfully fabricated through electrospinning. The effects of LA-SA eutectic amount on the morphology, structure and thermal energy storage properties of electrospun PAN/LA-SA composite fibers were studied. Scanning electron microscope (SEM) images showed that PAN/LA-SA composite fibers have good formation. Fiber fineness increased with the increase of LA-SA eutectic content. Fourier transform infrared (FTIR) showed in the PAN/LA-SA composite fiber there was no chemical bonds and the main interaction between PAN and LA-SA was physical. Differential scanning calorimetry (DSC) analysis indicated that heat enthalpies values of the phase change composite fibers gradually increased with the increase of LA-SA eutectic amount, and their onset melting temperatures ranged from 33.3°C to 38.9°C. Thermal gravimetric (TG) analysis showed that PAN/LA-SA composite phase change fiber has good thermal stability below 100°C.

Keywords: electrospinning; LA-SA eutectic; PAN; composite phase change fibers

INTRODUCTION

Adaptive phase change material is one of the representatives of smart materials. Phase change is a process of energy release or absorption, thus the environment temperature can be adjusted during this process. Phase change process is a physical process and there is no chemical reaction during this process, since it is only the change of the physical state. Based on these characteristics, phase change materials can be used as a smart green material. In the past decades, PCMs have been studied and applied successfully in the various applications such as solar energy storage, energy efficient buildings, space and water heating, waste heat utilization, cooling and air-conditioning, medical application, cooling of energy, thermal regulating fibers and smart textiles [1–5].

So far, among a variety of latent heat energy storage phase change materials, solid-liquid types have been widely concerned, for their desired properties and characteristics such as the volume stability during phase change, suitable range of melting temperature,

high capacity of latent heat [6–8]. However, liquid is produced during phase change process, which brings inconvenience to the practical application. To solve this problem, one method is to develop a form-stable phase change material [9–13]. The shape-stable amorphous phase change materials are generally composed of substrate matrix and phase change materials. At present polymer is widely used as matrix to afford structural and mechanical support, meanwhile, solid-liquid phase change materials are dispersed in the three-dimensional structure of the polymer to form a new composite material. The composite material is solid in macro during phase change process and less prone to leakage and can be made into different shapes and specifications of products according to the needs of practical application.

The used solid-liquid PCMs can be generally classified into inorganic type (such as salt hydrate $Na_2SO_4 \times 10H_2O$, $CaCl_2 \times 6H_2O$) and organic type (such as paraffins, fatty acids). Fatty acid have been extensively studied as a promising type due to the desired properties and/or characteristics including

low price, suitable melting temperature, high capacity of latent heat, little or no super cooling during phase transitions, low vapor pressure of melts, environment friendly and good chemical stability [14–16]. However, their phase transition temperature is high for climatic requirement which can limit their practical applications. To overcome this disadvantage, fatty acid eutectic mixtures were widely researched and prepared successfully by many researchers [17–20]. Based on the reports in the literature, many researchers have discovered that the phase transition temperatures of fatty acid eutectic are lower than that of corresponding individual fatty acid, but phase change latent heats of the mixtures can be maintained at a sufficient level. Polymer and fatty acid have many similarity in compositions and properties, according to similarity and intermiscibility principle, by melt blending or blending spinning or in-situ polymerization method, the three-dimensional network structure of the polymer can well coated with organic phase change material to form a shape stabilized composite phase change material [21–25].

Electrospinning is a simple, convenient, and versatile technique for generating ultrafine fibers from wide variety of polymers. These electrospun ultrafine fibers possess special properties for example high porosity, large specific surface area, high surface energy and high activity. In this study, to utilize the multi-scaled porous structure of electrospun fiber mats, electrospinning technique has been tried to develop innovative form-stable PCMs. The form-stable phase change composite fibers consisting of binary lauric-stearic acid (LA-SA) eutectic and polyacrylonitrile (PAN) acted as a supporting material were successfully fabricated by electrospinning.

EXPERIMENTAL PART

Materials

The PAN chip (Mw=50000) was obtained from Shanghai Plastics Co. (Shanghai, China). Lauric acid [LA, $CH_3(CH_2)_{10}COOH$], stearic acid [SA, $CH_3(CH_2)_{16}COOH$] and n,n-dimethyl-formicaci (DMF) were supplied by Sinopharm Group Chemical Reagent Co. ltd. (Shanghai, China).

Preparation of binary lauric-stearic acid (LA-SA) eutectic

Based upon the lowest eutectic point theory, two fatty acids can be blended together with eutectic ratio to achieve the eutectic temperature, which is lower than those of individual fatty acids. The eutectic ratios of fatty acid mixtures were calculated by the Schrader equation [25, 26].

$$T_m = \frac{1}{1/T_A - (R 1n X_A)/H_A} \qquad (1)$$

$$H_m = T_m \left(\frac{X_A H_A}{T_A} + \frac{X_B H_B}{T_B} \right) \qquad (2)$$

Where T_m is the melting temperature of a eutectic mixture, K; T_A and T_B is melting temperature (K), X_A

and X_B is molar fraction percentage ($X_A + X_B$ = 1), and H_A and H_B is melting latent heat (J/mol) of component A and B in the binary system, respectively; and R is the gas constant, 8.315 J/(mol×K). By using equation 1, mass ration for LA-SA binary system can be calculated.

The binary eutectic system was prepared with fatty acids LA and SA. With the calculated eutectic ratio, LA and SA weighed and mixed together in a sealed flask; the flask was then kept in an oven at 80°C for 2h. After fully melted, the mixture was treated with ultrasonic vibration at 60°C for 5 min. After that the mixture was cooled at ambient temperature and kept for use.

Preparation of PAN/ LA-SA composite fiber

PAN pellets were dissolved in n,n-dimethyl-formicaci (DMF) and magnetically stirred for at least 3h to obtain 12%wt PAN solution. LA-SA binary eutectic material of different mass content was blended with PAN solution and fully dissolved in solution. The mass ratio of LA-SA and PAN was 0.5:1, 0.7:1, 1:1 and 1.2:1 respectively. After that, the blend solution was filled in a 10 ml plastic syringe with a blunt-end stainless-steel needle. Inside diameter of the needle was 0.5 mm. The spin dope was supplied by a syringe pump with a flow rate of 1 ml/h. The discharged voltage was 15 kV. The received distance was 20cm. The electro-spun fibers were collected as overlaid fibrous mats.

Characterization

Scanning electron microscope (SEM, JEOL, JSM-6510LV) was used to observe the surface morphology of the electrospun ultrafine composite fibers with acceleration voltage of 10 kV. All samples were sputtered and coated with gold under vacuum prior to SEM observation.

Fourier transform infrared (FTIR) spectrum of neat PAN electrospun fiber and PAN/LA-SA composite fibers were scanned using Bruker Alpha TENSOR 27X. The spectra were recorded between 600 cm^{-1} and 4000 cm^{-1} by 32 scans for each.

Differential scanning calorimetry (DSC, NETZSCH DSC 204F1) and thermal gravimetric (TG, NETZSCH STA409PC) were employed to investigate the thermal behaviors of individual fatty acids, binary fatty acid eutectics and electrospun ultrafine composite fibers. DSC testing was carried out from 25°C to 100°C with inflowing nitrogen atmosphere (50 mL/min) at a heating and cooling rate of 8°C/min. Measurement precisions for calorimeter and temperature was ±2.0% and ±2.0°C, respectively. TG testing was carried out from 20°C to 800°C with inflowing nitrogen atmosphere (50 mL/min) at a heating rate of 100°C/min. Each sample was about 5 mg.

RESULTS AND DISCUSSION

Thermal properties of individual fatty acids and binary fatty acid eutectics

From the DSC curves of LA and SA (figure 1), the obtained melting temperature of LA and SA is 43.9°C

Fig. 1. DSC curves of LA and SA

THERMAL PROPERTIES OF LA AND SA BINARY MIXTURES			
LA/SA (%)	80:20	86.5:13.5	90:10
Onset melting temperature (°C)	39.1	38.8	39.5
Peak melting temperature (°C)	41.7	44.1	42.7
End melting temperature (°C)	44.6	48.2	44
Latent heat (kJ/kg)	146.5	135.1	127.9

Table 1

Table 2

THEORETICAL AND EXPERIMENTAL LATENT HEAT VALUES OF LA AND SA BINARY			
Parameters	**Molar fraction (%)**	**Melting temperature (°C)**	**Latent heat of fusion (kJ/kg)**
Theoretical value	86.7:13.3	40.7	167.5
Experimental value	86.5:13.5	38.8	135.1
Absolute error	0.2	1.9	32.4
Relative error	0.23%/1.5%	4.7%	19.3%

Note: Among 0.23%/1.5%, 0.23% is calculated based on value 86.7% and 1.5% based on value 13.3%.

and 69.1°C, and latent heat of LA and SA is 161.8 and 219.2 kJ/kg, respectively.

The molecular weight of LA and SA is 200.32 and 284.48, respectively. Combining these parameters and equation 1 and 2, the calculated mass ration for LA-SA binary system is 86.7:13.3 (LA:SA), the melting temperature and latent heat is 40.7°C and 167.5 kJ/kg respectively. In order to verify the accuracy of the above formula, LA and SA was mixed with different molar ratios and melting temperature and latent heat of the binary mixture were tested. The experimental results are shown in table 1.

It can be seen from table 1, the melting temperature of LA–AS binary mixtures (80:20, 86.5:13.5, 90:10) was 39.1°C, 38.8°C and 39.5°C respectively.

The latent heat of fusion values was 146.5, 135.1 and 127.9 kJ/kg, which shows that LA-SA binary mixtures have enough latent heat of fusion in the range of 127–147 kJ/kg and suitable melting temperature around 39°C. Latent heat and temperature of phase change vary with the molar fraction change of LA and SA. The phase transition temperature and enthalpy of both pure fatty acids are higher than that of the mixture. When the molar ratio of LA and SA is 86.5:13.5, the binary mixture has lowest melting temperature, which means that a binary eutectic can be formed between LA and SA. And the results are consistent with the theoretical calculation values. The comparison between experimental and theoretic results is presented in table 2. The calculated results agree well with the experimental values, thus 86.7:13.3 was selected as molar ratio of the binary mixture.

Morphology observation of PAN/LA-SA composite fibers

LA-SA binary eutectic and PAN was blended with different mass ratio and PAN/LA-SA composite fibers were prepared through electron spinning successfully. The morphology of composite fiber was investigated by SEM. The images are shown in figure 2.

a   b   c   d   e
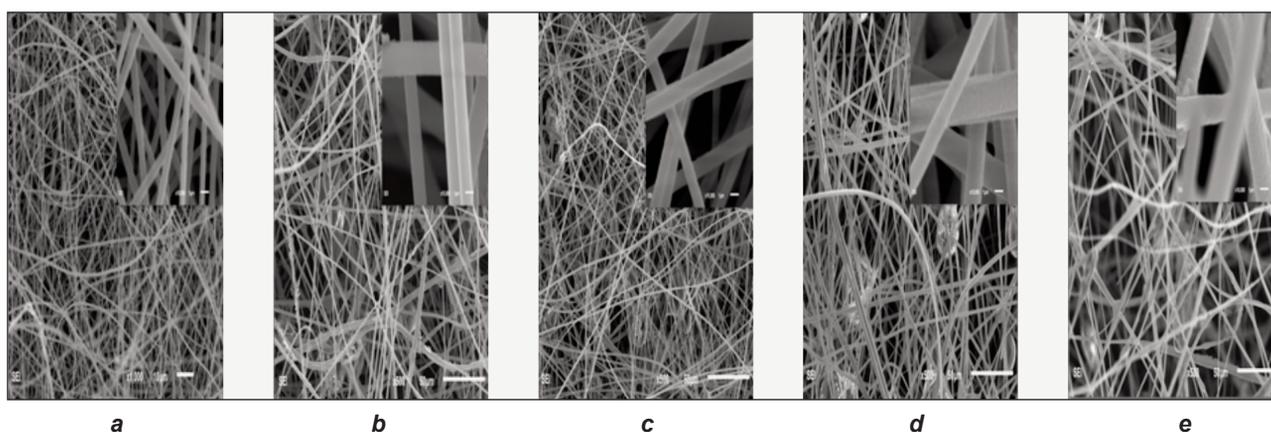
Fig. 2. SEM images of PAN/LA-SA composite fibers: mass ratio of LA-SA and PAN:
a – 0; b – 0.5:1; c – 0.7:1; d – 1:1; e – 1.2:1

As shown in figure 2, *a*, the neat PAN fibers are quite uniform in diameters and have fine diameter and smooth surfaces. It is observed that the composite fibers with LA-SA/PAN mass ratio of 0.5/1, 0.7/1, 1.2/1 are also smooth and cylindrical in shape. However, with the increase of LA-SA eutectic mixture proportion in the composite fibers, the grooves and wrinkles on the surface of the composite fibers are clearly observed. And fiber diameter also becomes coarse. The morphology of electrospun fibers is affected by many factors, such as polymer molecular weight, concentration and conductivity and viscosity of spinning solution, solvent volatilization and spinning process parameters. Hydrogen bonds between carbonyl (C°N) in PAN and carboxyl (–COOH) in LA-SA binary eutectics might exist, which also resulted in the change of electrospun dope properties and thus the change of fiber morphology. However, due to the protection and support of the PAN matrix, LA-SA eutectic material can be combined into the polymer and the obtained PAN /LA-SA composite fibers have good formation.

FTIR analysis of PAN/LA-SA composite fiber

FTIR spectrum of neat PAN ultrafine fibrous mats and PAN/LA-SA composite fibrous mats were shown in figure 3.

It can be observed spectrum of PAN (a) shows typical absorption band at about 2252, 2940 and 1447 cm^{-1}, which is belong to stretching vibration of cyanogroups –C°N, asymmetric and symmetric bending vibrations of methylene groups (–CH2–) in PAN molecular chains, respectively. Comparing to spectrum of PAN, some typical absorption peaks of fatty acid appear in spectrum of PAN/LA-SA (b). The band at 1702, 1278 and 949 cm^{-1} was belong to C=O, C–O and –OH stretching vibrations in LA-SA binary eutectics, respectively. The characteristic adsorption peak at 2842 cm^{-1} is ascribed to C–H symmetric stretching vibrations in fatty acid. Spectrum results indicated that no chemical reaction

happened between PAN and LA-SA and PAN was just a supporting matrix of LA-SA binary eutectics.

Thermal energy storage properties

The thermal energy storage properties of electrospun PAN/LA-SA ultrafine composite fibers were investigated with DSC method. DSC curves of various PAN/LA-SA fibers are presented in figure 4. The characteristic temperatures and melting latent heat are shown in table 3. DSC curves indicated that the endothermic peaks of the composite fibers increased with the increase of binary fatty acid eutectics content, which means the increase of melting latent heat. Binary fatty acid eutectics mass percentage in the composite fibers became the dominating factor for the variations of latent heat. Though enthalpy value of PAN/LA-SA can reach 88.08 kJ/kg, it is still far smaller than that of pure LA-SA eutectics (135.1 kJ/kg). During phase change processes, the movement of LA-SA may be confined by hydrogen bonding interaction between carbonyl (C°N) and carboxyl (–COOH) and limitation from PAN matrix, thus the crystallization process of LA-SA eutectics in fibers was retarded and the melting latent heat value was decreased [25]. It is observed that LA-SA mass content and PAN polymer has little effects on phase change temperature. Onset melting temperature varies from 33.3°C to 38.9°C, which is a suitable temperature range for energy storage application of composites fibers in textile and building field.
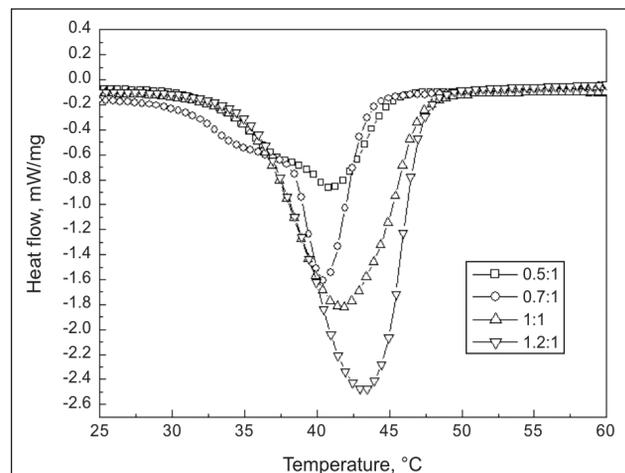
Fig. 4. DSC curves of PAN /LA-SA composite fibers

Fig. 3. FTIR spectrum of various fibers

Table 3

THERMAL PROPERTIES OF PAN/LA-SA COMPOSITE FIBERS				
Mass ratio of LA-SA and PAN	Onset melting temperature, °C	Peak melting temperatue, °C	End melting temperature, °C	Latent heat, kJ/kg
0.5:1	33.3	40.9	43.3	35.26
0.7:1	38.9	40.5	43.3	46.21
1:1	36.1	41.7	47.1	74.94
1.2:1	36.9	44.0	46.9	88.08

Table 4

THERMAL DEGRADATION VALUES OF PAN/LA-SA COMPOSITE FIBER							
LA-SA/PAN	0.5:1		0.7:1		1:1		1.2:1	
Area	Phase 1	Phase 2	Phase 1	Phase 2	Phase 1	Phase 2	Phase 1	Phase 2
Onset (°C)	176.4	311.1	187.6	311.1	195.7	330.8	193.0	315.9
End (°C)	217.1	346.5	216.8	342.8	241.1	324.3	238.4	330.1
Mass change (%)	22.11	33.03	25.89	29.39	37.17	19	50.14	18.42

Thermal gravimetric analysis

Phase change materials, especially organic phase change materials, are often subjected to the oxidation, decomposition, volatilization and other reactions when they are subjected to high temperature. Here PAN/LA-SA composite fibers are tested using TG and the results are shown in figure 5. The mass change and decomposition onset and end temperature are summarized in table 4. Obviously there are two main weight-loss areas. Phase 1 occurs from 176°C to 240°C, and it is mainly due to fatty acid carbonization and degradation. It can be observed that onset temperature of weight loss is delayed from 176.4°C to 193.0°C with the increase of LA-SA content, which might be due to inhibitory effect of strong hydrogen bond on LA-SA volatilization. Phase 2 happens from 311°C to 346°C, and it is mainly from PAN degradation. TG results showed that PAN/LA-SA composite phase change fiber has good thermal stability below 100°C, but when the environment temperature is higher than 100°C, fatty acid easily decomposes and volatiles and thus quality loss would happen. Therefore, the composite phase change fiber film is suitable for low temperature phase change heat storage areas, such as passive solar room, temperature-adjustable garments and phase change building materials.
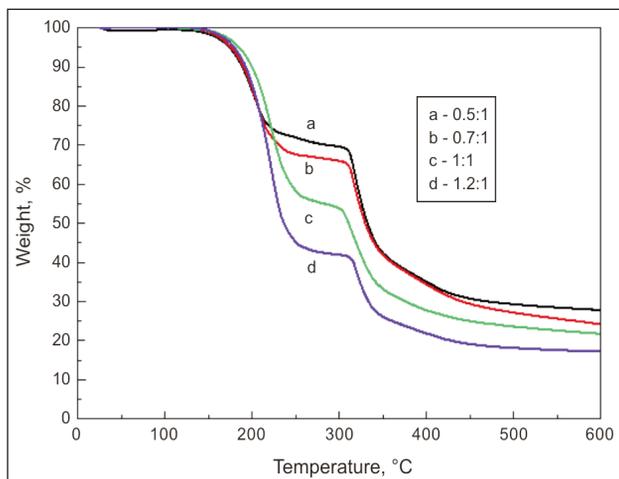
Fig. 5. TG curves of PAN/LA-SA composite fibers (mass ratio of LA-SA and PAN, *a* – 0.5:1, *b* – 0.7:1, *c* – 1:1, *d* – 1.2:1)

CONCLUSIONS

Lauric acid (LA) and stearic acid (SA) binary eutectics were prepared with molar ratio 86.7:13.3. The theoretical melting temperature was 38.8°C, close to experimental value 40.7°C, lower than that of pure LA or SA. PAN was taken as matrix and LA-SA as phase change material, and form-stable phase change composite fibers were electrospun successfully. The PAN/LA-SA composite fiber had good formation, while when LA-SA content was too high, fiber would become coarse and wrinkled. No chemical interaction happened between PAN and LA-SA eutectics. Latent heat value of PAN/LA-SA increased from 35.26 kJ/kg to 88.08 kJ/kg with the increase of LA-SA mass fraction, but it was far below the value of pure LA-SA eutectics (135.1 kJ/kg). Relatively speaking, the influence on phase transition temperature was small. The phase change temperatures of the composite fibers ranged from 33.3°C to 38.9°C. PAN/LA-SA composite phase change fiber had good thermal stability below 100°C. The composite phase change fiber is expected to use in low temperature phase change heat storage areas, such as passive solar room, temperature-adjustable garments and phase change building materials.

BIBLIOGRAPHY

[1] Zhang P., Xiao X., Ma Z.W. *A review of the composite phase change materials: Fabrication, characterization, mathematical modeling and application to performance enhancement*, In: Applied Energy, 2016, vol.165, pp. 472–510.

[2] Veerakumar C., Sreekumar A. *Phase change material based cold thermal energy storage: Materials, techniques and applications – A review*, In: International Journal of Refrigeration, 2016, vol. 67, pp. 271–289.

[3] Sharma A., Tyagi V.V., Chen C.R., Buddhi D. *Review on thermal energy storage with phase change materials and applications*, In: Renewable Sustainable Energy Reviews, 2009, vol. 13, issue 2, pp. 318–345.

[4] Zhou D., Zhao C.Y., Tian Y. *Review on thermal energy storage with phase change materials (PCMs) in building applications*, In: Applied Energy, 2012, vol. 92, pp. 593–605.

[5] Khadiran, T., Hussein, M.Z., Zainal, Z., Rusli, R. *Encapsulation techniques for organic phase change materials as thermal energy storage medium: A review*, In: Solar Energy Materials and Solar Cells, 2015, vol. 143, pp. 78–98.

[6] Sharmaa, R.K., Ganesana, P., Tyagib, V.V., Metselaara, H.S.C., Sandaranc, S.C. *Developments in organic solid–liquid phase change materials and their applications in thermal energy storage*, In: Energy Conversion and Management, 2015, vol. 95, pp. 193–228.

[7] Sua, W., Darkwab, J., Kokogiannakisc, G. *Review of solid–liquid phase change materials and their encapsulation technologies*, In: Renewable and Sustainable Energy Reviews, 2015, vol. 48, pp. 373–391.

[8] Castell, A., Solé, C. *An overview on design methodologies for liquid–solid PCM storage systems*, In: Renewable and Sustainable Energy Reviews, 2015, vol. 52, pp. 289–307.

[9] Kenisarin, M.M., Kenisarina, K.M. *Form-stable phase change materials for thermal energy storage*, In: Renewable and Sustainable Energy Reviews, 2012, vol. 16, no. 4, pp. 1999–2040.

[10] Mu, S., Guo, J., Zhang, S., An, Q., Wang, D., Liu, Y., Guan, F. *Preparation and thermal properties of cross-linked poly(acrylonitrile-co-itaconate)/polyethylene glycol as novel form-stable phase change material for thermal energy storage*, In: Materials Letters, 2016, vol. 171, pp. 23–26.

[11] Ke, G., Yu, W. *Preparation and physical characteristics of porous phase change PU/PEG membrane*, In: Industria Textila, 2012, vol. 63, no. 6, pp. 283–289.

[12] Fu, X., Liu, Z., Wu, B., Wang, J., Lei, J. *Preparation and thermal properties of stearic acid/diatomite composites as form-stable phase change materials for thermal energy storage via direct impregnation method*, In: Journal of Thermal Analysis and Calorimetry, 2016, vol. 123, no. 2, pp. 1173–1181.

[13] Konuklu, Y., Paksoy, H.O. *The Preparation and Characterization of Chitosan-Gelatin Microcapsules and Microcomposites with Fatty Acids as Thermal Energy Storage Materials*, In: Energy Technology, 2015, vol. 3, no. 5, pp. 503–508.

[14] Yuan, Y., Zhang, N., Tao, W., Cao, X., He, Y. *Fatty acids as phase change materials: A review*, In: Renewable and Sustainable Energy Reviews, 2014, vol. 29, pp. 482–498.

[15] Jiao, C. M., Ji, B. H., Fang, D. *Preparation and properties of lauric acid-stearic acid/expanded perlite composite as phase change materials for thermal energy storage*, In: Materials Letters, 2012, vol. 67, no. 1, pp. 352–354.

[16] Kenisarin, M.M. *Thermophysical properties of some organic phase change materials for latent heat storage, A review*, In: Solar Energy, 2014, vol. 107, pp. 553–575.

[17] Sari, A. *Eutectic mixtures of some fatty acids for latent heat storage: thermal properties and thermal reliability with respect to thermal cycling*, In: Energy Conversation Management, 2006, vol. 47, pp. 1207–1221.

[18] Yuan, Y., Tao, W., Cao, X., Bai, L. *Theoretic prediction of melting temperature and latent heat for a fatty acid eutectic mixture*, In: Journal of Chemical and Engineering Data, 2011, vol. 56, no. 6, pp. 2889–2891.

[19] Listona, L.C., Farnamb, Y., Krafcikc, M., Weissb, J., Erkc, K., Taoa, B.Y. *Binary mixtures of fatty acid methyl esters as phase change materials for low temperature applications*, In: Applied Thermal Engineering, 2016, vol. 96, pp. 501–507.

[20] Fauzi, H., Metselaar, H.S.C., Mahlia, T.M.I., Silakhori, M., Ong, H.C. *Thermal characteristic reliability of fatty acid binary mixtures as phase change materials (PCMs) for thermal energy storage applications*, In: Applied Thermal Engineering, 2015, vol. 80, pp. 127–131.

[21] Li, M., Wu, Z.S., Kao, H.T. *Study on preparation and thermal properties of binary fatty acid/diatomite shape-stabilized phase change materials*, In: Solar Energy Materials and Solar Cells, 2011, vol. 95, no. 8, pp. 2412–2416.

[22] Sari, A., Alkan, C. *Preparation and thermal energy storage properties of poly(n-butyl methacrylate)/fatty acids composites as form-stable phase change materials*, In: Polymer Composites, 2012, vol. 33, no. 1, pp. 92–98.

[23] Sari, A., Alkan, C., Kolemen, U., Uzun, O. *Eudragit S(methyl methacrylate methacrylic acid copolymer)/fatty acid blends as form-stable phase change material for latent heat thermal energy storage*, In: Applied Polymer, 2006, vol. 101, no. 3, pp. 1401–1406.

[24] Sari, A., Karaipekli, A. *Thermal conductivity and latent heat thermal energy storage characteristics of paraffin/expanded graphite composite as phase change material*, In: Applied Thermal Engineering, 2007, vol. 27, pp. 1271–1277.

[25] Ke, H., Pang, Z., Peng, B., Wang, J., Cai, Y., Huang, F., Wei, Q.J. *Thermal energy storage and retrieval properties of form-stable phase change nanofibrous mats based on ternary fatty acid eutectics/polyacrylonitrile composite by magnetron sputtering of silver, In: Journal of Thermal Analysis and Calorimetry*, 2016, vol. 123, pp. 1293–1307.

[26] Zhang, Y.P., Su, Y.H., Ge, X.S. *Prediction of the melting temperature and the fusion heat of (quasi-) eutectic PCM*, In: Journal of University of Science and Technology of China, 1995, vol. 25, pp. 474–478.

Authors:

GUIZHEN KE
JIAFENG PEI
KUNDI ZHU
Department of Textile Science and Engineering, Wuhan Textile University
Yangguang Road Number 1, Jiangxia District
Wuhan City (Zip Code: 430020), China

Corresponding author:

GUIZHEN KE
e-mail: kgz66@126.com, guizhen.ke@wtu.edu.cn

Shrink resistant finishing and mechanism analysis on the silk/hemp fabric

SHU-QIANG LIU
GAI-HONG WU

YI CUI
HONG-XIA GUO

REZUMAT – ABSTRACT

Analiza mecanismului de finisare rezistentă la contracție asupra țesăturii de mătase/cânepă

Țesăturile de mătase/cânepă sunt populare pentru caracteristicile de biodegradare, permeabilitate excelentă, finețe și beneficiile pentru sănătate, dar au un dezavantaj evident, acela de a se contracta foarte mult la spălare. În scopul rezolvării acestei probleme, în această lucrare au fost aplicate tehnologii de finisare fizică și chimică. S-au studiat efectele parametrilor de prelucrare a finisării fizice, temperaturii și timpului de imersie asupra gradului de contracție și au fost studiate alte proprietăți ale țesăturii de mătase/cânepă. Mai mult, au fost investigați parametrii chimici de finisare, cum ar fi raportul dintre acidul citric (CA)/acidul (poli)maleic (PMA), dozele de PMA, CA și catalizatorul de hipofosfit de sodiu (SHPP). Rezultatele au arătat că parametrii optimi de imersie au fost la 65°C timp de 60 de minute. Condițiile optime de procesare a finisării chimice au fost următoarele: raportul 3:1 CA/PMA, doza de 40 g/L PMA și CA și doza de de 30 g/L catalizator SHPP. După procesarea prin finisarea fizică și chimică optimă, gradul de contracție al țesăturilor de mătase/cânepă a scăzut la 0%. Mecanismul de contracție a fost discutat, de asemenea, pentru a evalua în viitor deformarea fibrelor la astfel de tratamente.

Cuvinte-cheie: țesătură de mătase/cânepă, finisare rezistentă la contracție, finisare pre-conracție, finisare fizică și chimic

Shrink resistant finishing and mechanism analysis on the silk/hemp fabric

Silk/hemp fabrics are popular with people for their biodegradation, excellent permeability, smooth and healthy, but they have one obvious drawback of shrink seriously in the wash. Aiming at solving this problem, the physical and chemical finishing technologies were applied in this paper. The effects of processing parameters of physical finishing, immersion temperature and time, on the shrinkage ratio and other properties of silk/hemp fabric were studied. Moreover, the chemical finishing parameters, such as the ratio of citric acid (CA)/poly (maleic acid) (PMA), dosages of PMA, CA, and catalyst of Sodium Hypophosphite (SHPP) were also investigated. The results showed that the optimal immersion parameters were at 65°C for 60 min. The optimal processing conditions of chemical finishing were as follows: 3:1 ratio of CA/PMA, 40 g/L dosage of PMA and CA, and 30 g/L dosage of catalyst SHPP. After processed by the optimal physical and chemical finishing, the shrinking percentage of silk/hemp fabrics declined to 0%. The shrinkage mechanism was also discussed to further disclose the deformation of fibres under such treatments.

Keywords: silk/hemp fabric; shrink resistant finishing; pre-shrink finishing; physical and chemical finishing

INTRODUCTION

As a kind of natural protein fibre, silk has many outstanding performances, such as smooth and soft handle, gentle luster, antibiotic property, so it always is people's most favorite product [1–5]. Meanwhile, hemp, as another kind of natural cellulose fibre, also possesses many superior features, as good moisture permeability, high strength, small deformation, bactericidal ability, etc. [6–10], which was often applied in various types of garments. So the fabrics blended with silk and hemp fibres, would assemble these excellent characteristics of silk and hemp, including soft luster, admirable draping quality, cool feeling, excellent air permeability and many others. Thus the silk/hemp fabrics are deemed to be one most promising material for summer clothing. However, the silk/ hemp fabrics shrink seriously when washing, which usually leads to distortion and deformation to. Even worse, the superior properties of silk/hemp fabrics

would be weakened. So the shrink resistant treatments to silk/ hemp fabrics are absolutely necessary. Review of the literatures revealed the shrink resistant treatments were almost for wool fabrics [11–15]. For instance, Eslahi applied extracted feather protein to improve the shrinkage of wool fabric [16]. Gao used the polymeric biocide polyhexamethylene biguanide (PHMB) to resist the shrinkage of wool woven fabric [17]. Only small proportion of literatures made research on the shrinkage resistance of silk fabrics, and most of treatment methods adopted in these literatures were chemical finishing techniques [18–20]. For example, Yang applied natural chemical agent 'Chorangak liquid' to reduce the shrinkage of silk fabrics [21]. Based on literature research, it was found that there was almost no literature studying shrink resistant on silk/hemp fabric. Besides that, the physical and chemical techniques were usually used separately, but both of the two techniques could make contributions towards the shrinkage resistance [22].

So to achieve better shrink resistance, the physical and chemical finishing techniques were both used in this paper. Firstly the silk/hemp fabrics were preshrunk in warm water directly, which belonged to physical treatment. Following the chemical agents were used to improve the shrinkage of silk/hemp fabrics. It is worth mentioning that all chemical agents employed in this study were harmless and environmentally friendly. Then, the influences of processing parameters of physical and chemical finishing on the shrinkage and other properties of silk/hemp fabrics were studied. Finally, the optimal parameters of shrink resistant could be obtained. Moreover, the mechanism of shrinkage resistance was also investigated.

EXPERIMENTAL WORK

Materials

Silk/hemp fabrics, whose warp yarns were mulberry silk and weft yarns were hemp/cotton blending yarns, were supplied by Shanxi Jilier Lu Silk Industry (China). And their fibre contents were 34% silk, 36% hemp and 30% cotton, the weight was 89 g/m^2, as well as the static shrinkage percentage was 5.2%.

Chemical reagents used in this experiment were as follows: Citric Acid (CA, $C_6H_8O_7$) from Beijing Chemical Works, China; Poly (Maleic Acid) (PMA $C_4H_4O_4$, Mn≤2000) from Luoyang Tengyi Chemical Company, China; Sodium Hypophosphite (SHPP, $NaH_2PO_2 \cdot H_2O$) from Yueqiao Reagent Plastic Co., Ltd, Taishan, China; Trolamine [TEA, $(HOCH_2CH_2)_3N$] from Zhengzhou Chemical Reagent No.2 Factory, China; Boric Acid (BA, H_3BO_3) from Chaoyang Chemical Factory; Primary Alcobol Ethoxylate [AEO, $C_{12}H_{25}O \cdot (C_2H_4O)_7$] from Xingfasheng Chemical Company, Shanxi, China.

Processing of shrink resistant finishing

Firstly, physical finishing technique was used to dispose the fabrics. The fabric was placed in the water bath (HH-8, Ningbo Textile Instrument Factory, China) under certain immersion temperature (20, 35, 50, 65, 80°C) and time (30, 60, 90, 120, 150 min). Then it was pressed by two rollers to squeeze out excess water in the fabric. After that, the fabric was dried in an oven (DHG-9070, Ningbo Textile Instrument Factory, China) under 65°C for 5 min. In the process of physical finishing, 2 parameters, immersion temperature and immersion time, were employed to investigate their effects on shrinkage resistance of silk/hemp fabrics.

Following, the fabrics were disposed by chemical finishing. They were dipped in the chemical treating solution (CA, PMA, SHPP, TEA, BA and AEO was dissolved in water to prepare the solution with concentrations of 20g/l TEA, 5g/l BA, 2g/l AEO, 40g/L SHPP, 40g/L CA and the ratio of CA to PMA was set as 1:1, 2:1, 3:1, 4:1, 5:1) until completely soaked, and then squeezed by rollers to remove the excess liquid. The dip-squeeze processing was repeated 2 times. The whole processing was called "double-dips-double-squeezes". Based on previous literatures, this research adopted single factor experiment to investigate the effect of these parameters on shrinkage resistance [23–24]. After that, the fabrics were dried in an oven at 170°C for 3 min. In chemical finishing, 3 parameters, the ratio of CA/PMA, dosage of PMA and CA and the catalyst dosage of SHPP were studied. Notably, in this experiment the physical and chemical finishing approaches were joined together to improve the shrinkage of silk/hemp fabrics.

Fabric testing

The static shrinkage of fabric was measured by a Fabric Shrinkage Test Machine (YG-703, Wenzhou Fangyuan Instrument Co., Ltd., China). The tensile properties of fabric were tested by Fabric Strength Machine (YG(B)026D-500, Wenzhou Darong Textile Instrument Co., Ltd., China) at 20 mm/min test speed and 200 mm test length. And the drape coefficient of fabric was measured by Fabric Drape Tester (YG811E, Wuhan Guoliang Instrument Co., Ltd., China).

RESULTS AND DISCUSSION

Effect of immersion temperature on shrinkage of fabric

The silk/hemp fabrics were soaked into a water bath for 50 min, and then dried in an oven at 65°C for 5 min. The effects of immersion temperature on shrinkage of fabrics are shown in figure 1.

Figure 1 showed that the weft shrinkage changed slightly from 0% to –0.3%, which expressed that the immersion temperature hardly affected the weft shrinkage of fabric, and would cause a little elongation in the weft direction. The reason was that the weft yarn of fabric was made of hemp and cotton fibres, and this yarn would swell after absorbing water in bath. So its diameter would increase, while the length of hemp/cotton yarn was hardly increased. Therefore the weft yarn or the weft of fabric hardly shrink and have just a little elongation.

Comparing to the weft direction, the warp shrinkage changed obviously with the rise of immersion temperature, firstly decreased and then increased. The
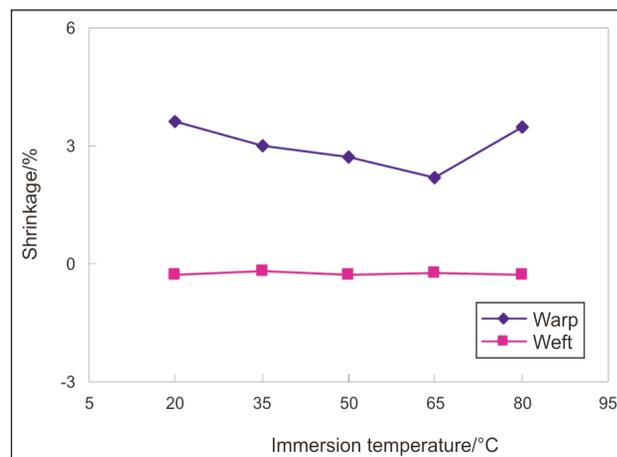
Fig. 1. Shrinkage varied with the rise of immersion temperature

warp shrinkage was lowest at 65°C. The cause of this phenomenon was attributed to the warp yarn which was made of silk fibers. When the silk yarns were in moist and heat condition, they would form extremely small jagged shape, and then shrink. Besides that, when the hemp/cotton weft yarn swelled and grew bigger in diameter, the silk warp yarn, which was interwoven with the bigger weft yarn, would be obliged to shrink. Moreover, the shrink formed in water bath was hard to recover when drying. Therefore, the processing of water bathing was called as "pre-shrinking". Through pre-shrinking, the shrinkage of warp of fabric would decline to the original fabric. As figure 1 showed, the pre-shrinking became more effective with the rise of immersion temperature and warp shrinkage decreased even more.

However, when the immersion temperature was too high (above 80°C), part of crystal structure inside of silk macromolecule decomposed and the orientation degree of silk decreased. Consequently, the stability of silk declined, and further the silk warp yarns couldn't preshrink completely in water bath. Then the shrinkage of silk warp increased.

Thus it drew the conclusion that the optimal immersion temperature was 65°C.

Effect of immersion time on shrinkage of fabric

Figure 2 showed that the weft shrinkage changed slightly (less than 0.3%) with the rise of immersion time. The hemp/cotton yarn would swell after absorbing water and its diameter would increase, but the length of hemp/cotton yarn was hardly affected by water bathing, so the weft shrinkage was very small and changed little.

As for the warp direction, the shrinkage decreased firstly, but then almost invariant when the immersion time was longer than 60 min. In water bath, the pre-shrinking of silk warp became more effectively for longer immersion time, so the warp shrinkage decreased firstly. Then the immersion time was long enough (longer than 60 min), the pre-shrinking effect of silk warp changed slightly, so the warp shrinkage changed slightly.
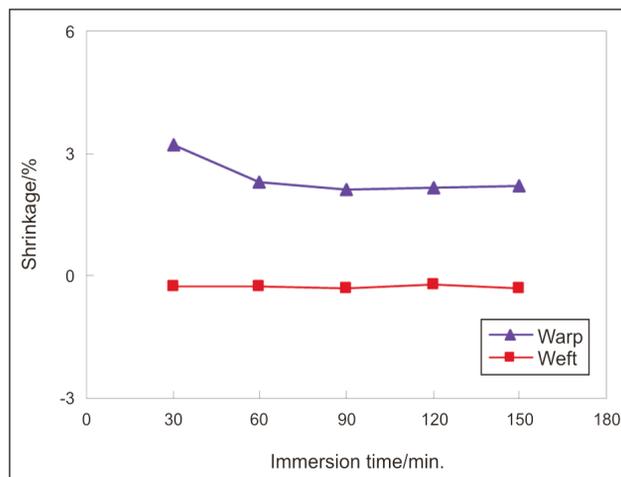
Fig. 2. Shrinkage varied with the immersion time

From the view of shrinkage and energy saving, optimum immersion time was 60 min.

Effect of ratio of CA/PMA on shrinkage of fabric

In the chemical treatment solution, the concentration of catalyst SHPP was 40 g/L, and CA was 40 g/L. And the dosage of PMA was adjusted according to the ratio of CA/PMA of 1:1, 2:1, 3:1, 4:1, 5:1.
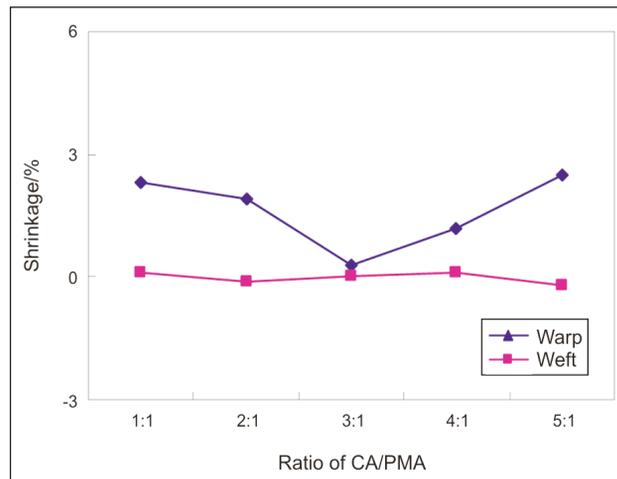
Fig. 3. Shrinkage change with the ratio of CA/PMA

Figure 3 showed that the weft shrinkage was keeping on fluctuating around the vicinity of 0%, which illustrated that the weft of fabric would no longer shrink essentially after chemical finishing.

The warp shrinkage of fabric decreased firstly and increased afterward with the ratio of CA/PMA. And the warp shrinkage was smallest at 3:1. It was because the α-hydroxyl groups of CA could react with carboxyl groups of PMA, and formed polybasic carboxylic acid copolymers (PMA-CA) which had bigger structures. This copolymer in high temperature could be dehydrated into anhydride. Moreover, this anhydride reacted with catalyst of SHPP and further formed an intermediate product, which could react with hydroxyl and amino groups on the macromolecular chain of fibres. Then a system with network cross-linked structure was formed. Based on the network cross-linked structure, the macromolecular chains of fibre entangled, so the relative slippage between large molecules was limited. Certainly, the shrinkage of silk/hemp fabric would be reduced.

On the basis of the above reactions, the PMA and CA reacted more completely, the warp shrinkage of fabric would be smaller. As the figure 3 showed the optimum ratio of CA/PMA was 3:1.

Effect of catalyst dosage of SHPP on shrinkage of fabric

The chemical reagent SHPP was used as catalyst [25] in the experiment. The dosage of SHPP was appropriate when the ratio of CA/PMA was 3:1 (40 g/L CA and 13.33 g/L PMA). The effect SHPP on shrinkage of fabric was shown in figure 4.
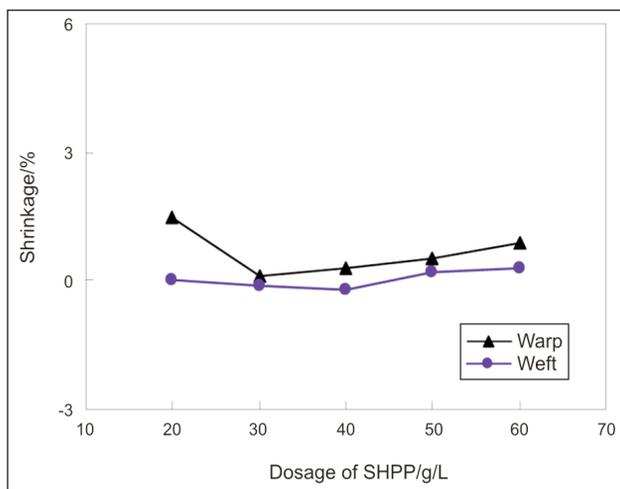
Fig. 4. Effect of dosage of SHPP on shrinkage of fabric
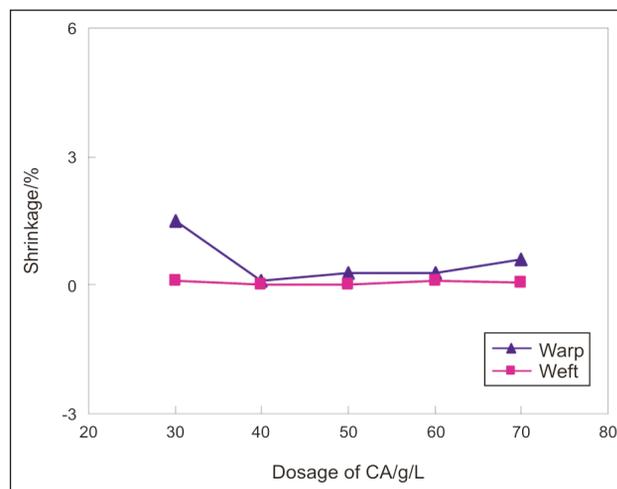
Fig. 5. Effect of dosages of CA on shrinkage of fabric

It can be seen in figure 4 that the weft shrinkage fluctuated around 0%, which expressed that the dosage of SHPP affected slightly on the weft shrinkage.

But the warp shrinkage of fabric changed obviously with the rise of dosage of SHPP, firstly decreased and then increased. Because more amounts of SHPP could accelerate crosslinking reaction between chemical agents and fiber's macromolecules, so the warp shrinkage decreased firstly. At 30 g/L of SHPP dosage, the warp shrinkage was smallest. But when dosage of SHPP exceeded 30 g/L, the warp shrinkage increased conversely. After the crosslinking reactions of finishing agents and fiber' macromolecules completely, it would cause hydrolysis of finishing agents and fibre's macromolecules. So the optimal dosage of SHPP was 30 g/L.

Effect of dosage of PMA and CA on properties of fabric

The ratio of PMA/CA was 1:3, and the dosage of SHPP was 30 g/L, and the dosage of PMA and CA was designed as listed in table 1. The effect of dosage of CA on shrinkage of fabric was shown in figure 5.

Figure 5 showed that with the rise of dosage of CA, the weft shrinkage had fluctuated around 0%, while the warp shrinkage declined firstly (the lowest value at 40 g/L), and then increased slowly. This mainly caused by a number of hydroxyl groups in silk/hemp fabric, which reacted with the chemical agents (e.g. PMA and CA). When the dosage of finishing agents was small (below 30 g/L CA), the hydroxyl groups could not reacted with finishing agents (PMA and CA) completely, hence the warp shrinkage was big. When the dosage of finishing agents was appropriate, these hydroxyl groups would thoroughly react with finishing agents, so the warp shrinkage was small. While, when the dosage of finishing agents were over high (e.g. 50–70 g/L CA), the finishing agents might accumulate on the surface of silk/hemp fabric, which impeded the pre-shrink processing of chemical finishing, then the warp shrinkage would increase again over 50 g/L.

Table 1

DOSAGES OF PMA AND CA	
Dosage of CA (g/L)	Dosage of PMA (g/L)
30	10
40	13.33
50	16.67
60	20
70	23.33

From the experimental results, it can be drawn that the optimal dosage of CA was at 40 g/L, and the dosage of PMA was at 13.33 g/L.

Optimum process and verification

According to the above analysis, the optimal parameters of physical and chemical finishing are as follows: 65°C immersion temperature; 60 min immersion time; 3:1 ratio of CA/PMA; 30 g/L SHPP; 40 g/L CA and 13.33 g/L PMA.

In order to verify the optimal process, the silk/hemp fabric was treated by physical and chemical finishing under these parameters. The qualities of treated silk/hemp fabric were given in table 2.

Table 2 showed that the warp shrinkage of fabric reduced significantly and the weft shrinkage went down slightly after shrink resistant finishing. It revealed that the optimal shrink resistant finishing was effective, especially for warp direction.

The strength of fabric declined after shrink resistant finishing. The strength of warp declined by a large margin, while the weft declined a little. It suggested that the shrink resistant finishing would lead to some damages on silk/hemp fabric, especially for the warp yarns.

The static drape coefficient of fabric showed in table 2 decreased a little after shrink resistant finishing, which can be the case that the fabric' structure become tighter after physical finishing (or pre-shrink finishing) and the cracks in fabric was filled by the

Table 2

QUALITIES OF TREATED SILK/HEMP FABRIC					
Qualities	Shrinkage (%)		Strength of fabric (cN)		Static drape coefficient (%)
	Warp	Weft	Warp	Weft	
Original fabric silk/hemp fabric	5.20±0.01	0.10±0.01	368.2±0.1	688.5±0.1	38±1
Silk/hemp fabric treated by optimum shrink resistant finishing	0.01±0.01	0.08±0.01	325.6±0.1	680.6±0.1	40±1

chemical agents after chemical finishing, so the fabric became stiff, then the draping of fabric got worse slightly.

Shrinking and shrink-resistant mechanisms of silk/hemp fabric

In this paper the reasons of shrinkage for silk/hemp fabric were also analyzed. There may be two reasons: one is that the silk warp yarn would shrink after
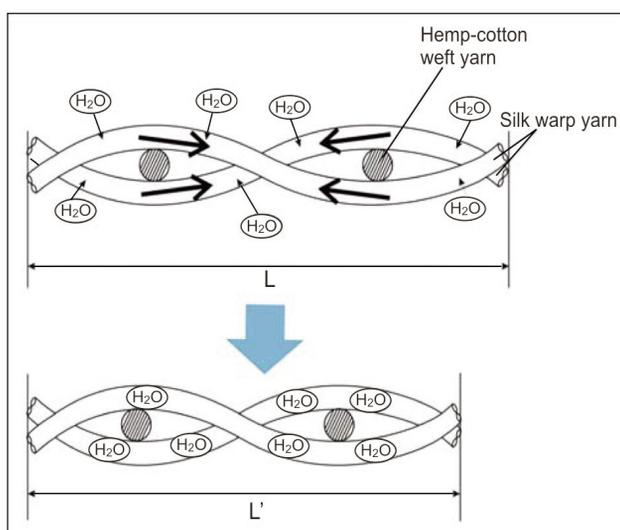
Fig. 6. Silk warp yarn would shrink after absorbing water
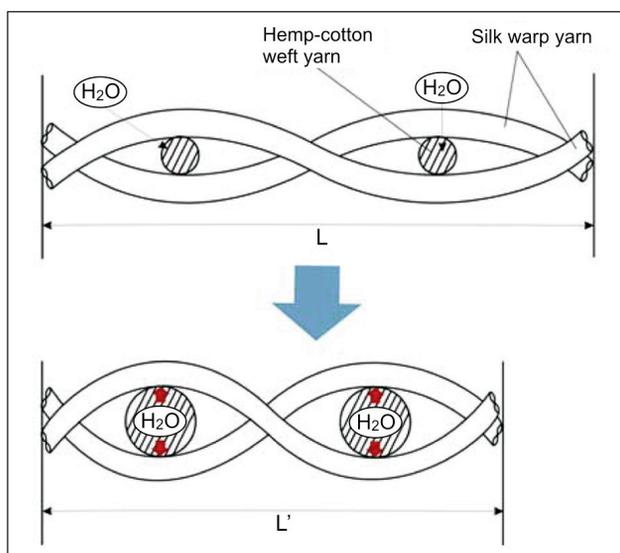
absorbing water. And the shrunk silk warp yarn couldn't recover completely after dried, so it caused the resistance of warp yarns. According to the test, the shrinkage of pure silk fabric was about 3%. The shrinkage caused by the silk warp yarn after absorbing water was illustrated in figure 6.

The other reason is that the hemp/cotton weft yarn would swell after absorbing water and its diameter increased. Thus, the silk warp yarn would be uplifted under stress of the swollen hemp/cotton weft yarn, so the length of fabric in warp-wise would shrink. The shrinking process was illustrated in figure 7.

For the two reasons, the shrinkage of fabric in warp-wise increased to about 5%.

Therefore, the physical finishing and chemical finishing were both applied to solve the problem of shrinking. In physical finishing, the fabric was pre-shrunk under the actions of water and heat. In chemical finishing, there were two processes to stop shrinking. One is the chemical agents reacted and linked with the fiber, then the yarns were coated with chemical finishing agents. Thus the water molecules were not easy to enter into the yarns and the fibers, therefore, the water absorption of yarn and fiber decreased as shown in figure 8.

The other process is that the chemical finishing agents formed a bond among silk fibers or yarns, and

Fig. 7. Hemp/cotton weft yarn would swell after absorbing water
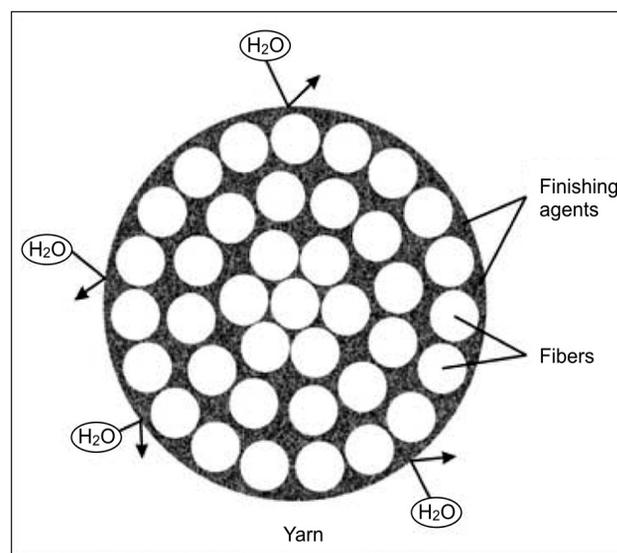
Fig. 8. The yarn and fibers were coated with the chemical finishing agents
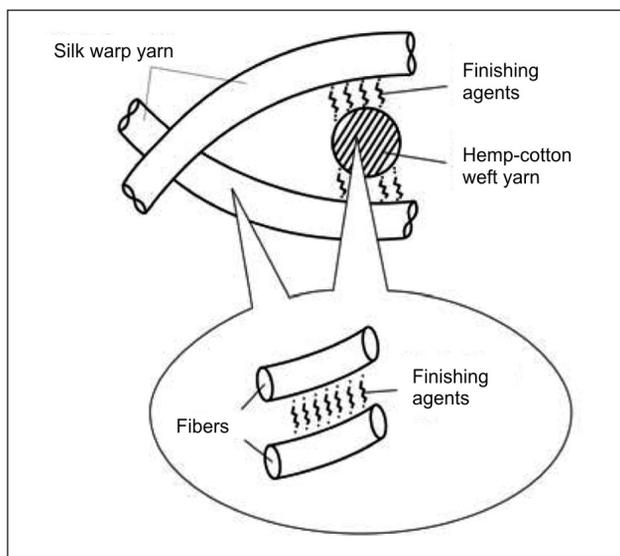
Fig. 9. The chemical finishing agents formed a bond among fibers or yarns

then the weft yarn and warp yarn couldn't slip with each other. So the dimension of fabric became stable as shown in figure 9.

As a whole, after processed by physical and chemical finishing, the shrinkage of silk/hemp fabrics was improved greatly.

CONCLUSION

The optimal processes of shrinkage resistance finishing for silk/hemp fabric can be divided into two steps. The first step, that is physical finishing, is to soak the general silk/hemp fabric into a water bath at 65°C for 60 min, and then dry it in an oven at 65°C for 5 min. The second step, that is chemical finishing, is to treat the fabric in chemical solution and squeeze twice, then dry it in an oven at 170°C for 3 min. Through the shrink resistant finishing, the fabric warp shrinkage reduced significantly, as the weft shrinkage changed slightly. Based on the experimental results, the optimal technical parameters, which were 3:1 ratio of CA/PMA, 40 g/L dosage of PMA and CA, and 30 g/L dosage of catalyst SHPP, were obtained. Further, the shrinking and shrinkage mechanism were also analysed. The internal and external of the fibres in the fabric had changed under chemical regents, so its shrinking percentage had been declined.

BIBLIOGRAPHY

[1] Binkowska, B., Sapieja, A., Marszalek, R., et al., *Protective properties against UV radiation of natural silk textiles.* In: Industria Textila, 2015, vol. 66, no 1, pp. 19–22.

[2] Xing, T.L., Li, X.Y., Guo, S.J., et al., *Preparation and properties of silk fabric grafted with-polylysine by tyrosinase.* In: Textile Research Journal, 2015, vol. 85, no 16, pp. 1743–1748.

[3] Mohsin, M., Ramzan, N., Ahmad, S.W., et al*., Development of environment friendly bio cross-linker finishing of silk fabric*, In: Journal of Natural Fibers, 2015, vol. 12, no. 3, pp. 276–282.

[4] Kan, C.W., Lam, Y.L.,*The effect of plasma treatment on water absorption properties of silk fabrics*, In: Fibers and Polymers, 2015, vol. 16, no. 8, pp. 1705–1714.

[5] Ma, M.B., You, L.X., Chen, L.C., et al., *Effects of ultrasonic laundering on the properties of silk fabrics,* In: Textile Research Journal, 2014, vol. 84, no. 20, pp. 2166–2174.

[6] Hwang, M.S., Ji, D.S., *The effects of yarn number and liquid ammonia treatment on the physical properties of hemp woven fabrics*, In: Fibers and Polymers, 2012, vol. 13, no. 10, pp. 1335–1340.

[7] Petrulyte, S., Velickiene, A., Petrulis, D., *Water vapour absorption of terry fabrics with linen and hemp pile loop,* In: Fibres & Textiles in Eastern Europe, 2013, vol. 21, no. 2, pp. 90–95.

[8] Misnon, M.I., Islam, M.M., Epaarachchi, J.A., et al., *Analyses of woven hemp fabric characteristics for composite reinforcement*, In: Materials & Design, 2015, vol. 66, pp. 82–92.

[9] Li, J., Feng, J.H., Zhang, H., et al., *Wear properties of hemp, ramie and linen fabrics after liquid ammonia/crosslinking treatment*, In: Fibres & Textiles in Eastern Europe, 2010, vol. 18, no. 5, pp. 81–85.

[10] Zhang, H., Zhang, L.M., *Structural changes of hemp fibres modified with chitosan and BTCA,* In: Industria Textila, 2010, vol. 61, no. 2, pp. 51–56.

[11] Jeong, A., Kimjongjun, *A study on physical properties of wool with shrink-resist treatment and felting*, In: Journal of Fashion Business, 2015, vol. 19, no. 2, pp. 23–35.

[12] Chakraborty, J.N., Madan, P.P.S., *Imparting anti-shrink functionality to wool by individual and simultaneous application of keratinase and papain*, In: Indian Journal of Fibre & Textile Research, 2014, vol. 39, no. 4, pp. 411–417.

[13] Nagashima, N., Tahara, M., Cho, S.M., et al*., Shrink resistance of pulse corona discharge/keratinase treated wool fabrics: relation between shrink resistance and strength*, In: Sen-i Gakkaishi, 2012, vol. 68, no. 8, pp. 225–228.

[14] Takagishi, T., Nagashima, N., *Eco-friendly textile processing: shrink proofing of wool*, In: Sen-i Gakkaishi, 2012, vol. 68, no. 9, pp. 256–260.

[15] Wang, P., Wang, Q., Fan, X.R., et al., *Effects of cutinase on the enzymatic shrink-resist finishing of wool fabrics,* In: Enzyme and Microbial Technology, 2009, vol. 44, no. 5, pp. 302–308.

[16] Eslahi, N., Moshggoo, S., Azar, S. K., et al., *Application of extracted feather protein to improve the shrink resistance of wool fabric,* In: Journal of Industrial Textiles, 2015, vol. 44, no 6, pp. 835–848.

[17] Gao, Y., Yu, X., Pierlot, A.P., et al., *A simultaneous antimicrobial and shrink resistance treatment of wool woven fabrics using the polymeric biocide polyhexamethylene biguanide*, In: Journal of Materials Science, 2011, vol. 46, no. 9, pp. 3020–3026.

[18] Jeon, D. W., Kim, J. J., *A study on the shrinkage of silk fabric by Ca(NO_3)_2 solution*, In: Journal of Fashion Business, 2009, vol. 13, no. 3, pp. 136–148.

[19] Lee, Y.W., *Studies on the shrinkage of silk yarn by neutral salts*, In: Korean Journal of Sericin Science, 1991, vol. 33, no. 2, pp. 87–92.

[20] 이난영, *A study on the development of new fabric design applying sericin finishing of silk-based on the shrinkage effect,* In: Journal of the Korean Society of Design Culture, 2009, vol. 15, no. 1, pp. 202–210.

[21] Yang, J.S., *A study on the shrinking of the silk treated with the natural chorangak liquid*, In: Journal of the Korean Society of Design Culture, 2008, vol. 14, no. 4, pp. 293–300.

[22] Siritientong, T., Srichana, T., Aramwit, P., *The effect of sterilization methods on the physical properties of silk sericin scaffolds*, In: AAPS Pharmscitech, 2011, vol. 12, no. 2, pp. 771–781.

[23] Wu, C.S., Liao, H.T., *Study on the preparation and characterization of biodegradable polylactide/multi-walled carbon nanotubes nanocomposites*, In: Polymer, 2007, vol. 48, pp. 4449–4458.

[24] Seligra, P.G., Nuevo, F., Lamanna. M., et al., *Covalent grafting of carbon nanotubes to PLA in order to improve compatibility*, In: Composites: Part B, 2013, vol. 46, pp. 61–68.

[25] Hashemikia, S., Montazer, M., *Sodium hypophosphite and nano TiO_2 inorganic catalysts along with citric acid on textile producing multi-functional properties Original Research Article*, In: Applied Catalysis A: General, 2012, vol. 417–418, pp. 200–208.

Authors:

SHU-QIANG LIU[1]
GAI-HONG WU[1,2]
YI CUI[1]
HONG-XIA GUO[1]

[1] College of Textile Engineering, Taiyuan University of Technology,
Taiyuan 030021, China;
[2] Fashion Institute of Design, Donghua University,
Shanghai, 200051, China

Corresponding author:

SHU-QIANG LIU
e-mail: liushuqiang8866@126.com

Model of thermal absorptivity of knitted rib in dry state and its experimental authentication

ASIF ELAHI MANGAT
LUBOS HES
VLADIMIR BAJZIK

FUNDA BUYUK
MUDASSAR ABBAS

REZUMAT – ABSTRACT

Modelul absorbției termice a tricotului patent în stare uscată și autentificarea experimentală a acestuia

Absorbția termică este un factor important pentru confortul corpului uman și, din acest motiv, au fost realizate probe utilizând fire de poliester 100% cu o greutate plană deosebită și o variație semnificativă în profilul de suprafață al tricoturilor patent. Absorbția termică a tuturor probelor a fost măsurată utilizând aparatul Alambeta. Absorbția termică este un indicator al senzației calde-rece în timpul interacțiunii dintre materialul textil și corpul uman. S-a constatat că există o corelație semnificativă între absorbția termică și profilul de suprafață al tricotului patent. Folosind analiza de regresie, a fost dezvoltată o ecuație pentru predicția absorbției termice a tricotului. Această ecuație este destul de utilă pentru designerii de îmbrăcăminte pentru a-i ajuta să producă o confecție care nu dă senzație de rece în timp ce aceasta este purtată într-un mediu rece.

Cuvinte-cheie: profil de suprafață, absorbție termică, senzație de rece, tricoturi patent, analiza de regresie, îmbrăcăminte

Model of thermal absorptivity of knitted rib in dry state and its experimental authentication

Thermal absorptivity is an important factor in comfort of human body, for this samples were produced using 100% polyester yarn with particular planar weight and significate variation in the surface profile of rib knit fabrics. Thermal absorptivity of all samples was measured using Alambeta. Thermal absorptivity is an indicator of warm-cool feeling during the interaction between the fabric and the human hand. It was found that there is a significant correlation between thermal absorptivity and surface profile of the knitted rib. Using regression analysis, we have developed an equation for the prediction of thermal absorptivity of the fabric. This equation is quite helpful for clothing designers to help them manufacture a fabric, which does not give cool feeling while wearing in a cold environment.

Keywords: surface profile, thermal absorptivity, cool feeling, rib knit fabrics, regression analysis, clothing

INTRODUCTION

Thermal absorptivity is a vital property of material fabrics and it is the subject of numerous studies as well. It relies on the thermal conductivity of fibers, density of fabric and specific heat of the material. Thermal absorptivity demonstrates the capacity of a material to give warm-cool feeling when a material is touched for a short time approximately for two seconds. Thermal conductivity is anisotropic in nature and generally relies on the structure of the material. Density of fabric depicts the mass per unit volume of a fabric. It indicates the ratio of solid and void area in the fabric. Fabric consists of polymers (filaments), air caught inside fabric and dampness in voids. Thermal absorptivity $Ws^{0.5}m^{-2}K^{-1}$ is linked with the thermal conductivity $[Wm^{-1}K^{-1}]$ and thermal capacity of fabric $[Jm^{-3}K^{-1}]$. Thermal capacity is a product of density $[Kgm^{-3}]$ and specific heat $[JKg^{-1}K^{-1}]$. Any change in the thermal conductivity and fabric thickness will change the thermal absorptivity of a fabric.

Prediction of changes in thermal absorptivity is quite useful because variety in surface profile is required while fabric is intended for apparels utilized as undergarments. Models ready to anticipate the thermal absorptivity are helpful for manufacturing clothing architecture of undergarments. The result of this study is a mathematical statement, which foresees thermal absorptivity of a fabric having different surface profiles. Undergarments are normally manufactured using cotton or comforting cotton combinations with other fabrics. On the other hand, polypropylene is additionally used to make undergarments including vests for players, which help in evaporating the sweat from skin to environment. It happens because of non-retentive nature of polypropylene. In this study, we have created specimen utilizing polyester.

This study is an effort to add to a model of thermal absorptivity of the fabric [1–5]. Thermal absorptivity (*b*) of fabrics was introduced by, which is an indicator of warm feeling (heat level) amid short contact with human skin with the fabric surface [6]. Given that the time of high temperature contact τ between the human skin and the material takes place for a few seconds, the measured fabric can be disentangled into semi-unbounded homogenous mass with certain warm limit represented by ρc $[Jm^{-3}]$ and starting temperature t_2. Unstable temperature field between the human skin (with steady temperature t_1) and fabric regarding of limit conditions offers a relationship,

which empowers to focus the heat stream q [Wm^{-2}] that passes through the fabric b Ws$^{0.5}$m^{-2}K^{-1} t [°C]

$$q = \frac{b(t_1 - t_2)}{\pi\tau^{0.5}} \qquad (1)$$

$$b = \lambda\rho c \qquad (2)$$

Where ρc (Jm^{-3}K^{-1}) represents the thermal capacity of the fabric and the term b represents thermal absorptivity Ws$^{0.5}$m^{-2}K$^{\varepsilon 1}$ of fabrics. The higher the thermal absorptivity of the fabric is, the cooler its inclination will be. In the material praxis, this parameter ranges from 20 Ws$^{0.5}$m^{-2}K^{-1} for fine nonwoven networks to 600 Ws$^{1/2}$m^{-2}K^{-1} for overwhelmingly wet fabrics. Thermal absorptivity is the objective measurement of the warm-cool feeling of fabrics. When a human touches a garment that has a different temperature than the skin, heat exchange occurs between the hand and the fabric. If the thermal absorptivity of clothing is high, it gives a cooler feeling at first contact [7]. In conventional manufacturing technology of cloth- development and technical progress in the field of engineering the industrial system, the body-clothing correspondence is often assessed in stores according to the stock products which remain. Unsold products do not reflect that they are obsolete or don't have the best quality in terms of accuracy of manufacturing technology, appropriate use of raw and auxiliary materials, but they were not purchased because they corresponded to the dimensional morphological requirements of the users [8].

THERMO-PHYSIOLOGICAL COMFORT

Work of Olaru, S., et al. is quite relevant to our study, they explained that warm-cool feeling is the first sensation [9]. They concluded that higher thermal absorptivity of clothing gives a cooler feeling during the initial contact with the human skin. They found that in both cotton and polyester fabrics, the interlock fabrics with highest thermal absorptivity values provide the coolest feeling at the beginning of skin contact due to specific construction of the fabric surface. The surface area between the fabric and skin is bigger for smooth fabric surfaces and these structures have a cooler feeling as mentioned. This study describes that the thermal absorptivity depends upon the surface profile of a fabric. Smooth surface provides maximum contact points and heat transfers between the skin and the fabric. More heat transfer means higher thermal absorptivity and more intense warm-cool feeling. Clothing comfort can be induced by thermal, pressure-related and tactile properties. Among these factors affecting clothing comfort, the thermal factor is the most decisive one affecting the comfort level. Thermal factors are often important in determining whether a given clothing ensemble is suitable for the use under specified condition have studied physiological impact of resin-treated fabrics including tencel and other cellulosic fibers [10–12]. They included thermal absorptivity as one of the important parameters of thermos-physiological comfort. Findings of Varga et al. show that the thermal absorptivity of a fabric is an indicator of the amount of heat taken away from the surface of the fabric per unit time. In case, if a fabric does not conduct heat away from its surface, it will have a warm feeling, which shows low thermal absorptivity. High thermal absorptivity values indicate cool feeling in the initial touch, which is not preferred for undergarments. Polypropylene is a commonly used, inexpensive synthetic polymer. PP fibres belong to the textile raw materials being frequently used. The surface of such monofilaments is really smooth, and this makes the modification procedure and the process control easier investigated the moisture management and thermal absorptivity properties of double-faced Knitted fabrics [13–14]. Rib is also a double knitted fabric. They observed that double faces are more effective for high Moisture transfer from skin to the environment, which makes garments made up of such fabric more functional And comfortable. For their study, they developed double knit fabrics. This fabric has different or same yarn Combinations in the front and back sides. Supuren et al. used distinctive types of yarn (cotton–cotton, cotton–polypropylene, polypropylene–cotton and polypropylene–polypropylene) for both sides of the fabric. Alambeta was used for characterization of maisture management properties and thermal absorptivity values. Their findings show that the polypropylene (cotton from inside and fabric from outside) fabric has better moisture management properties, which provides high levels of comfort and they should be preferred for summer and sportswear. Another parameter showing the comfort is warm–cool feeling. When the human touches a garment that has a different temperature than the skin, heat exchange occurs between the hand and the fabric, and the warm–cool feeling is the first sensation. Which feeling is better depends on the customer; for hot summer garments a cooler feeling is demanded, whereas in winter warmer feeling is preferred [3]. This supports our selection of polyester for developing of mode. It is important to note that polypropylene is quite sensitive to heat due to low melting point as compared to polyester. Polypropylene garments cannot be ironed to remove wrinkles due to its low melting point. It is one of the limitations of Polypropylene, which did not let it become popular for dresses.

EXPERIMENT AND RESULTS

Sample description

This study took into account knitted rib fabrics in order to verify the above mentioned thermal absorptivity model. A weft-knitted rib fabric is highly dense in nature. 14 kinds of samples were produced on Flat knitted machine 12 gauge all samples were produced with same yarn 100 % polyester but keeping the thickness same and 50 yarn count was used for the production of the samples only surface area is changed from sample to sample, see table 1.
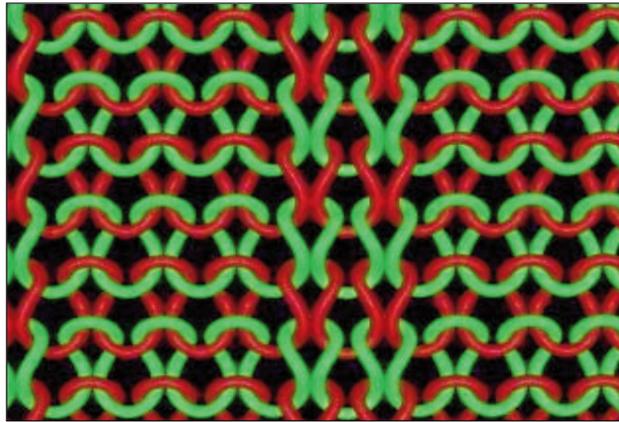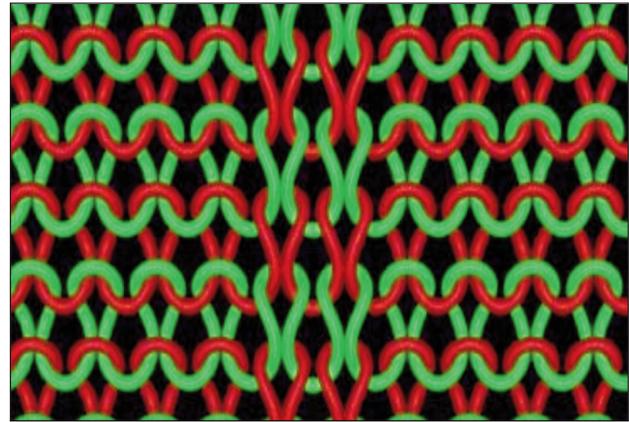
Fig. 1. Geometrical shapes of samples: *a* – 3x2 rib type; *b* – 4x4 rib type

Table 1

Sample no.	Rib types	Planar weight (gm²)	Thickness (h) (mm)	Porosity [1]
1	1.1	481	1.91	0.818
2	1.2	400	2.00	0.855
3	2.1	541	1.96	0.800
4	2.2	560	2.00	0.797
5	2.3	462	2.05	0.837
6	3.1	523	2.05	0.815
7	3.3	477	2.06	0.833
8	3.4	471	2.02	0.831
9	4.1	485	1.98	0.823
10	4.2	548	2.26	0.824
11	4.3	540	2.06	0.810
12	4.4	540	2.23	0.825
13	1.1	378	1.99	0.862
14	2.1	422	2.01	0.848
15	3.1	447	1.98	0.836
16	4.1	474	1.92	0.821
17	5.1	501	2.01	0.819
18	6.1	470	2.11	0.839

Some of the samples geometrical were developed with the help of software to get a more detailed idea of samples and there surface profile, in figure 1 it is clear from (a) rib type 3x2 is used and if increase in the number of ribs the surface area will also be changed. Elongation at break (similarly maximum force to rupture) demonstrates fabrics knitted in tuck-rib stitch patterns. Elongation at break of tuck-rib stitch fabrics Knitted in a basis of 1×1 and 1×1×1×2 rib is the same in course and wale direction. And elongation at breaking course direction of tuck-rib stitch fabrics knitted basis of 2×2 rib is about twice greater than in wale direction [15].

Testing procedure

The determination of thermal absorptivity of the fabric in a dry condition requires the use of a special testing instrument that enables a researcher to record a measurement quickly. One of the unique instruments, through which, the full signal is achieved within less than three minutes is Alambeta (Sensora Czech Republic). The Alambeta is a computer-controlled, semiautomatic, nondestructive thermal tester for testing textile fabrics. The biggest advantage of the Alambeta testing is that the instrument immediately displays the thermal absorptivity levels of the tested fabrics. The Alambeta has been used in various other studies as well. Selection of Alambeta is based on its effectiveness, efficiency and scope in many studies [6, 16, 17].

Samples were kept in a testing lab in the open air of the lab, where the temperature was maintained between 20°C and 22°C, and the relative humidity was between 24% and 25%. This was all done to minimize the impact of moisture in the knitted rib fabric. Each sample were measured were tested 5 times to get the better reading and all samples were fall on the same values.

Humans are sensitive to humidity because the human body uses evaporative cooling, enabled by perspiration, as the primary mechanism to rid itself of waste heat. Perspiration evaporates from the skin more slowly under humid conditions than under arid conditions. Because humans perceive a low rate of heat transfer from the body to be equivalent to a higher air temperature, the body experiences greater distress of waste heat burden at high humidity than at lower humidity, given equal temperatures.

The air temperature is 24°C (75°F) and the relative humidity is zero percent, then the air temperature feels like 21°C (69°F). If the relative humidity is 100 percent at the same air temperature, then it feels like 27°C (80°F). In other words, if the air is 24°C (75°F) and contains saturated water vapour, then the human body cools itself at the same rate as it would if it were 27°C (80°F) and dry. The heat index and the humidex are indices that reflect the combined effect of temperature and humidity on the cooling effect of the atmosphere on the human body.

Porosity calculation

In this study, volumetric approach proposed by Militky and Havrdova has been used to measure the porosity, as shown in equation 3

$$P_{HW} = 1 - \frac{\upsilon_y}{\upsilon_V} \qquad (3)$$

Where P_{HW} [1] represents the porosity based on volumetric density, υ_y shows the volume covered by fiber, and υ_V depicts the whole accessible volume. Following prediction equation has been developed for the prediction of contact thermal absorptivity of rib knit fabrics.

$$b = b_p \, A \, (1 - P_{HW}) \qquad (4)$$

where b represents the thermal absorptivity [Ws$^{0.5}$m^{-2}K^{-1}] of fabric and b_p is thermal absorptivity of polyester in solid form, P_{HW} shows porosity [1], and A is contact area [1] between human skin and surface of fabric. Porosity and contact area both are unit less values. In this approach, value of thermal absorptivity of polyester was calculated using standard values of thermal conductivity, density and specific heat capacity values of polyester in solid form and putting in equation 2 and then the calculated value of thermal absorptivity of polyester in solid form is multiplied with the porosity and contact area of knitted rib to find thermal absorptivity of rib knit fabrics. This is a novel approach, which proves that using this method, thermal absorptivity of any material can be predicted. The porosity of samples used in this study is high due its structure and knit structure has many air gaps due to insertion of loop and they can be well seen in the following images taken from microscope while measuring the contact area.

RESULTS AND DISCUSSION

This study aims to develop an equation for the prediction of thermal absorptivity using contact area. As discussed in the previous pages, thermal absorptivity is a function of thermal conductivity and thermal capacity of a fabric. Thermal capacity is a product of density and specific heat of a material. We used SPSS software to find the regression analysis. We calculated contact area with the help of a microscope, which was fitted inside the camera. For measuring contact area, images of the samples have been used. These images were taken using electronic microscopes and then images were analyzed. As it is clear from figure 1, knitted rib has two types of surface. Elevated portion touches the hand when hand is put on the fabric surface. Using these images, elevated area and non-elevated area have been measured, which gave the percentage of contact area of rib when it is touched with any human hand or any plate we measured distance between the two wales (grooves) and thickness of the top of the fins (table 2).

Correlation between contact area and thermal absorptivity

Table 3 shows correlation between contact area and thermal absorptivity. Significance of this correlation is 0.01, which is quite less than 0.05. It proves that there is a significant correlation between contact area and thermal absorptivity. This test supports our findings that contact area of knitted rib is highly influential on thermal absorptivity.

Linear regression model

We applied linear regression model technique to have an equation for the prediction of thermal absorptivity. Figure 2 shows that there is a significant correlation between thermal absorptivity and

Table 2

Sample no.	Rib type	Height (mm)	Thickness of fins (a) (mm)	Distance between adjacent wales (grooves) (mm)	Contact area fraction	Contact (%)
1	1x2	2	1.8	2.15	0.46	45.57
2	2x3	2.05	3.4	3.3	0.51	50.75
3	2x1	2	3.3	3	0.52	52.38
4	3x4	2.02	5.15	4.33	0.54	54.32
5	1x1	2.13	2.45	2	0.55	55.06
6	2x2	2	3.4	2.4	0.59	58.62
7	1x1	2	1.47	1	0.6	59.51
8	3x3	2.06	4.9	3.14	0.61	60.95
9	4x4	2.15	6.2	3.3	0.65	65.26
10	2x1	1.96	3.16	1.26	0.71	71.49
11	4x3	2.06	6.3	2	0.76	75.9
12	4x2	2.11	6	1.6	0.79	78.95
13	3x1	2.05	4.7	1.1	0.81	81.03
14	4x1	1.98	5.8	0.7	0.89	89.23

		Contact area (%)	Predicted thermal absorptivity
Contact area (%)	Pearson correlation	1	1.000**
	Sig. (2-tailed)		.000
	N	18	18
Predicted thermal absorptivity	Pearson correlation	1.000**	1
	Sig. (2-tailed)	.000	
	N	18	18

Table 3

** Correlation is significant at the 0.01 level (2-tailed)

Fig. 2. Thermal absortivity measured

contact area of the knitted rib. It is obvious from the R^2 values (0.96). It shows that 96.9% changes in thermal absorptivity take place due to changes in the contact area.

We applied regression analysis and found that the model developed is significant. Table 3 shows that un-adjusted R square value is 0.870 which shows that 87 % of data is well explained by the graph and the readings which were measured on ALAMBETA are correlating with each other, which is too high and its p-value is 0.000, which is quite less than 0.05 at 95% confidence level.

We can write an equation based on the coefficient (table 4) in the following way:

$$y = -9.34 + 2.31b \qquad (5)$$

Here y shows the thermal absorptivity while b represents contact area (%). We have compared measured
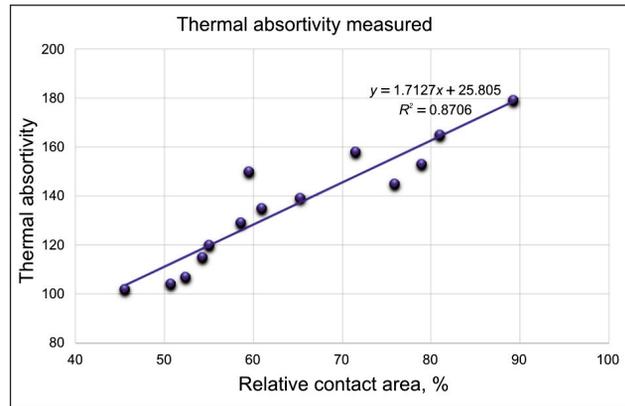
and predicted values of thermal absorptivity. Table 4, table 5, and table 6 show that their correlation is 0.984 while their p value is 0.836. As p value is greater than 0.05, it shows that there is no significant difference between the two sets of values.

CONCLUSIONS

The suggested model has been used to predict thermal absorptivity values of knitted rib fabric model using 100% polyester and exploiting structure of knitted rib fabric. For development of knitted rib fabric, double-knit rib knitting machine has been used. Samples were kept under standard conditions and they were tested using Alambeta. Thermal absorptivity was measured by changing the surface area and

Table 4

Model		Unstandardized coefficients		Standardized coefficients	t	Sig.
		B	Std. Error	Beta		
1	(Constant)	−9.341	6.715		−1.391	.183
	Contact area (%)	2.307	.103	.984	22.350	.000

Table 5

		Mean	N	Std. deviation	Std. error mean
Pair 1	Measured thermal absorptivity	138.9444	14	24.12095	5.68536
	Predicted thermal absorptivity	139.1556	14	23.77817	5.60457

Table 6

		N	Correlation	Sig.
Pair 1	Measured thermal absorptivity & predicted thermal absorptivity	14	.984	.000

Table 7

		Paired differences					t	df	Sig. (2-tailed)
		Mean	Std. deviation	Std. error mean	95% confidence interval of the difference				
					Lower	Upper			
Pair 1	Measured thermal absorptivity − predicted thermal absorptivity	−.2111	4.24856	1.00139	−2.32387	1.90165	−.211	17	.836

hence it has showed a significant result that as the contact area is increasing the thermal absorptivity value is also increasing suggested models can be used for prediction of thermal absorptivity of any material having distinct surface Their thermal absorptivity was measured and finally, the measured values were compared with model values. The results show that there is a substantial agreement between experimental and calculated values. The study shows that this model can be used for the prediction of thermal absorptivity of the studied fabrics. Considering this study and keeping in view the application of this model for the knitted rib manufactured by using 100% polyester can be used for other types of fabrics as well, However this study was only done on same yarn but changing surface area from 45–89 % check the graph again which gives manufacturer a clear idea which contact area is better for both wearer and comfort.

BIBLIOGRAPHY

[1] Crow, R.M. *Heat and moisture transfer in clothing systems,* In: *Part 1. Transfer through materials, A literature review.* 1974, DTIC Document.

[2] Hes, L. and Loghin, C. *Heat, moisture and air transfer properties of selected woven fabrics in wet state.* In: Journal of Fiber Bioengineering and Informatics, 2009, 2(3), pp. 141–149.

[3] Özdil, N., Marmaralı, A., Kretzschmar, S.D. *Effect of yarn properties on thermal comfort of knitted fabrics.* In: International Journal of Thermal Sciences, 2007, 46(12): pp. 1318–1322.

[4] Yamashita, Y., Yamada, H., Miyake, H. *Effective thermal conductivity of plain weave fabric and its composite material made from high strength fibers,* In: Journal of Textile Engineering, 2008, 54(4), pp. 111–119.

[5] Zhu, F., Zhang, W., Song, G. *Thermal performance assessment of heat resistant fabrics based on a new thermal wave model of skin heat transfer,* In: International Journal of Occupational Safety and Ergonomics, 2006, 12(1), pp. 43–51.

[6] Hes, L., *Non-destructive determination of comfort parameters during marketing of functional garments and clothing,* In: Indian J. Fibre Text. Res, 2008, 33(3), pp. 239–245.

[7] Pac, M.J., et al. *Warm-cool feeling relative to tribological properties of fabrics,* In: Textile Research Journal, 2001, 71(9), pp. 806–812.

[8] Olaru, S., et al. *Morphological assessment of human body for clothing patterns design,* In: DE REDACTIE, 2013, 1, p. 254.

[9] Oğlakcioğlu, N., Marmarali, A. *Thermal comfort properties of some knitted structures,* In: Fibres & Textiles in Eastern Europe, 2007, 15(5-6), pp. 64–65.

[10] Raja, D., et al. *A study on thermal properties of single-jersey knitted fabrics produced from ring and compact folded yarns,* In: The Journal of the Textile Institute, 2015, 106(4), pp. 359–365.

[11] Varga, K., et al. *Physiological investigation of resin-treated fabrics from TENCEL® and other cellulosic fibres,* 2008.

[12] Varga, K., et al. *Physiological investigation of resin-treated fabrics from TENCEL® and other cellulosic fibres,* 2009.

[13] Stawski, D., et al. *Application of the layer-by-layer technique for knitted fabrics/Aplicarea tehnologiei de depunere strat cu strat pe materiale textile tricotate,* In: Industria Textila, 2014, 65(4), p. 190.

[14] Süpüren, G., et al. *Moisture management and thermal absorptivity properties of double-face knitted fabrics,* In: Textile Research Journal, 2011: p. 0040517511402122.

[15] Mikučionienė, D., Čiukas, R., Mickevičienė, A. *The influence of knitting structure on mechanical properties of weft knitted fabric,* In: Mater Sci, 2010, 16(3), pp. 221–225.

[16] Karaca, E., et al. *Effects of fiber cross sectional shape and weave pattern on thermal comfort properties of polyester woven fabrics,* In: Fibres & Textiles in Eastern Europe, 2012.

[17] Schacher, L., Adolphe, D., Drean, J.-Y. *Comparison between thermal insulation and thermal properties of classical and microfibres polyester fabrics,* In: International Journal of Clothing Science and Technology, 2000, 12(2), pp. 84–95.

Authors:

ASIF ELAHI MANGAT[1]
LUBOS HES[1]
VLADIMIR BAJZIKH[1]
FUNDA BUYUK[2]
MUDASSAR ABBAS[3]

[1] Technical University of Liberec, Faculty of Textile Engineering, Department of Textile Evaluation

[2] Technical University of Liberec, Faculty of Textile Clothing

Studentska 2, Liberec, 461 17, Czech Republic

[3] School of Textile and Design, University of Management and Technology, Lahore, Pakistan

Corresponding author:

ASIF MANGAT
e-mail: asifmangat@gmail.com

Absorption and moisture transfer through knitted fabrics made of natural and man-made fibers

DANIELA NEGRU
LILIANA BUHU
EMIL LOGHIN

IONUT DULGHERIU
ADRIAN BUHU

REZUMAT – ABSTRACT

Absorbția și transferul de umiditate prin materiale tricotate din fibre naturale și artificiale

Această lucrare prezintă cercetări legate de evaluarea caracteristicilor care influențează confortul produselor de îmbrăcăminte, și anume: hidrofilia, indicele de vaporizare, higroscopicitatea și porozitatea, în funcție de natura materiei prime (bumbac, măstase artificială și PES) pentru diverse structuri textile tricotate. Tricoturile au fost fabricate din fire de bumbac și diferite amestecuri cu o finețe de Nm54/1. Matricea experimentală a luat în considerare următoarele variabile de intrare: structura tricotului și compoziția firului. În ceea ce privește comportamentul în mediul umed al grupurilor de materiale tricotate, cercetarea experimentală are drept rezultat posibilitatea unei analize complexe asupra hidrofiliei, higroscopicității, permeabilității și porozității la vapori. Deoarece confortul fiziologic depinde de toți parametrii analizați, rezultatele conduc la concluzia că toate structurile tricotate analizate și diversele amestecuri utilizate sunt optime pentru articolele de îmbrăcăminte care oferă confort utilizatorului.

Cuvinte-cheie: hidrofilicitate, permeabilitate la vapori, higroscopicitate, porozitate, materiale tricotate

Absorption and moisture transfer through knitted fabrics made of natural and man-made fibers

This paper presents researches related to the assessment of the characteristics that influence the comfort of clothing products, namely: hydrophilicity, vaporization index, hygroscopicity and porosity, depending on the nature of the raw material (cotton, rayon and PES) for various knitted textile structures. The knitted fabrics were made using cotton yarns and various blends with fineness Nm54/1. The experimental matrix took into consideration the following input variables: fabric structure and yarn composition. With regard to the behaviour in the humid environment of groups of knitted fabrics, experimental research results in the possibility of a complex analysis on hydrophilicity, hygroscopicity and vapor permeability and the porosity. Since the physiological comfort depends on all the parameters that were analyzed, the results lead to conclusion that all knitted structures under discussion and various blends used are optimal for garments that provide comfort to wearer.

Keywords: hydrophilicity, vapour permeability, hygroscopicity, porosity, knitted fabrics

INTRODUCTION

The main focus resulting from this research is the possibility of establishing the scientific role and effect of clothing during physiological processes of the human body and therefore the possibility to substantiate trough standardized parameters the garment production according to its destination. The complexity of this problem is due to necessity to orientate the production of clothing, in order to satisfy physiological demands, given the fact that the content of man-made fibres in the structure of modern clothing has increased considerably.

The textiles fabrics have affinity to moisture when an amount of fluid (i.e. water) is in contact with it. The phenomenon of water penetration inside the fiber is known as absorption, and the adhesion of the liquid to the fiber surface is called adsorption. It is necessary to take into account that both the moisture of materials, as well as their behaviour in the humid environment will depend on the nature of the polymer, the energy of intermolecular ties, as well as their crystallinity. The moisture resulting from perspiration cause heat release and entropy decrease depending

on the nature of the fiber [1–2]. Also the porosity of the materials, which represent the percentage of pores in the material, characterizes the volumetric storage capacity of a fluid in a particular environment [3].

Porosity affects obviously both the absorption and desorption of materials and with their voluminosity increase grows both the vapour permeability and permeability to air. A large volume of air represent a high volume of pores, so an additional condition for the maintenance and transport of moisture, favoring at the same time faster drying of skin when intense sweating [2, 4]. Otherwise the feeling of discomfort appears, accompanied by intense cooling of the surface of the skin, the sticking of wet first layer of clothing and the transport of a larger amount of heat from the surface of the skin and thus increasing the overall coefficient of heat transfer, which is dependent directly to the equivalent thermal conductivity coefficient [5].

The presence of water or ice in the pores of the material leads to a decrease in thermal insulation, i.e. thermal resistance, since the coefficient of thermal

conductivity increases considerably. And specific heat, which means the capacity of the material to absorb heat when the temperature increases, is directly influenced by the moisture content of the material [6–9]. Although behaviour in the humid environment is dependent on the structure of the material, structure of the yarn and nature of fibers, from the physical point of view it is treated under the following aspects: vapour permeability, hydrophilicity, hygroscopicity, reaction to sweating [10]. Although these characteristics cannot be separated from the physical properties of the material, they are treated in connection with the human body, in terms of creating the emissions balance results in different conditions, in this case the activity of the sweat glands.

Taking into account that as a result of sweating removes toxins, unpleasant odors and carbon dioxide, throughout the clothing in contact with these surfaces should be placed textile surfaces that influence skin flora, spaces created having an important role in this respect and to be hydrophilic, hygroscopic and allow a good passage of vapour.

The sweat glands, with a density of about 120 glands/cm^2 (total unfolded surface of the skin to a healthy adult ranges between 1.5 and 1.7 m^2), have the capacity to cool the body by evaporation, and clothes should be chosen so that it can take not only the heat produced at the surface of the body, but also the amount of moisture released by the skin in case of various daily activities. In choosing the materials for the realization of a clothing product, must be taken into account that in case of an insensible breath a quantity of humidity of about 400 ml per 24 hours is removed through the skin, and in the case of a active secretion determined of hard work, the amount of moisture may increase between 3.5 and 5 liter/24 hours.

The amount of moisture eliminated from the body in certain circumstances, can be correlated with the distribution of sweat glands on the surface thereof. Considering that number of sweat glands is around 120 per cm^2, the total number could reach 1.92 million if consider the average area of the body 1.6 m^2. It is also important to know the reactions occurring at the contact between the moistened skin covered or uncovered and different products that are used in auxiliary finishing textile chemical processes.

Researchers in the field of clothing physiology have come to the conclusion that maintaining health status is dependent on the possibility of keeping the area of the body dried. It was established that in the utmost comfort for clothing, depends on its capacity to carry fast perspiration by eliminating the moisture between body and clothing. It is necessary therefore to consider not only the loading with moisture, but also the drying speed, or the time in which the humidity accumulated will be ceded. Up to certain effort limits can be established a strong link between the above values and the possibility of taking the moisture given off by the body through clothing structure, taking into account that both wettability index and vaporization index varies between 0 and 50 g/m^2h.

The characteristics associated with the reaction in the humid environment cannot be analyzed separately from the influence of the comfort features that constitute a summary of the physical properties of textile materials (thermal conductivity, hygroscopicity, hydrophilicity, adsorption-desorption diagrams, reaction to sweating, air permeability etc.). Comfort is influenced by the draping, the crease and dimensional stability of textile materials into final products. In addition, all these features are conditioned by a series of structural factors that generate a complex structure parameter which is porosity and by chemical treatment of textile surfaces [11]. Differences from textile surfaces also arise if knitted, woven or obtained through unconventional technologies [12].

EXPERIMENTAL WORK

The yarns used as raw materials for the knitted samples were 100% cotton and different blends with PES and rayon. These yarns were chosen because they are most used for garments coming in contact with the skin, including for the cold season. Several variants of knitted fabrics were made, the categories of yarns used and the knitting patterns being summarized in table 1.

The warp knitted fabric was produced on a double bar warp knitting machine. The interlock 2 and 3 samples have similar stitch density, while sample interlock 1 has a higher stitch density.

Vapour permeability is the property of materials to let through water vapor in environments with high relative humidity in lower relative humidity environments, due to their porous capillary for the textiles. Due to this characteristic, it is possible to remove, by material or garment, moisture from the body surface, especially to its condensed phase. The sample of material is fixed on the top of a container (Herfeld type glass). The container holds 50 cm^3 of distilled water, and analyzed assembly is placed in an environment with low relative humidity (recommendation is near to 0%). Due to the difference in partial pressure, the vapor formed in the space between the water surface and the material will diffuse through the material to the outside.

The value of vapor permeability is obtained by calculating the weight differences of the analyzed ansembly (1):

$$P_v = M_i - M_f, \text{ (g)} \qquad (1)$$

where:
M_i is the initial mass of the analyzed ansembly (g);
M_f – the final mass of the analyzed ansembly maintened a specific period of time "τ" in an environment with $\varphi = 0\%$, (g).

The vaporisation index is calculated with the formula (2):

$$\mu = \frac{P_v}{S_v \cdot \tau} , \left(\frac{g}{m^2 h}\right) \qquad (2)$$

Table 1

Fabric	Sectional wale representation of knitted fabric	Fibrous composition	Mass (g/m²)
interlock 1		67 % cotton / 33 % rayon	195
interlock 2	Ri	100 % cotton	140
interlock 3		50 % polyester / 50 % rayon	150
single jersey with miss stitches	R3 R2 R1 1/1' 2/2' 3/3' 4/4'	75 % cotton / 25 % polyester	190
single jersey with cross miss	IV III II I 1 2 3 4	100 % cotton	135
single jersey with miss stitches	IV III II I 1 2 3 4	100 % cotton	100
single jersey	R3 R2 R1 1 2 3 4	100 % cotton	120
warp knitted fabric	-	78 % cotton / 22 % polyamide	250
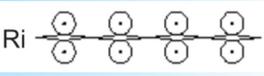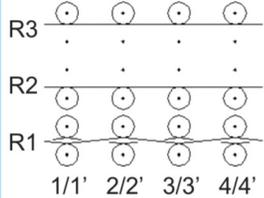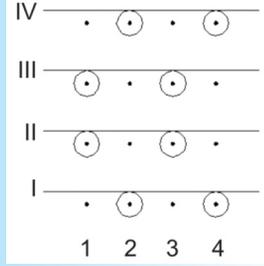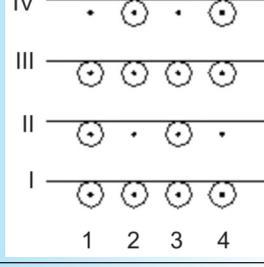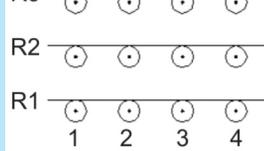
where:

P_v is vapour permeability of the material [g];

S_v – the surface of the glass covered with the textile material [m²];

τ – the time of exposure to a environment with 0% relative humidity [h].

Hydrophilicity is a body's ability to absorb water. The textile material generally has a porous surface which has a high content of air, which in the process of wetting is removed from the micro or macro capillaries by the water. Hydrophilicity was determined by a method based on the principle of capillarity, knowing that the fabrics can be treated with systems more or less homogeneous capillaries. The method consists in following the rise of the water in the sample of textile material partially immersed in the water. Water penetrates through the pores within the structure of the fiber, yarn and textile surface analyzed respectively. For testing it used a stand which consists of a container with distilled water and a sample suspension device. For each sample there is a graduated scale for reading the height of rising water level, measured from its container level. The samples are cut to the length of 280 ± 2 mm and a width of 30 ± 1 mm, four in each direction of knitting fabric (wale and course). The test samples were originally conditioned. The samples are immersed in water at least 20 mm. The water rise in samples and the reading of the height of ascent value of 10 to 10 minutes up to 30 minutes represent the value of hydrophilicity.

The materials used in the production of clothing must be hygroscopic. Material's ability to absorb or to yield or to withhold water vapor is called **hygroscopicity.** To ensure hygienic conditions and thermo-physiological comfort to worn clothing, textiles (mainly those for the first layer) must have a minimum moisture content of 6%, in standard atmospheric conditions. The samples with the sizes of 10×10 cm², preconditioned, remain a time (τ) in a tightly closed humid environment (exicator). To analyze the influence of

the duration of time in wet environment, the samples are conditioned prior to $\Phi = 65\%$ relative humidity, and then maintained at relative humidity of $\Phi = 100\%$ weighed at time intervals of 30 minutes. The value of higroscopicity can be calculated as a relative indicator which indicates the proportion of the mass of vapor absorbed (yielded or retained) in the total mass of the sample (3):

$$H = \frac{M_1 - M_2}{M_2} \cdot 100, \ (\%) \tag{3}$$

Where:
M_1 is the mass of the conditioning sample [g];
M_2 – the mass of the sample mantained in an environment with a specific relative humidity [g].
Since the hygroscopicity of materials is dependent on the surface exposed to the environment, and also the duration of maintaining in the environment, it can be appreciated by an indicator that reports the amount of vapor (mass difference) per unit area and per unit time, which is the absolute indicator of wettability (4), i_H [g/m²h]:

$$i_H = \frac{M_1 - M_2}{S} \cdot t, \ (\text{g/m}^2\text{h}) \tag{4}$$

where:
S is the surface of the sample [m²];
t – the time while the sample is mainained in moist environment [h].

The porosity can be defined as the ratio between the mass of air contained in the fabric under some pressure and mass of material without air. The porosity is a very important feature of comfort that is part of the physiological properties of clothing, depending on the raw material fiber composition, the value of twist, the fineness of the yarns and the knitt pattern and also the chemical treatments of textile surfaces. The porosity is determined using the picnometric method and is calculated with the formula (5):

$$Pz = \frac{\gamma_r - \gamma_a}{\gamma_r} \cdot 100, \ (\%) \tag{5}$$

where:
γ_r is relative density of the textile material [g/cm³];

γ_a – the apparent density of the textile material [g/cm³].
The apparent density of textile material is determined with the formula:

$$\gamma_a = \frac{M}{1000 \cdot \delta}, \ (\text{g/cm}^2) \tag{6}$$

where:
M is mass per unit area [g/cm²];
δ – the thickness of the material [mm].
The relative density of textile material is determined with the formula:

$$\gamma_r = \frac{M_s \cdot \gamma_l}{M_2 - M_1}, \ (\text{g/cm}^2) \tag{7}$$

where:
M_s is the mass of the sample [g];
γ_l – the density of toluene 0,871 [g/cm³];
M_1 – the mass of the picnometer with toluene [g];
M_2 – the mass of the picnometer with toluene plus the sample [g].

RESULTS AND DISCUSSIONS

The paper develops the theoretical aspects of some important parameters characterizing the behaviour in the humid environment and experimental research on several groups of knits, highlights achievements that have allowed some interpretations, marked by the limits shown in graphs, histograms and related tables.
In order to highlight how the fiber composition and structure changes over time, values for recorded parameters (hydrophilicity, vaporization index, hygroscopicity and hygroscopicity index) were summarized in table 2, which correspond to eight types of knitted fabrics made from yarn with fineness Nm 54/1. Because these features depend on porosity, this parameter was also established.
The experimental matrix took into consideration the following input variables: fabric structure and yarn composition.
Experimental results regarding the hydrophilicity refer to the same group of materials as in the case of vapour permeability and are contained in table 2, and

Table 2

Fabric	Hydrophilicity h [cm]						Vaporization index μ [g/m²h]	Hygroscopicity		Porosity Pz [%]
	Wale [min]			Course [min]				H [%]	I$_H$ [g/m²h]	
	10	20	30	10	20	30				
interlock 1	8.2	10.6	12.6	7.9	9.6	19.2	20.77	8.4	0.764	73.48
interlock 2	5.7	6.6	7.65	4.0	5	5.25	8.02	6.7	0.289	80.04
interlock 3	7.5	9	12.25	4.5	7	8.75	8.78	6.3	0.227	69.47
interlock with miss stitches	6	7	7.45	6.8	7.9	8.4	19.36	5.4	0.324	80.12
single jersey with cross miss	5.8	7.3	8.4	5.3	6.9	8.1	5.57	7.3	0.236	78.85
single jersey with miss stitches	4.8	5.7	6.6	4	4.5	5.85	6.63	8.7	0.24	81.37
single jersey	5	5.5	5.96	3	3.1	3.35	11.29	12	0.122	75.55
warp knitted fabric	6.2	8.4	9.15	4.8	6.3	7.9	8.41	6.8	0.464	81.41
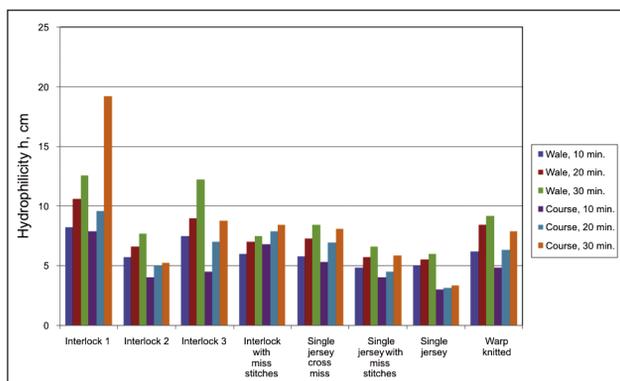
Fig. 1. Hydrophilicity histogram
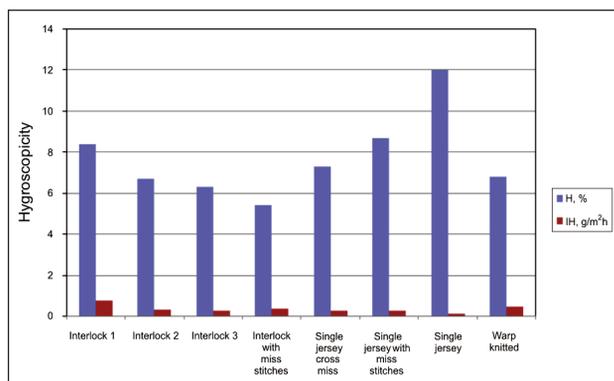
Fig. 3. Hygroscopicity histogram
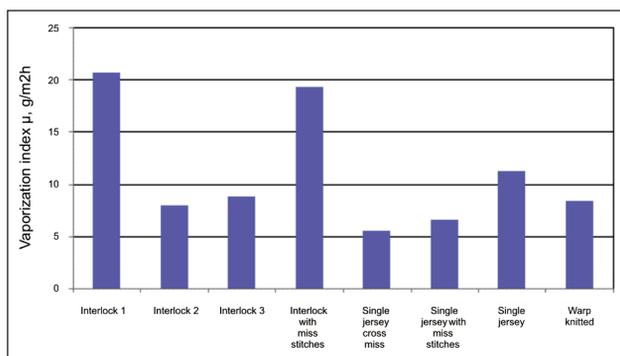
Fig. 2. Index of vaporization
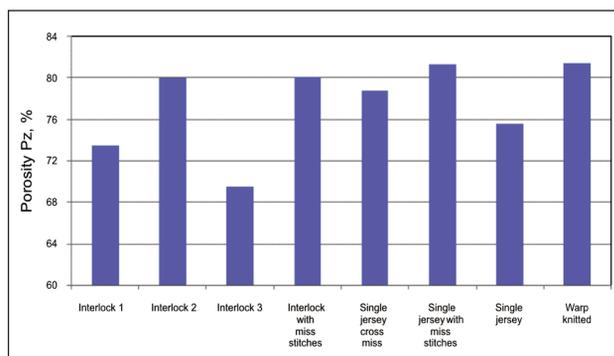
Fig. 4. Porosity histogram

the histogram in figure 1. Hydrophilicity has close values on the two sides, which is a slight increase in the sense of knitting, i.e. the wale direction.

The values given in table 2 and the histogram in figure 2 show how the more fibrous composition can result in increased vaporization index.

Experimental results regarding the hygroscopicity and hygroscopicity index are presented in table 2, the elements of comparison resulting also from the histogram shown in figure 3, which highlights the limits on hygroscopicity of cotton materials or cotton type.

Discussions relating to the vapour permeability, hydrophilicity and hygroscopicity are associated with porosity (table 1). The histogram in figure 4 allows comparative analyses between the knitted structures considered.

The minimum value of hydrophilicity (3 cm) was obtained for a single jersey knit from 100% cotton yarn. The maximum value (19.2 cm) was obtained for an interlock knit pattern from 67% cotton and 33% rayon yarns. The vaporization index ranged between 5.57 g/m^{2}h for cross miss single jersey knit from 100% cotton yarn and 20.77 g/m^{2}h for the interlock knit from 67% cotton and 33% rayon yarn. In terms of hygroscopicity, it has values ranging from 5.4% to interlock with miss stitches knit from 75% cotton and 25% polyester yarn and 12% for single jersey knit from 100% cotton yarn. Minimum and maximum porosity values are 69.47% and 81.41%, corresponding to interlock knit from 50% polyester and 50% rayon yarns, respectively single jersey with miss stitches knit from 100% cotton yarns.

Hydrophilicity maximum values give us information regarding the optimal structure of the fabric, which could be a simple interlock or interlock with miss stitches; the maximum value is obtained for a blend of cotton and rayon, knowing that rayon has a special behavior in wet conditions. Lower hydrophilicity values were noted for cotton knits with single jersey structure, so from the standpoint of this parameter is not sufficient to use a hydrophilic raw material, but also the structure used plays an important role.

High hygroscopicity values have proven interlock knits from cotton and rayon blends and single jersey knits from 100% cotton. However, a value of hygroscopicity more than 6% is accepted, and it can be observed on interlock knit from 100% cotton, a close value can be seen in the structure interlock with the fiber composition of 50% polyester and 50% rayon. So this blend can replace successfully cotton yarns. Values higher than 6% are observed in all knitted structures and all combinations of fiber blends, unless for interlock with miss stitches, which can be attributed to the polyester fibers and to the structure that shows the miss stitches, resulting in a lower specific weight and hence a reduced ability to yield/absorb water vapor from/to ambient environment. Values higher than 50% for porosity indicates good capacity to maintain and transport moisture while favoring faster dry skin to intense sweating, noticing that all structures analyzed shows high porosity, which make them optimal for use in garments that come in direct contact with skin. Note that the maximum

porosity was obtained for single jersey with miss stitches with 100% cotton.

Since the physiological comfort depends on all the parameters that were analyzed, it can be concluded that all knitted structures under discussion and various blends used are optimal for garments that provide comfort to wearer.

CONCLUSIONS

The human body gives out, through the sweat, an important quantity of moisture, even in rest conditions, which if it stays on the skin's surface, would negatively influence the biological balance of the body. The clothes must be consistently favorable environment to eliminate the moisture, as well as other harmful emissions. Thus, between the amounts of moisture gave it by the body under certain conditions and its ability of storing and transport by clothing products there must be a close connection. Therefore, a comprehensive study was required, and conducting a case study, given the multitude of factors that determine behavior in the humid environment of fabrics, as well as the creation of this environment in terms of wearing.

With regard to the behavior in the humid environment of groups of knits made of cotton type yarn with the same fineness, experimental research results in the possibility of a complex analysis on hydrophilicity, hygroscopicity and vapor permeability; at the same time stands the porosity, which in case of knits has values that may exceed 80%. Porous structure with higher values in knits, compared to other textile surfaces increases the moisture content no matter whether it is liquid or vapor form. It also noted a decrease in the index of evaporation which increases the material's compactness. The appreciation of the limits of those parameters must be taken into account for the purpose of articles of clothing and also the weight of those characteristics studied in quality of fabrics and clothes.

BIBLIOGRAPHY

[1] Mitu, S., Hâncu, S., Căprariu, C., Capmare, L., Țuca, M. *Heat and mass transfer through clothing*, In: Industria Textila, 2007, vol. 58 (5), pp. 178–185.

[2] Vircan, A., Ionesi, D., Mitu, S., Dabija, A., Capmare, L. *Interdependence between anthropometric parameters specific for the age group 7–10 years,* In: Industria Textila, 2013, vol. 64, Issue 4, pp. 188–194.

[3] Sekkeli, M., Kececioglu O. *Scada based an energy saving approach to operation of stenter machine in a textile plant using waste heat recovery system*, In: Tekstil ve Konfeksiyon, 2012, Issue 3, pp. 248–257.

[4] Lefter, C., Maier, S., Maier, V., Popa, M., Desbrieres, J. *Engineering preliminaries to obtain reproducible mixtures of atelocollagen and polysaccharides*, In: Mater. Sci. Eng. C. Mater. Biol. Appl., 2013, vol. 33, Issue 4, pp. 2323–2331.

[5] Oğlakcioğlu, N., Marmarali, A. *Thermal comfort properties of cotton knitted fabrics in dry and wet states*, In: Tekstil ve Konfeksiyon, 2010, vol. 20, Issue 3, pp. 213–217.

[6] Dulgheriu, I., Cozmanciuc, C. *Mecanical tests carried out on composite materials specific to safety jackets*, In: Industria Textila, 2012, Vol. 63, Issue 2, pp. 97–104.

[7] Matenciuc, C.C., Dulgheriu, I. *Quality evaluation model for cloting materials*, In: Industria Textila, 2011, vol. 62, Issue 2, pp. 99–104.

[8] Iorgoaea-Guignard, M., Fărîmă, D., Ciobanu, L., Ciocoiu, M., Giraud, S., Campagne, C., Broască-Asavei, G. *Comfort properties of knitted fabrics with massaging effects*, In: Industria Textila, 2013, volume 64, Issue 1, pp. 34–39.

[9] Abramiuc D., Popescu, C., Dunca, S., Muresan, A. *Improving cotton textile materials properties by treating with chitosan and metallic salts*, In: Industria Textila, 2013, vol. 64, Issue 4, pp. 204–209.

[10] Oglakcioglu, N., Marmarali, A. *Thermal comfort properties of some knitted structures*, In: Fibres and Textiles in Eastern Europe, 2007, vol. 15, no. 5–6, pp. 94–96.

[11] Ozçelik, G., Çay, A., Kirtey, E. *A study of the thermal properties of textured knitted fabrics*, In: Fibres and Textiles in Eastern Europe, 2007, vol. 15, no. 1(60), pp. 55–60.

[12] Frydrych, I., Dziworska, G., Bilska, J. *Comparative analysis of the thermal insulation properties of fabrics made of natural and man-made cellulose fibres*, In: Fibres & Textiles in Eastern Europe, 2002, pp. 40–44.

Authors:

DANIELA NEGRU[1], LILIANA BUHU[1], EMIL LOGHIN[1], IONUT DULGHERIU[1]
ADRIAN BUHU[1]

[1] «Gheorghe Asachi» Technical University of Iasi, Faculty of Textiles, Leather and Industrial Management

Corresponding author:

DANIELA NEGRU
dnegru@tex.tuiasi.ro

The role of microcapsules in masking bad odors of cotton fabrics

TÜLAY GÜLÜMSER

REZUMAT – ABSTRACT

Rolul microcapsulelor în mascarea mirosurilor neplăcute ale țesăturilor de bumbac

Interesul consumatorilor pentru materialele textile funcționale și inovatoare este în creștere. Textilele parfumate cu efect de lungă durată reprezintă unul dintre aceste produse populare care reușesc să mascheze mirosurile neplăcute. Tehnologia de microîncapsulare este foarte avantajoasă pentru utilizarea textilelor care eliberează parfumuri pe termen lung. În acest studiu, microcapsule parfumate au fost aplicate pe țesături de bumbac. Au fost analizate capacitatea de mascare a mirosurilor neplăcute, rezistența la spălare și rezistența în timp a parfumurilor. Rezultatele indică faptul că microcapsulele ar putea combate diverse mirosuri neplăcute, cum ar fi mirosul de ceapă și pește.

Cuvinte-cheie: microcapsule, parfum, textile inovatoare, mascarea mirosului neplăcut

The role of microcapsules in masking bad odors of cotton fabrics

The interest of consumers for functional and innovative textile materials is increasing. Long lasting perfumed textiles are one of these popular products and they are successful in masking the unpleasant smells. Microcapsulation technology is very advantageous in order to provide long-term fragrance releasing textiles. In this study ready-made fragranced microcapsules were applied to cotton fabrics. Stink-masking ability, resistance to washing and strength of the fragrances were inspected. The results indicate that microcapsules could overcome some bad odors such as onion and fish smells.

Keywords: Microcapsule, fragrance, innovative textiles, stink masking

INTRODUCTION

Breathing is vital, humans cannot live without breathing. A person inhales smell molecules with every breath so smelling has a different place in our lives. In a day, approximately over 23,000 breaths are taken and tiny molecules of scents enters in our body, that makes smelling involuntary. Even when a person sleeps he smells. Of the five senses, only our sense of smell is linked directly to the limbic lobe of the brain, our emotional control center. Fear, anxiety, depression, anger, and joy all emanate from this region of the brain [1–2].

Although humans' odor detection ability is lower than animals, a person can feel approximately 10,000 different odor molecules. Smell is directly related with the sense of taste; most of the taste of the foods cannot be detected if capacity of smell is lost. Today taste enjoyment and using perfumes for various reasons occupy our smell sense unlike its duty of saving from dangers which was more important for humans in the past. Perfumery industry has been growing more and more as interest on fragrance increases. Fragrance is taking place not only in perfumes but also in many products to attract the attention of consumers and make them wish to buy those products. Fragrance may be used as an additive in food, drinks, detergents, soaps, household cleaners, fabric softeners, cigarettes etc. Smelling good can also be a sign of cleaning with fresh fragrances [3].

For many ages the pleasantness of the smell of many natural products has attracted humans. Our ancestors in ancient Egypt and Greece developed the first methods to extract odorants from different natural sources. The developments of extraction methods lead to the creation of the fine fragrances. Then modern synthetic organic chemistry enlarged the number of compounds that can be used in perfumes besides volatile organic molecules isolated from plants and other natural sources. Perfumes are generally complex mixtures of a broad variety of natural or synthetic fragrance raw materials with a multitude of chemical functional groups such as alcohols, aldehydes, ketones, esters, lactones, ethers, and nitriles [4–5].

As the fragrance production technology developed, fragrances are considered normal components of everyday lives. People feel the need to wear a fragrance in order to feel good. Today, fragrances enhance the quality of life, and researchers claim that the use of fragrance can have a strong psychological impact, boosting and altering moods, keeping people alert, providing a feeling of calmness, and may even enhance the learning process and alleviate stress. Perfumes have a widely usage areas in personal and household products such as creams, lotions, detergents, softeners and many other. They are mainly used to neutralize the unpleasant odors. Many people apply perfume on clothes not only to mask unpleasant smells but also to protect themselves from perfumes that are not good for skin and body. To increase the durability of fragrances many studies have been made. One of the techniques that provide long lasting usage capabilities is microcapsulation. It can also meet the demands such as user-friendliness, manufacturability and ecological considerations [4, 6–8].

Microencapsulation is the coating of small solid particles, liquid droplets, or gas bubbles with a thin film of coating or shell material. Microencapsulation can modify the color, shape, volume, apparent density,

reactivity, durability, pressure sensitivity, heat sensitivity, and photosensitivity of the encapsulated substance. By this technology it is also possible to preserve a substance in a finely divided state, and release the substance from the enclosed capsule as required. There are many fields of application and industries using microcapsulation. Increasing research and development activities about this technology is producing a steadily increasing number of commercially successful products that utilize microcapsules. Encapsulated perfumes and flavors contain a coating of scent-filled capsules which break and release scent when the insert is torn open. This product is widely used as a marketing tool, primarily for new perfumes. The storage life of a volatile compound can be increased markedly by microencapsulation. Active agents like scents, essential oils, or perfumes which are used in these products often lose their activity while being stored or immediately during usage. Many flavors and fragrance compounds can be prevented from evaporating by microencapsulation [9–26].

Microencapsulation is an effective technique to control the release of fragrances and to produce more durable fragrant finishing on textiles. The application of microcapsules into textiles presents also several advantages in terms of fragrance performance and health benefits: reduces perfume dermatitis in humans and protects the fragrance material from aggressive external agents or media. Such kind of innovative textile product is designed, from the beginning, as a luxury product. Thus, although the incorporation of a fragrance scent will make it more expensive, it will also make the product more valuable and exclusive. Using this technique, the encapsulated perfume will be released upon breakage of the microcapsules. During the daily use of the suit, fragrances will diffuse into the air and release a pleasant smell by this way. To evaluate this product, the durability of the odor is important and should be evaluated because they will face abrasion, washing, and dry cleaning and similar activities. Nowadays, the perfume encapsulation technology is being used for the development of innovative textile products in order to offer a long-lasting fragrance release. The microcapsules can be applied by stamping works, exhaustion dyeing, impregnation, spraying and coating. Besides, microcapsules can be incorporated in the fiber directly without modifying its touch and color [27–39].

The microencapsulation of essential oils has led to many novel applications, including children's garments, hosiery, sheets, towels, cushions, fragrant ties and shoe insoles, as a consequence not only of the pleasant smell of the essential oils released but also of the wide variety of therapeutic benefits. Some of them help with insomnia, some provide relief from respiratory problems, some stimulate mental and some of them give antimicrobial effect [11].

By applying scented microcapsules to the textile materials, olfactory tests are in a new state, determining the amount of odors after rubbing (breaking the capsules and releasing more scent), and durability of fragranced microcapsules to washing.

In this research, cotton fabrics were treated to have some bad odors and scent microcapsules were used to mask these bad odors. When talking about bad odors, fried fish and roasted onion comes to mind esp. to the persons dealing with cooking. In daily life, most of the people complain about these odors after cooking or eating in a room full of these smells. The effectiveness and durability of scent microcapsules were tested against these odors.

EXPERIMENTAL PART

Materials

Plain weaved and scoured 100% cotton fabric was used. The specifications are:

weight: 120 g/m^2; yarn/cm: in the weft direction: 55 yarns/cm, in the warp direction: 30 yarns/cm; yarn number: weft yarn: 42 Ne, warp yarn: 45 Ne.

Cotton fabric pieces that would be used in the experiments were cut as 20 cm × 20 cm.

Microcapsule and binder were supplied from a national supplier, NUY Tekstil San. ve Dış Tic. Ltd. Şti. in slurry (viscous mixture containing high concentration of microcapsules) form.

Microcapsules contained 30–40% fragrance, 35–45% dry extracts and pH = 7–9. The size of the capsules was 4–6 μm. The fragrance of the microcapsules was designed as to give freshness. It was claimed that (statement needs revision) this design was made in order to mask unpleasant odors rather than to give perfume effect, but have a fresh feeling. The extract was composed of: pomegranate, bergamot, orange blossom, apple, juniper and musk.

Application solution was prepared step by step. First binder was put in pure water and mixed. The solution should not be below 25° C. Slurry form of microcapsule was added to the binder solution by mixing 30 minutes.

In washing trials ECE Reference Detergent: Nonphosphate Reference Detergent (A) – Base powder without optical brightener agent SDC, Type 2 was used. To get fried fish and roasted onion odors, anchovy fish and onion were supplied from a local supermarket.

Method

In order to test the capability of microcapsules to mask the bad odors of cotton fabrics, two methods were applied:

1) Microcapsules were applied to the cotton fabrics and then fabrics were exposed to the odors of fish and onion.

2) Cotton fabrics were exposed to the odors of fish and onion and then microcapsules were applied to the cotton fabrics.

Application of microcapsules to the cotton fabrics:

Two different methods were tried to apply the microcapsules to the cotton fabrics:

Exhaust method: Treatments were made at 40°C for 20 minutes with a L.R= 1:20. Thermal laboratory type

dyeing machine was used. A recipe of 0.6 g/l microcapsule and 0.25 g/l binder was applied by the advice of the chemical producer for exhausting.

Padding method: Fabrics were impregnated by AF: 80%, dried at 80°C for 3 minutes and fixed at 120°C for 2 minutes. Ernst Benz Laboratory type foulard, ATAC GK 40 Laboratory type stenter were used.

The recommendation of the chemical producer for padding is a recipe of 2–8 g/l microcapsule and 0,8–2,5 g/l binder, so following experimental design was composed (table 1):

		Table 1
Trial	**Microcapsule concentration (g/l)**	**Binder concentration (g/l)**
1	2	2.5
2	4	1.8
3	4	2.5
4	6	0.8
5	6	1.8
6	6	2.5
7	8	1.8
8	8	2.5

Application of bad odors to the cotton fabrics:
The application of these odors was performed in a closed glass cabinet (75 × 70 × 45 cm) with a rod in it to hang fabrics.

Fried fish odor: 350 gr. of anchovy fish was fried in a Philips Deep fryer at 160° C for 7 minutes. This deep fryer was put in the cabinet during frying and the cotton fabrics were hanged down from the rod in the cabinet to absorb the odors.

Roasted onion odor: 100 gr. onion was roasted in a pan full of 20 ml of olive oil over a hot plate for 5 minutes. This pan was put in the cabinet during roasting and the cotton fabrics were hanged down from the rod in the cabinet to absorb the odors.

Panel Tests:
All the tests were performed by trained experienced panelists who had minimum 10 years in the evaluation & execution of objective tests (perfume intensity and softness etc.). The panelists are trained at regular intervals by fragrance experts to maintain their acuity. The training was recently validated by Firmenich, an international producer of perfumery and flavor chemicals since 1895. The evaluation group for this study was composed of 20 female individuals with high olfaction endowment. The testers all worked in a Research and Development Center dealing with textiles. It was forbidden for the evaluators to smoke and to drink coffee during the test day upon the advice of Firmenich.

Scent evaluation:
The assessments of the scent of the cotton fabrics were done by panelists after smelling the samples with the in-house scale below:
0: Scentless
1–2: Light Scented (very low)
3–4: Fair Scented
5–6: High Scented (strong)

7–8: Very High Scented (very strong).
Assessment of perfume intensity was made for 8 fabrics before rubbing and after rubbing in order to feel the effects of microcapsules. The same assessments were made after washing to the cotton fabrics again to test the durability of microcapsules to washing.

Washing tests:
In order to test the durability of scented microcapsules to washing conditions and the abilities of masking bad odors after washing, fabrics that were treated with microcapsules and bad odors in two ways were washed in Atlas Linitest Plus laboratory type washing device successively 5 cycles. In these cycles rinsing was applied, but drying was not made. The fabrics were washed by 4 g/l ECE detergent at 40°C for 30 minutes.

Surface characterization Scanning Electron Microscope (SEM):
Surface characterization of the samples was made by SEM Analysis by using Phillips XL- 30S FEG type electron microscope. The fabric samples were coated with gold in order to provide max. 20 nm of conductivity.

Statistical evaluation:
The results were evaluated statistically by SAS program. The evaluations were made according to the least significant difference.

RESULTS AND DISCUSSIONS

I. Determination of recipes

In this part of the study, the recipes for padding and exhausting method were tried in order to decide the recipes to be used in application of bad odors.

The presence of microcapsules was detected by Scanning electron microscope (SEM).

After the application of microcapsule and binder to the cotton fabrics in different methods and concentrations, SEM images were taken. SEM images of applied padding recipes are given in figure 1–4, SEM image of applied exhausting recipe is given in figure 5.
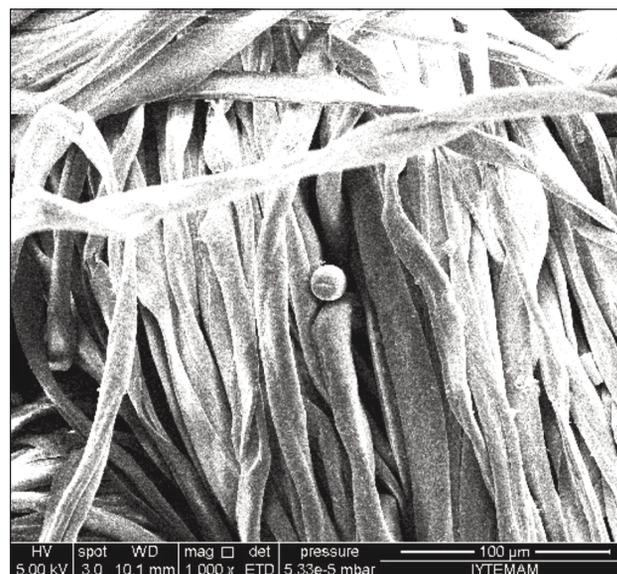
Fig. 1. SEM images of 2 g/L microcapsule and 2.5 g/L binder applied fabrics (1000 x)
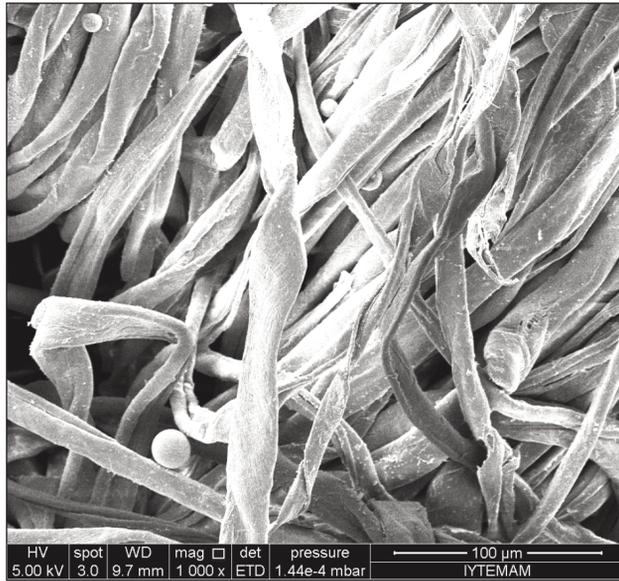
Fig. 2. SEM images of 4 g/L microcapsule, 1.8 g/L binder (left, 1000 x) and 2.5 g/L binder (right, 400 x) applied fabrics
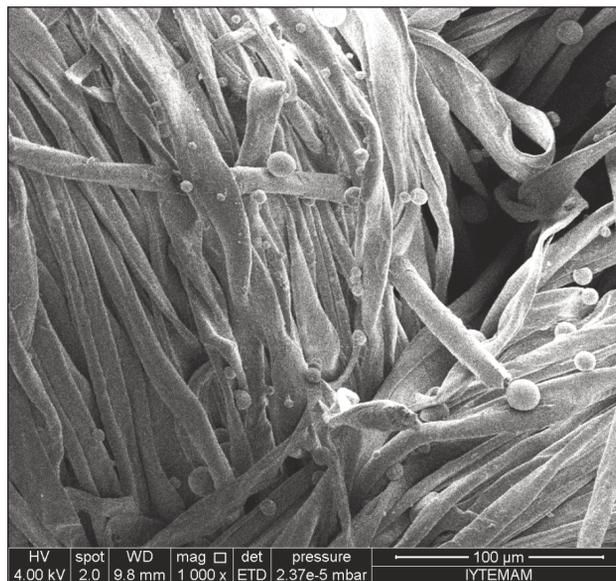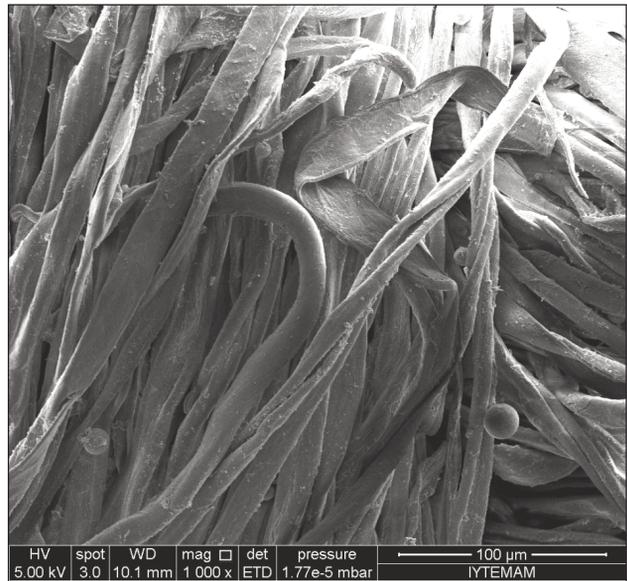
Fig. 3. SEM images of 6 g/L microcapsule, 0.8 g/L binder (upper left) and 1.8 g/L binder (upper right)
and 2.5 g/L binder (down) applied fabrics with a magnification of (1000 x)
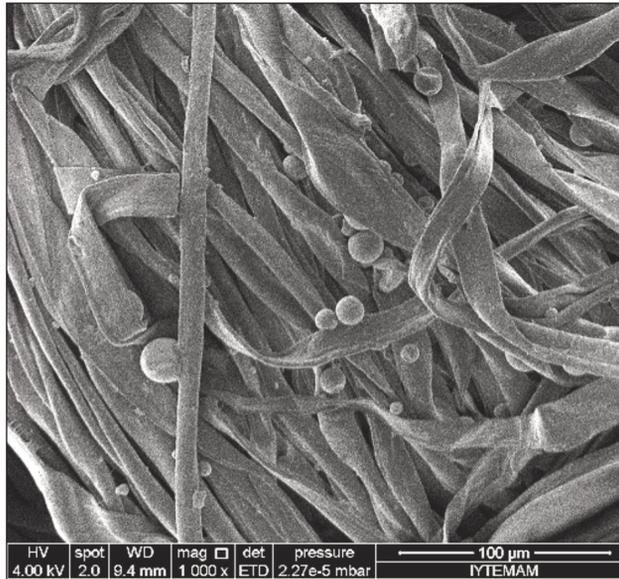
Fig. 4. SEM images of 8 g/L microcapsule, 1.8 g/L binder (left) and 2.5 g/L binder (right) applied fabrics with a magnification of (1000 x)

In figure 1, the microcapsules are very few because of the application of microcapsules in low concentration.

In figure 2, the dimensions and distributions of the microcapsules are similar, but there is not a remarkable increase in the quantity of microcapsules over the fabrics. The increase of the binder concentration does not seem to have a positive effect.

In figure 3, it is obvious that microcapsules are distributed homogenously over the fabrics. There seems no difference about the dimensions and forms of the capsules. When these images of figure 3 are compared with the ones of figure 1 and 2, the amounts of microcapsules increase as the concentration of microcapsules increase. The increase of binder concentrations also has a positive effect over the transfer of microcapsules to the fabrics. Especially the difference between 0.8 g/L and 2.5 g/L binder concentration is remarkable.

In figure 4, the microcapsules seem to have similar dimensions and forms. The change of binder concentration does not affect the amount of microcapsules transferred to the fabric. But it is obvious that there are more microcapsules than the concentrations of 2 g/L and 4 g/L. There is no significant difference between the microcapsule concentrations of 6 g/L and 8 g/L. So for the studies with padding method microcapsule concentrations of 2 g/L and 6 g/L were chosen with the constant binder concentration of 2.5 g/L.

At the end of the studies made with exhausting method, the physical appearance of the microcapsules did not change, but the amount of microcapsules applied to the fabrics seemed less than the ones applied with padding method. So the trials went on with padding method.

II. Evaluation

At this step, fabrics were treated with bad odors and microcapsules as described above with the chosen
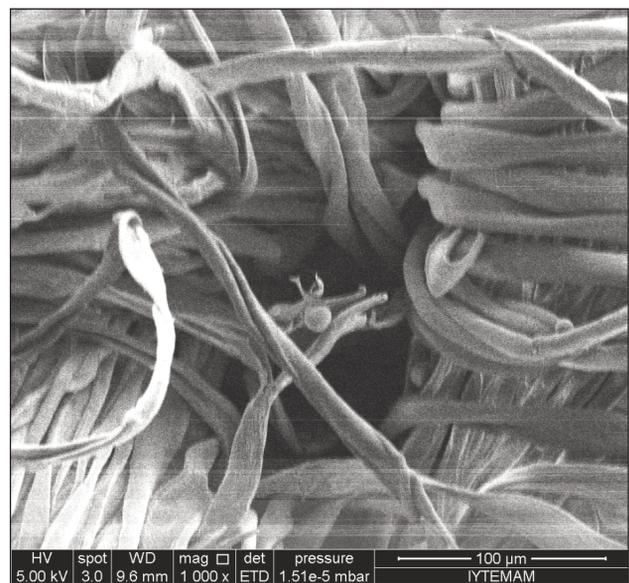
Fig. 5. SEM images of fabrics treated with exhausting method (1000 x)

recipes. 8 treated fabrics' scents were then evaluated by the panel tests before and after washing. In these evaluations, the grades were taken before rubbing and after rubbing to determine the effect of microcapsules. The average values were taken and Least Significant Difference (LSD) values were given. Scents were evaluated by means of bad odor and perfume intensity.

Fabrics were coded by the treatments:
• O2M: Fabric, exposed to the onion odor and then 2 g/L microcapsules were applied;
• O6M: Fabric, exposed to the onion odor and then 6 g/L microcapsules were applied;
• M2O: Fabric, applied 2 g/L microcapsules and then exposed to the onion odor;
• M6O: Fabric, applied 6 g/L microcapsules and then exposed to the onion odor.

Same coding was made for the fabrics exposed to the fish odor.

Washed fabrics were coded by adding "W" to the end of the previous code. Panel tests are given in figures 6–9. In addition to the evaluations described above, panel test was also applied to the cotton fabrics (table 2–5) that had only bad odors (without scented microcapsule application). The average grades are: fabric for the onion odor: 7, fabric for the fish odor: 7.25

When onion and fish odors are compared generally, it can be pointed out that it is harder to mask fish odor.

The increase of microcapsules increased the perfume's odor of both washed and unwashed fabrics. The result is similar before and after rubbing.

Microcapsules applied after exposing to the bad odor are more effective in decreasing bad odors.

When washing results are compared, perfume odors are still effective after rubbing, but it can be said that the values of bad and perfume odor are both lower. During washing some of the capsules are cracked by the mechanical effect of washing.

Table 2

Onion	Least signifi-cant dif-ference	Perfume before rubbing	Perfume after rubbing	Bad odor before rubbing	Bad odor after rubbing
O2M	0.958	1.900	7.700	5.200	0.800
O6M	1.361	3.500	7.800	4.400	0.500
M2O	1.496	2.800	7.500	4.900	1.100
M6O	0.799	3.100	7.600	4.500	0.700
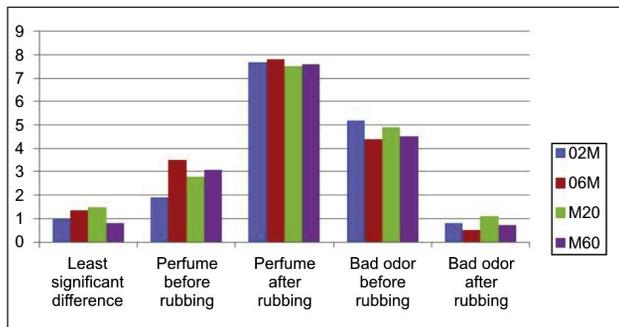
Fig. 6. Panel test results of onion odor

Table 4

Fish	Least signifi-cant dif-ference	Perfume before rubbing	Perfume after rubbing	Bad odor before rubbing	Bad odor after rubbing
O2MW	1.489	2.300	5.600	1.700	1.600
O6MW	1.219	3.100	6.800	2.000	0.500
M2OW	0.907	2.500	5.700	1.500	0.900
M6OW	0.982	2.600	5.900	1.500	0.400
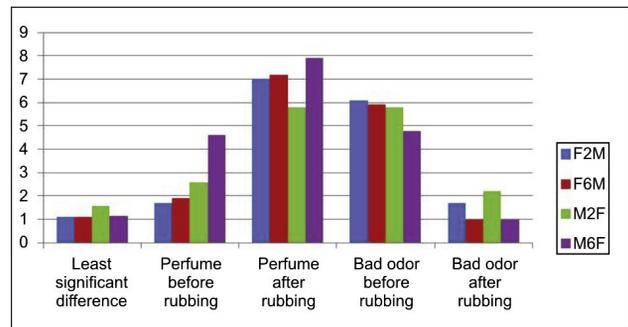
Fig. 8. Panel test results of onion odor after washing

Table 3

Onion wash-ing	Least signifi-cant dif-ference	Perfume before rubbing	Perfume after rubbing	Bad odor before rubbing	Bad odor after rubbing
F2M	1.122	1.700	7.000	6.100	1.700
F6M	1.105	1.900	7.200	5.900	1.000
M2F	1.565	2.600	5.800	5.800	2.200
M6F	1.140	4.600	7.900	4.800	1.000
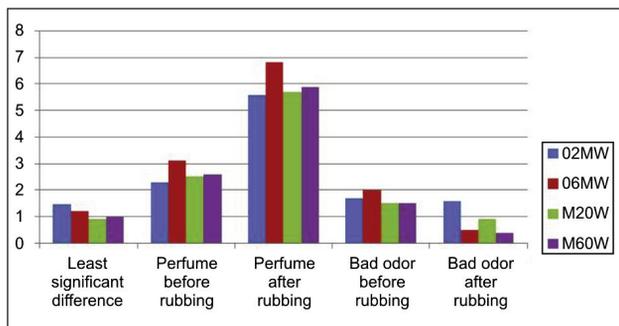
Fig. 7. Panel test results of fish odor

Table 5

Fish wash-ing	Least signifi-cant dif-ference	Perfume before rubbing	Perfume after rubbing	Bad odor before rubbing	Bad odor after rubbing
F2MW	1.397	1.900	4.600	2.500	1.000
F6MW	1.277	2.500	6.400	1.900	0.800
M2FW	1.357	2.100	5.000	2.100	1.300
M6F	1.220	2.200	5.800	1.700	0.500
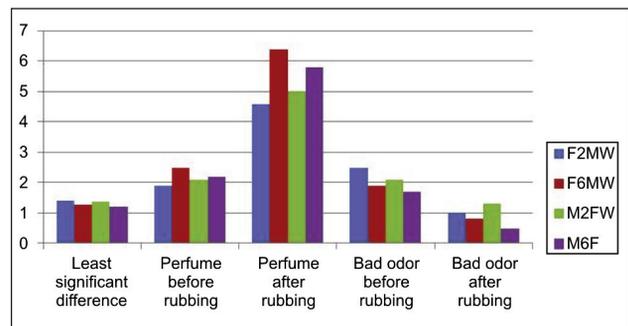
Fig. 9. Panel test results of fish odor after washing

CONCLUSIONS

Fragranced textiles are at the focus of consumer interest in recent years. These fragranced textiles have many usage fields such as apparel, fashion accessories, shoes, and bags. They are accepted as new and innovative by consumers. Finishing textile materials with long-term fragrance-releasing properties is an attractive commercial aim, as well as a significant textile chemical and engineering challenge. Microencapsulation is a technique that enables the persistence of fragrances over textiles with controlled release properties. It is advantageous to apply microcapsules into textiles in terms of fragrance performance and health benefits.

In this study, the masking abilities of scent microcapsules were tried over bad odors such as onion and fish. Durability and performance of odors were evaluated against washing and rubbing. The order of applying odors was also tried. It was concluded that intensive bad odors could be overcome by the application of chosen fragranced microcapsules to the cotton fabrics.

BIBLIOGRAPHY

[1] Becker, R.A. *You smell: The mysterious science of scent*, In: Master of Science in Science Writing at the Massachusetts Institute of Technology September, 2015.

[2] Shepherd, G.M. *Smell images and the flavour system in the human brain*, In: Nature, 444, 2006, pp. 316–31.

[3] Gülümser, T., Balpetek, F.G., Demir, A. *Durability of fabric softeners' odors used in home type of washings at cotton products during wearing*, In: Tekstil ve Konfeksiyon, 25(3), 2015, pp. 263–269.

[4] Herrmann, A. *Controlled release of volatiles under mild reaction conditions: from nature to everyday products,* In: Angewandte Chemie Ind. Ed., 46, pp. 2007, 5836–5863.

[5] Elia, R., Guo, J., Budijono, S., Normand, V., Benczedi, D., Omenetto, F., Kaplan, D.L. *Encapsulation of volatile compounds in silk microparticles*, In: J Coat Technol Res. 12(4), July 2015, pp. 793–799.

[6] Kayar, M. *Effects of perfume on mechanical and color properties of cotton fabrics,* In: International Journal of Clothing Science and Technology, vol. 27 no. 1, 2015 pp. 6–16.

[7] Xiao, Z., Liu, W., Zhu, G., Zhou, R., Niu, Y. A *Review of the preparation and application of flavour and essential oils microcapsules based on complex coacervation technology,* In: J Sci Food Agric 94, 2014, pp. 1482–1494.

[8] Kim, R.H. *Development and emotional evaluation of scented clothing using microcapsules,* In: 6th International Conference on Applied Human Factors and Ergonomics (AHFE 2015) and the Affiliated Conferences, AHFE 2015, Procedia Manufacturing 3, 2015, pp. 558–565.

[9] Kirk-Othmer, *Microencapsulation,* In: Kirk-Othmer Encyclopedia of Chemical Technology, vol. 16, pp. 438–463.

[10] Lamprecht, A., Bodmeier, R. *Microencapsulation,* In: Ullmann's Encyclopedia of Industrial Chemistry, pp. 157–172

[11] Golja, B., Sumiga, B., Tavcer, P.F. *Fragrant finishing of cotton with microcapsules: comparison between printing and impregnation*, In: Coloration Technology., 129, 2013, pp. 338–346.

[12] Theisinger, S., Schoeller, K., Osborn, B., Sarkar, M., Landfester, K. *Encapsulation of a fragrance via miniemulsion polymerization for temperature – controlled release,* Macromol. In: Chem. Phys., 210, 2009, pp. 411–420.

[13] Gray, A., Egan, S., Bakalis, S., Zhang, Z. *Determination of microcapsule physicochemical, structural, and mechanical properties,* In: Particuology, 24, 2016, pp. 32–43.

[14] Khan, P.F.K.A., Rohit, P.C.P.A., Sanap, M.D., Guajarati, N.A., Rane, B.R., Pawar, S.P. *A review on microencapsulation*, In: Pharma Science Monitor 6(2), Apr-Jun, 2015, pp. 38-49.

[15] Knez, E., Kukovic, M., Pipa, V., Boh, B. *Microcapsules on woven and non-woven materials,* In: Intern. J. Polymeric Mater., vol. 41, 2000 pp. 693–699.

[16] Bonet, M.A., Capablanca, L., Monllor, P., Diaz, P., Montava, I. *Studying bath exhaustion as a method to apply microcapsules on fabrics*, In: The Journal of The Textile Institute, vol. 103, no. 6, June, 2012, 629–635.

[17] Li, Y., Huang, Y.Q., Fan, H.F., Xia, Q. *Heat-resistant sustained-release fragrance microcapsules,* In: J. Appl. Polym. Sci., 2014, 40053, pp. 1–7.

[18] Chao-Xia, W., Shui-Lin, C. Anchoring β-cyclodextrin to retain fragrances on cotton by means of heterobifunctional reactive dyes, In: Color. Technol., 120, 2004, pp. 14–18.

[19] Jing, H., Zuobing, X., Rujun, Z., Shuangshuang, M., Mingxi, W., Zhen, L. Properties of aroma sustained-release cotton fabric with rose fragrance nanocapsule, In: Chinese Journal of Chemical Engineering, 19(3), 2011, pp. 523–528.

[20] Yang, Z., Zeng, Z., Xiao, Z., Ji, H. Preparation and controllable release of chitosan/vanillin microcapsules and their application to cotton fabric, In: Flavour Fragrance Journal, 29, 2014, pp.114–120.

[21] Abdmanaf, M., Jai, J., Raslan, R., Subuki, I., Mustapa, A.N. Microencapsulation methods of volatile essential oils – a review, In: Advanced Materials Research, vol. 1113, 2015, pp. 679–683.

[22] Bakry, A.M., Abbas, S., Ali, B., Majeed, H. Abouelwafa, M.,Y., Mousa, A., Liang, L.*, Microencapsulation of oils: a comprehensive review of benefits, techniques, and applications,* In: Comprehensive Reviews in Food Science and Food Safety, vol. 15, 2016, pp. 143–182.

[23] Kisilak, D., Lajnšček, M., Golob, D., Vončina. B. *Cosmetotextile as innovation in the production of protective clothing,* In: Sigurnost, 53 (2), 2011, pp. 103–108.

[24] Cheng, S.Y., Yuen, C.W.M., Kan, C.W., Cheuk, K.K.L., Tang, J.C.O. *Systematic characterization of cosmetic textiles*, In: Textile Research Journal, vol. 80 (6), pp. 524–536.

[25] Salaün, F., Vroman, I., Elmajid, I. *A novel approach to synthesize and to fix microparticles on cotton fabric,* In: Chemical Engineering Journal, 213, 2012, pp. 78–87.

[26] Vankeviciute, D., Petrulyte, S., Petrulis, D. *Study on the possibilities to graft microencapsulated essential oil on natural fibres and terry fabrics,* In: Fibres & Textiles in Eastern Europe, 23, 5(113): 2015, pp. 48–54.

[27] Teixeira, M.A., Rodriguez, O., Rodrigues, S., Martins, I., Rodrigues, A.E. *A case study of product engineering: performance of microencapsulated perfumes on textile applications*, In: AIChE Journal, June, vol. 58, no. 6, 2012, pp. 1939–1950.

[28] Nelson, G. *Application of microencapsulation in textiles,* In: International Journal of Pharmaceutics, 242, 2002, pp. 55–62.

[29] Yoh, E. Adoption of fragranced textile products by segmented markets: *Application of the innovation adoption theory*, In: JOTI, vol. 96, no.3, 2005, pp. 157–167.

[30] Li, S., Lewis, J.E., Stewart, N.M., Qian, L., Boyter, H. *Effect of finishing methods on washing durability of microencapsulated aroma finishing*, In: The Journal of The Textile Institute, TJTI, vol. 99, no. 2 , 2008, pp. 177–183.

[31] Rodrigues, S.N., Martins, I.M., Fernandes, I.P., Gomes, P.B., Mata, V.G., Barreiro, M.F., Rodrigues, A.E. Scentfashion®: *Microencapsulated perfumes for textile application,* In: Chemical Engineering Journal, 149, 2009, pp. 463–472.

[32] Panisello, C., Pena, B., Oriol, G.G., Constanti, M., Gumí, T., Valls, R.G. *Polysulfone/vanillin microcapsules for antibacterial and aromatic finishing of fabrics*, In: Ind. Eng. Chem. Res., 52, 2013, pp. 9995−10003.

[33] Pena, B., Panisello, C., Areste, G., Valls, R.G., Gumí, T. *Preparation and characterization of polysulfone microcapsules for perfume release*, In: Chemical Engineering Journal 179, 2012, pp. 394–403.

[34] He, Y., Bowen, J., Andrews, J.W., Liu, M., Smets, J., Zhang, Z. *Adhesion of perfume-filled microcapsules to model fabric surfaces*, In: J Microencapsul, 31(5), 2014, pp. 430–439.

[35] Petrulyte, S., Vankeviciute, D., Petrulis, D. *Characterization of structure and air permeability of aromatherapic terry textile*, In: International Journal of Clothing Science and Technology, vol. 28, no. 1, 2016 pp. 2–17.

[36] Wang, C.X., Chen, S.L. *Aromachology and its application in the textile field*, In: Fibres& Textiles in Eastern Europe January/December, vol. 13, no. 6 (54), 2005, pp. 41–44.

[37] Hu, J., Xiao, Z.B., Zhou, R.J., Ma, S.S., Li, Z., Wang, M.X. *Comparison of compounded fragrance and chitosan nanoparticles loaded with fragrance applied in cotton fabrics,* In: Textile Research Journal, 81(19), 2011, pp. 2056–2064.

[38] Vasquez, R.V.T., Esteller, L.J., Bojarski, A.D. *Multiscale modeling approach for production of perfume microcapsules*, In: Chem. Eng. Technol., 31, no. 8, 2008, pp. 1216–1222.

[39] Azizi, N., Chevalier, Y., Majdoub, M. *Isosorbide-based microcapsules for cosmeto-textiles*, In: Industrial Crops and Products, 52, 2014, pp. 150–157.

Authors:

TÜLAY GÜLÜMSER

Ege University Textile Engineering Department, Turkey

Corresponding author:

TÜLAY GÜLÜMSER

tulay.gulumser@ege.edu.tr

Study on the use of textiles to manufacture mattresses in order to prevent decubitus ulcers due to post-fracture immobilization syndrome in the elderly patient

CLAUDIA-CAMELIA BURCEA
CONSTANTIN CIUCUREL
COSMIN MEDAR
MARIA GLENCORA COSTACHE
LILIANA PĂDURE

MARIUS IVAȘCU
RĂZVAN PETCA
AIDA PETCA
LUMINIȚA GEORGESCU
CLAUDIA NICULESCU

REZUMAT – ABSTRACT

Studiu privind utilizarea materialelor textile pentru confecționarea saltelelor în prevenirea escarelor de decubit din cadrul sindromului de imobilizare postfracturi la pacientul vârstnic

Lucrarea prezintă un studiu experimental și rezultatele acestuia privind optimizarea strategiilor de intervenție în sindroamele de imobilizare prin identificarea combinațiilor dintre programele de recuperare funcțională și procedurile/metodele moderne de profilaxie și/sau tratament cu accent pe analiza eficienței utilizării saltelelor antiescară ca mijloc terapeutic. Experimentul s-a realizat pe două grupe, o grupă experimentală și o grupă martor, ambele cuprinzând câte 10 subiecți cu fracturi ale articulației șoldului. Programul de profilaxie aplicat a fost diferit: La lotul martor a fost aplicată terapia kinetică obișnuită, iar la lotul experimental s-a aplicat pe lângă programul kinetic și un program de prevenire a complicațiilor generale ce apar în perioada de imobilizare prin utilizarea saltelelor și pernelor antiescară, purtarea de botoșei (pernițe) antiescară pentru călcâie, folosirea îmbrăcămintei și lenjeriei de pat din bumbac. Saltelele antiescară utilizate au fost din spumă cu înaltă elasticitate și densitate foarte mare (HR35), cu piese crenelate detașabile, pernele antiescară au fost din spumă tip CMHR, cu densitate de 38–40 Kg/mc, cu duritate de 200 Newtoni, iar la pacienții cu risc mare și mediu de apariție a escarelor s-a utilizat salteaua antiescară dinamică, cu pompă de presiune alternantă, salteaua antiescară din PVC pneumatică cu compartimente cilindrice și compresor de presiune alternantă. Toate saltelele au fost acoperite cu un material impermeabil, respirabil, antifungic, antialergenic si ignifug. De asemenea, pacienții au utilizat îmbrăcăminte și lenjerie de pat din fibre de bumbac, cu țesătură cu desime mare și au fost folosite aleze, în special în cazul persoanelor cu incontinență urinară. În urma experimentului s-a constatat regresul în evoluția escarelor sau limitarea expansiunii lor, în lotul experimental, ca o consecință a utilizării saltelelor antiescară din spumă cu înaltă elasticitate și densitate mare și a alezelor absorbante.

Cuvinte-cheie: fractură, saltea antiescară, spuma poliuretan, recuperare, textile funcționalizate

Study on the use of textiles to manufacture mattresses in order to prevent decubitus ulcers due to post-fracture immobilization syndrome in the elderly patient

This work presents a pilot study and its results regarding the optimization of intervention strategies in the immobilization syndromes by identifying combinations between functional rehabilitation programs and modern procedures/methods for prophylaxis and/or treatment, focusing on the analysis of the effectiveness of anti-bedsore mattresses as therapeutic means. The experiment was conducted on two samples, experimental and control, both consisting of 10 subjects each with hip joint fractures. The prophylaxis programme applied was different: usual kinetic therapy was used on the control sample, and the experimental sample underwent, apart from the kinetic programme, a prevention programme related to general complications arising during the immobilization period by using anti-bedsore mattresses and pillows, wearing anti-bedsore boots (cushions) for heel protection, using cotton clothing and bed linens. The anti-bedsore mattresses used were made of high density and elastic foam (HR35), with detachable castellated parts, the anti-bedsore pillows were made of foam type CMHR with density applied of 38–40 Kg/mc with hardness of 200 Newton, and for the patients at high and average risk of developing bedsore, the dynamic anti-bedsore mattress was used with an alternating pressure pump, the pneumatic PVC anti-bedsore mattress featuring cylindrical compartments and alternating pressure compressor. All mattresses were covered by an impermeable material, breathable, antifungal, antiallergenic and uninflammable. Also, patients were given cotton fiber clothing and bed linens, with dense fabric and absorbent bed pads, especially for people with urinary incontinence. Following this experiment, the regression or, at least, limiting, of bedsores evolution was found in the experimental sample, as a consequence of using anti-bedsore mattresses made of high density and elastic foam and absorbent bed pads.

Keywords: fracture, anti-bedsore mattress, polyurethane foam, rehabilitation, functionalized textiles

INTRODUCTION

The continuous development of the mattresses materials made, used to prevent or treat pressure ulcers, has made life expectancy to expand and to increase elderly patient's quality of life. Pressure ulcers are decubitus wounds which develop on the skin and tissue of the patient's body after prolonged immobilization [1]. Senectute features a series of functional impairments affecting directly the organs' functional capacity, the body's systems on account of a gradual

and differential degradation process [2]. Given the increase in longevity, third age persons develop a number of conditions, mostly degenerative, which cause favorable premises for fractures. High incidence of fractures in the elderly population segment is due to the bone metabolism changes which diminish bone toughness [3]. Diminished bone density (osteoporosis) also leads to diminished load, causing fractures [4–8]. Frequently encountered diseases in this population segment, such as hemiparesis, Alzheimer's dementia, Parkinson, osteomalacia, are all susceptible to falls, thus favoring fractures. Overlay of one of these conditions with a fracture causes the patient's immobilization for a variable length and subsequently limitation of activity results in decrease of their quality of life and increase of morbidity and mortality [9–10]. The elderly patient's immobilization brings forward, apart from the clinical signs relating to fracture and lung stasis, renal stasis, edemas and tegumentary lesions in the peripheral regions, compression/decubitus ulcers [11–12]. Anti-bedsores mattresses made of high elasticity and resilience foams allow ventilation of teguments, do not favor sweating (maintain the teguments dry), drop the pressure on teguments. All these characteristics represent the premises for using these mattresses both in order to avoid pressure ulcers, and to protect an already present bedsore.

EXPERIMENTAL PART

The purpose of this study was to manage from clinical and functional points of view the pathology identified (existent fractures and tares) in the subjects selected and to optimize the intervention strategies in the immobilization syndromes by identifying the combinations between functional rehabilitation programs and modern methods/procedures for prophylaxis and/or treatment of these subjects with a view to improve and/or preserve the health status and increase the quality of life.
Study objectives:
– To identify the clinical-functional and mental state of patients;
– To identify correlations between the clinical-functional and mental state of patients and the presence of compression ulcers;
– To identify the most effective operational (possibilities) structures to reduce risks of developing compression ulcers;
– To set out tests and assessment tools to measure the quality and effectiveness of the means applied.
– To experiment and analyze the effectiveness of anti-bedsore mattresses and other related techniques in relation to immobilization syndromes as a therapeutic means.
– To show the results obtained and to statistically interpret them.

Material and methods used in the research

Presentation of the groups of subjects which underwent the intervention and rehabilitation process. The experiment was conducted on two groups, experimental and control, both consisting of 10 subjects each, with hip joint fractures. All subjects had hip fractures, as well as co morbidities, such as: atherosclerosis with cerebral, coronary, peripheral manifestations, chronic ischemic cardiomyopathy, essential hypertension, osteopenia/osteoporosis, spinal and peripheral osteoarthritis with mono- or pluri-articular movements.

Research criteria for both groups

Case selection was carried out based upon the main diagnosis and patients' consent (for Alzheimer's patients, consent was taken from the family) for inclusion into one of the groups (experimental or control). Differentiation between experimental and control sample was made using a different prophylaxis programme: the control sample underwent usual kinetic therapy, and the experimental sample underwent, apart from the kinetic programme, a prevention programme for general complications arising during the immobilization period and prophylaxis of tardy complications.

Place and conditions for the experiment

Functional rehabilitation and patients' prophylaxis were conducted at their place of residence.

Preparing personalized strategies for rehabilitation, primary and/or secondary prophylaxis of decubitus/compression ulcers

The operational objectives and means used were:
– Improve pain and prevent the inflammatory process: antialgesic and anti-inflammatory medication;
– Sparing joints: joint rest, use of walking aids, crutches and walking sticks;
– Reduce swelling and stimulate venous return: anti-peripheral postures ("Bürger"-like gymnastics);
– Maintain normal range of movement and articular structures' trophicity (carried out manually by the kinesiotherapist, then by family members); passive exercises;
– Re-educate active control of lower limb: neuro-muscular facilitation techniques;
– Maintain and increase strength and elasticity in various muscle groups: controlled active exercises;
– Increase muscle strength and resilience in the moderate protection phase of the injured lower limb: exercises involving resistance;
– Prevent physical deconditioning and reduce recovery time: counter-lateral exercises;
– Oxygenate blood: breathing exercises;
– Treat /protect existent bedsores: brushing;
– Prevent decubitus/compression ulcers, ventilate teguments, maintain the teguments dry (avoid sweating), drop pressure on the teguments: use of anti-bedsore mattresses an pillows, wearing anti-bedsore boots (cushions) for heel protection, using cotton clothing and bed linens.
Early mobilization of patients with hip fractures, tared, was achieved for the purpose of preventing: bronchopneumonia due to lung stasis, compression

ulcers, decubitus edemas caused by loss of vascular reflexes in the peripheral regions, urinary infection caused by renal stasis [13]. Given that some of the patients had decubitus ulcers since the initial assessment was carried out, we thought it was essential to educate patients, and their family/next of kin, regarding the correct treatments and their immediate application and prevention of other bedsores [14]. We must mention that the bedsores present were stage 2, which are discontinuity solutions on the teguments, being superficial lesions affecting the epidermis and dermis. If treated inadequately, they shall lead to open wounds.

In order to protect the bedsores already developed and to prevent others from occurring, in patients at very high risk, we recommended the use of anti-bedsore mattresses made of high density and elastic foams (HR35) and anti-bedsore pillows made of foam type CMHR, with density applied of 38–40 Kg/mc, with hardness of 200 Newton. The seating surface is made up of 3 parts: head, torso and leg. The mattress's manufacture allows the air to travel freely, thus avoiding dampness. Patients at high and average risk of developing bedsores were recommended to use the dynamic anti-bedsore mattress with alternating pressure pump which inflates/deflates cyclically the pneumatic chambers inserted inside the smart foam, type CMHR (polyurethane foam) and PVC compartments, anti-bedsore air mattress made of nylon/PVC (polymerized vinyl chloride manufactures as per the European standards, EN71), with cylindrical compartments and alternating pressure compressor [9–10]. The mattresses were covered by functionalized textile material, impermeable, hygienic and breathable, antifungal and antiallergenic. The material is flame-resistant and it has a long shelf life.

gives cotton fibers gracefulness and resilience, elasticity, finishing capacity and specific chemical properties. Also, the use of bed pads was recommended especially for persons with urinary incontinence, thanks to the higher protection level they provide for sheets/blankets from the cellulose flakes layer and outer impermeable film (polyethylene), as well as due to the fact that the contact surface is soft, silky, delicate to touch [16].

RESULTS AND DISCUSSIONS

The data obtained in the experimental group of patients was summarized and analyzed statistically.

Upon analysis of subjects' *gender*, we noticed the control sample was made up of 6 female patients (standing for 60% of the total) and 4 male patients (standing for 40% of the total), and the experimental sample was made up of 7 female patients (standing for 70% of the total) and 3 male patients (standing for 30% of the total), as can be noticed in the frequency table shown below at table 1.

Regarding the age of the control group, we found that the average age was 77.2 years old with a minimum of 68 years old and maximum 92 years old, standard deviation of 8.06 and the average age of the experimental group was 82 years old, with a minimum of 70 years old and a maximum of 95 years old, standard deviation of 7.27. This data is shown below in the table with descriptive statistical indicators at table 2.

In both groups, the type of fracture was as follows:
– In the control sample: greater trochanteric fracture – 6 cases (standing for 60% of the total) and cervical hip fractures – 4 cases (40%);
– In the experimental sample: greater trochanteric fracture – 7cases (standing for 70% of the total) and cervical hip – 3 cases (30%).

				Table 1
SUBJECTS' GENDER – FREQUENCY				
Subjects gender	Control sample		Experimental sample	
	Absolute frequency	Relative frequency (%)	Absolute frequency	Relative frequency (%)
Male	4	40	3	30
Female	6	60	7	70
Total	10	100	10	100

Also, all patients were recommended to wear cotton clothing and to use cotton bed linens, with thick fabric, seeing as, less dense fabrics become asperous and form ridges or plies which increase the teguments' friction degree, thus favoring bedsores' occurrence. Thanks to its properties, such as, no allergenic (100% natural), cotton allows good body ventilation, absorbs and easily removes body moisture, can bear high temperatures without its quality or durability being affected; hence it may be sterilized, which makes it the perfect choice for eliminating risks of infections' occurrence and spreading [15]. The cellulose content

		Table 2
PATIENTS' AGE – STATISTICAL DESCRIPTIVE INDICATORS		
Statistical indicator	Control group	Experimental group
Mean	77.20	82.00
Median	77.50	80.50
Standard deviation	8.06	7.27
Minimum	68.00	70.00
Maximum	92.00	95.00

Table 3

TYPE OF FRACTURE – FREQUENCY				
Type of fracture	Control group		Experimental group	
	Absolute frequency	Relative frequency (%)	Absolute frequency	Relative frequency (%)
Cervical hip	4	40	3	30
Greater trochanter	6	60	7	70
Total	10	100	10	100

Table 3 shows the values of the researched variable. Related diseases present in the two research groups were the following, in order of their frequency:

– In the control group: spinal and peripheral osteoarthritis with pluri-articular movements (3 cases), cerebrovascular accident (3 cases), essential hypertension (4 cases), Alzheimer's disease (2 cases), chronic ischemic cardio-myopathy (3 cases), urinary incontinence (1 case), fracture of the distal radial epiphysis (1 case);

– In the experimental group: spinal and peripheral osteoarthritis with pluri-articular movements (5 cases), cerebrovascular accident (4 cases), essential hypertension (5 cases), chronic ischemic cardiomyopathy (2 cases), and urinary incontinence (1 case).

Hip mobility. In order to assess joint range of motion, we conducted the initial, then final tests, calculating subsequently the difference between the two tests. They were carried out for each patient separately and for all possible joint movements.

• Differences between tests inside the groups.

The descriptive statistical indicators table shows that mean differences values between the initial and final tests were:

– In the control group: flexion – 11.2^0; extension– 7.4^0; abduction – 4.8^0; adduction – 4.9^0; internal rotation – 6.6^0; external rotation – 4.7^0;

– In the experimental group: flexion – 12.1^0; extension – 7.8^0; abduction – 5.4^0; adduction – 6.3^0; internal rotation – 4.4^0; external rotation – 4.5^0.

• Differences between experimental and control group.

There are statistically significant differences between patients in the control group and those from the experimental group regarding the hip joint range of movement ($p < 0.05$), subjects in the experimental group registering better mobility.

Trends in the test results are illustrated by the synthetic table of basic statistical indicators shown below in table 4.

Concerning the presence and the degree of bedsores, the situation was as follows:

• Differences between tests inside the group.

– Initial: in the control group, 4 patients had bedsores (standing for 40% of the total), and 5 patients from the experimental group (standing for 50% of the total), all bedsores being stage 2;

– Final: 5 patients in the control group still had bedsores (standing for 50% of the total), and in the experimental group, there were 3 patients (standing for 30% of the total), all bedsores being stage 2.

• Differences between the experimental and the control group.

At the end of the rehabilitation program, there were statistically significant differences regarding the bedsores' presence, the highest progress being noticed in the experimental group.

These results are exemplified in the frequency table shown further in table 5.

The regions most frequently affected by bedsores were: heel, sacral, gluteal, trochanteric and occipital.

Table 4

MEAN VALUES OF DIFFERENCES BETWEEN TESTS (INITIAL AND FINAL) RELATING TO JOINT RANGE OF MOTION – DESCRIPTIVE STATISTICAL INDICATORS								
Difference between tests	Control group				Experimental group			
	Mean	Standard deviation	Minimum	Maximum	Mean	Standard deviation	Minimum	Maximum
Flexion	11.2^0	5.82	3	21	12.1^0	5.40	4	22
Extension	7.4^0	4.11	2	15	7.8^0	4.10	3	17
Abduction	4.8^0	2.29	2	10	5.4^0	2.95	3	11
Adduction	4.9^0	2.55	2	8	6.3^0	1.82	3	8
Internal rotation	6.6^0	4.27	2	13	4.4^0	2.83	2	12
External rotation	4.7^0	1.88	2	7	4.5^0	2.27	2	8

Table 5

Bedsores presence	Control group				Experimental group			
	Initial		Final		Initial		Final	
	Absolute frequency	Relative frequency (%)	Absolute frequency	Relative frequency (%)	Absolute frequency	Relative frequency (%)	Absolute frequency	Relative frequency (%)
Yes	4	40	5	50	5	50	3	30
No	6	60	5	50	5	50	7	70
Total	10	100	10	100	10	100	10	100

PRESENCE OF DECUBITUS/COMPRESSION ULCERS – FREQUENCY

CONCLUSIONS

- The presence of complications due to decubitus found in our study – bedsores, urinary infection, as well as aggravation of some preexisting conditions such as pulmonary and cardiovascular diseases represent immediate complications of hip fractures, which match the data in the published literature;
- Taking account of the patients' age and gender, we found out there is a significant increase in trochanteric fractures rate in the elderly, especially in females;
- The pathology presented in our study leads to significant need of reeducation, concerning the possibility to mobilize patients, in order to eliminate decubitus/compression ulcers, fact which proves the importance of patients/ their next of kin knowledge in respect of preventing ulcers and/or treating/protecting those already formed;
- The regression registered regarding the bedsores evolution or limitation of their expansion, identified in the experimental group is an outcome obtained following the use of anti-bedsores mattress made of high density and elastic foam and absorbent bed pads and textile materials with hygienic and protective role;
- Passive mobilizations, passive-active and active ones led to the significant improvement of functional parameters in the affected joints;
- Kinetic treatment related to a complex hygienic and sanitary care decreases the risk of direct complications caused by patient bed immobilization.

BIBLIOGRAPHY

[1] Guy H., Downie F., McIntyre L., Peters J. *Pressure ulcer prevention: making a difference across a health authority?,* In: British journal of nursing, 2013, vol. 22, no.12, pp. S4–S13.

[2] Bătrân D. *Îmbătrânirea, un proces ireversibil / Ageing, an irreversible process*, In: Revista de Administraţie Publică şi Politici Sociale, Anul I, nr. 3 / Iunie, 2010, pp. 40.

[3] Colon-Emeric C.S. *Postoperative management of hip fractures: interventions associated with improved outcomes,* In: Bonekey reports, Dec. 2012.

[4] Burcea C.C., Lupuşoru M.O., Negreanu L., et al. *Identification of osteoarthritis with multiple joint involvement in elderly institutionalized patients concomitant with psycho-kinesiotherapeutic intervention strategies – A Preliminary Study,* In: Modern Medicine, 2015, vol. 22, no. 4, pp. 351–354.

[5] Boddaert J., Raux M., Khiami F., et al. *Perioperative management of elderly patients with hip fracture*, In:Anesthesiology, 2014, vol. 121, pp. 1336–1341.

[6] Burcea C.C., Georgescu L., Armean P., et al. *Rehabilitation of knee mobility using hydrokinesitherapy in patients with gonarthrosis,* In: Medicina Sportivă – Journal of Romanian Sports Medicine Society, 2014, vol. 10, nr. 3, pp. 2406–2410.

[7] Lupuşoru M.O., Burcea C.C., Văcăroiu I.A., et al. *The rehabilitation of elderly institutionalized patients with osteoarthritis (multiple joint involvement) using alternative methods associated to drug therapy*, In: Modern Medicine, 2015, vol. 22, no. 4, pp. 355–358.

[8] Amin S., Achenbach S.J., Atkinson E.J., et al. *Trends in fracture incidence: a population-based study over 20 years*, In: J Bone Miner Res., 2014, vol. 29, no. 3, pp. 581–589.

[9] Carpintero P., Caeiro J.R., Carpintero R., et al. *Complications of the hip fractures: a review,* In: World J Orthop., Sep 2014, vol. 5, no. 4, pp. 402–411.

[10] Taylor N., Hogden E., Clay-Williams R., et al. *Older, vulnerable patient view: a pilot study of the patient measure of safety (PMOS) with patients in Australia,* In: BMJ Open, Jun 2016, vol. 6, no. 6.

[11] Jaul E. *Assessment and management of pressure ulcers in the elderly*, In: Drugs Aging, 2010, vol. 27, no. 4, pp. 311–325.

[12] Delic J. *The management of pressure ulcers, sixteenth annual European pressure ulcer advisory panel meeting*, In: Austria Center, Vienna, 28th – 30th August 2013, pp. 83.

[13] Singler K., Biber R., Wicklein S., et al. *A plea for an early mobilization after hip fractures. The geriatric point of view,* In: European Geriatric Medicine, 2013, vol. 4, no. 1, pp. 40–42.

[14] Agrawal K., Chauhan N. *Pressure ulcers: back to the basics*, In: Indian J Plast Surg., 2012, vol. 45, no. 2, pp. 244–254.

[15] Budimir A., Bischof Vukusic S., Grgac Flincec S. *Study of antimicrobial properties of cotton medical textiles treated with citric acid and dried/cured by microwaves,* In: Cellulose, 2012, vol. 19, no. 1, pp. 289–296.

[16] Bettez M., Tu L., Carlson K., et al. *Update: Guidelines for adult urinary incontinence collaborative consensus document for the Canadian Urological Association*, In: Can Urol Assoc J, 2012, vol. 6, no. 5, pp. 354–363.

Authors:

CLAUDIA-CAMELIA BURCEA[1]

CONSTANTIN CIUCUREL[2]

COSMIN MEDAR[1]

MARIA GLENCORA COSTACHE[3]

LILIANA PĂDURE[1]

MARIUS IVAȘCU[1]

RAZVAN PETCA[1]

AIDA PETCA[1]

LUMINIȚA GEORGESCU[2]

CLAUDIA NICULESCU[4]

[1] U.M.F. "Carol Davila" Bucharest / 37, Dionisie Lupu street, Bucharest, 020021, Romania
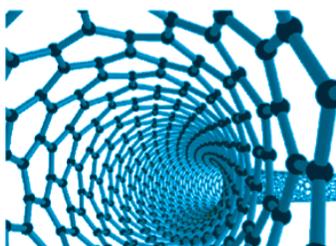
[2] University of Piteşti / 1, Targul din Vale street, Piteşti, Argeş, 110040, Romania

[3] U.M.F. Craiova / 2, Petru Rareș street, Craiova, Dolj, 200349, Romania

[4] The National Research & Development Institute for Textiles and Leather (INCDTP) 16, Lucretiu Patrascanu street, Bucharest, 030508, Romania

Corresponding author:

COSMIN MEDAR

cosmin78@gmail.com

Evaluation of electromagnetic shielding effectiveness of fabrics produced from yarns containing metal wire with a mobile based measurement system

E. KENAN ÇEVEN
AHMET KARAKÜÇÜK

A. EMIR DİRİK
UĞUR YALÇIN

REZUMAT – ABSTRACT

Evaluarea eficacității ecranării electromagnetice a țesăturilor fabricate din fire care conțin fir metalic cu un sistem de măsurare mobil

Această lucrare cuprinde o evaluare a eficenței ecranării electromagnetice a țesăturilor care conțin fir din oțel inoxidabil, cu o nouă metodă mobilă. Firele de bătătură hibride cu acoperire încrucișată au fost realizate cu fire din poliester și oțel inoxidabil. Țesăturile conductoare au fost produse prin utilizarea firelor de bătătură hibride și a firelor de urzeală din poliester texturat. Țesăturile au fost testate în poziții verticale și orizontale pentru a determina eficiența ecranării electromagnetice (EMSE). Toate măsurătorile EMSE au fost efectuate cu o metodă de testare mobilă. Această metodă se bazează pe principiul măsurării semnalelor GSM de către un software mobil și analizarea acestora prin metode statistice. Proprietatea EMSE a țesăturilor s-a dovedit a fi afectată de parametrii firelor hibride, cum ar fi parametrii determinați de numărul de straturi și de direcția acestora, după cum indică analizele statistice. Analizele bazate pe modelul Okumura-Hata au confirmat, de asemenea, rezultatele testelor. S-a ajuns la concluzia că noul sistem de măsurare mobil propus poate fi utilizat în mod corespunzător pentru a determina eficiența ecranării electromagnetice (EMSE) a țesăturilor conductoare.

Cuvinte-cheie: electromagnetic, ecranare, fire hibride, oțel inoxidabil, fir înfășurat

Evaluation of electromagnetic shielding effectiveness of fabrics produced from yarns containing metal wire with a mobile based measurement system

This paper comprises an evaluation of electromagnetic shielding effectiveness of woven fabrics containing stainless steel wire with a new mobile based method. Cross covered hybrid weft yarns were produced with polyester and stainless steel metal wires. The conductive fabrics were produced by using the hybrid weft and texturized polyester warp yarns. Fabrics were tested in vertical and horizontal positions to determine the electromagnetic shielding effectiveness (EMSE). All EMSE measurements were performed with a mobile based test method. This method is based on the principle of measuring GSM signals by mobile-based software and analyzing them by statistical methods. EMSE property of the woven fabrics was found to be affected by the hybrid yarn parameters like fabric parameters of ply number and ply direction, as indicated by statistical analyses. Analyses based on Okumura-Hata Model also verified test results. It was concluded that the proposed new mobile based measurement system can be used reliably to determine the EMSE of conductive fabrics.

Keywords: electromagnetic, shielding, hybrid yarns, stainless steel, wrapped yarn

INTRODUCTION

In recent decades, technological developments in the field of information and communications technology (ICT) provide many uses and easiness communication needs. However, they also increase electromagnetic radiation (EMR) in the environment, which is composed by both electric and magnetic components. The electric and magnetic fields can be transmitted from one medium to another. Electromagnetic waves lie in a spectrum of extremely low (ELF, 0 Hz ~ 300 Hz) to intermediate (IF, 300 Hz ~ 100 kHz), and audio frequency (RF, 100 kHz ~ 300 GHz) and their energy is proportional to their wave lengths [1–2].

Under operation, any electronic device such as computers, cell phones, household appliances, Wi-Fi systems and microwave ovens produce EMR. The broadusage of electronic devices has led to health problems. A person who is being exposed to such environment for a long period can show various health-related symptoms, such as depression, fatigue, loss of vision, and headaches. In addition, they may act as inhibitor to the immune system and accelerate cell mutation which may increase formation of cancer cells. Reproduction ability of males may also be affected negatively [3–5]. Thus, developing materials that could be protective against EMR are an area of interest. Recently, new materials, and methods to provide electromagnetic shielding are developed by researchers to reduce the harmful effect of the electronic devices on human health. Conductive textile materials are examples of these developments.

The developed techniques are manufacturing conductive metal wires from metal sheets, production of conductive fiber with different drawing methods, production of hybrid yarns from conductive filament and-staple fibers with spinning or wrapping together, coating fabrics with conductive paint, application of metal powders, metal oxides/salts, conductive carbon, or

polymers onto textiles. Fabrication of woven or knitted structures with the use of conductive yarns is mainly intended to integrate grids or lattices into the fabrics construction. Improving flexibility, durability and resistance to high-temperature and corrosionare also merits which are targeted. Electrical conductivity property of metal wires is making them a good candidate to achieve such properties. The frequently used conductive metal wires are stainless steel, carbon, nickel, copper, gold, silver and titanium and their alloys.

Örtleket et al. constructed weft-knitted EM shielding fabrics using hybrid yarns with stainless steel wires. They find that the amount, orientation, andlength of the metal wires as well as the applied frequency effected EMSE of fabrics. By integrating circuits to fabric structures based on hybrid special yarns made from steel threads and wrapped by copper wires, Grabowska et al. analyzed the attenuation of EM fields [6–7]. Bedeloglu, investigated the EM shielding characteristics of knitted fabrics made with hybrid-yarns having stainless wires, and illustrated that EM shielding of the fabricis related with the wire content and fabric structure [8]. Chen et al. fabricated a series of hybrid yarns with copper wire and polyamide filament as core and stainless steel wire as cover [9]. Türksoy et al. compared shielding effectiveness results measured with the coaxial transmission line method and the shielding chamber method. They developed a non-linear model to simulate SE results of the coaxial transmission line method according to shielding chamber method by using differential evolution algorithm [10].

The electromagnetic radiation shielding effectiveness measurement needs to use special devices, and results are dramatically effectedby various electrical, electromechanical, and electronic apparatus which emit electromagnetic energy in their normal operation. There are several methods with different advantages are available for EMSE measurement:

1. coaxial transmission line method;
2. shielded room method;
3. open field or free space method (without shielded-box or anechoic chamber);
4. shielded box (enclosure) method.

The first method is a standardized method. It consists of a network analyzer and two coaxial adapters as sample holders. Signals are transmitted through coaxial cable line. The test samples get compressed between the sides of the holder. For comparing measurement results of test samplesmade of different shield materials, the shielded box (enclosure) method is frequently used. The method comprises a metal box having a sample port on the wall, and a receiver inside the box. From outside the box, a transmitter is used to inject signals through the ports. The intensity of signals received through the open port and a sample fitted port is logged and analyzed to compute the EMSE for a range around 500 MHz. However, this does not cover higher frequencies such as GSM 1800. The shielded room method overcomesthis limitation, but it requires high numbers of sample size and the results generally depend on the usedexperimental arrangement and it is difficult to overcomethis dependency, which is a cause ofuncertainty in the results [11].

The purpose of this study is to present a new mobile based measurement method and evaluate EMSE of woven fabrics made of composite yarns consisting stainless steel. The proposed method is designated especially for rapid comparative measurements of fabric samples. To show usability of this method, EMSE of fabric sample set was tested by using this method and obtained results were compared.

The organization of the paper is as follows: In the next chapter, we will elaborate on the experimental design and the characteristics of fabrics, as well as its method of production and structure of the fabrics used in the experiment. Also in this chapter, the validity of the approach has been analyzed theoretically and statistically. For theoretical analysis, we used a model (Okumura-Hata Model) from the communication and wave propagation literature; whereas for statistical analysis, we used analysis of variance (ANOVA) and significance of differences (SNK) which will be expanded in detail in the related subsections. In the section "results and discussion", results acquired from the experiment will be given and they will be analyzed theoretically and statistically.

EXPERIMENTAL WORK

Materials

Characteristics of the weft and warp yarns, which were selected to producewoven fabric with electromagnetic shielding characteristic, are as follows:

1. Weft yarn: Wrapping process was adopted to produce composite yarns (figure 1) containing core yarn of metal wire and covering yarns (figure 2). Polyester yarns are cross covered over stainless steel metal wires on a hollow spindle spinning machine (table 1).
   1.1. Core yarn: Stainless steel metal wire having a diameter of 34 microns (70 denier), figure 3.
   1.2. Covering yarn: 75 denier textured FR (fire-resistant) polyester (figure 3).

Fig. 1. Hollow spindle spinning machine

Table 1

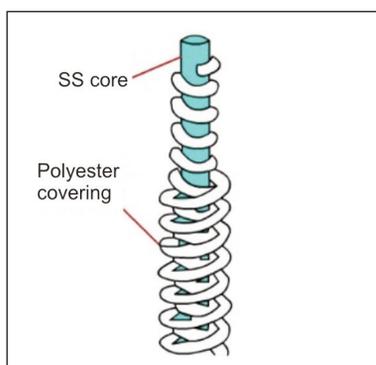| Composite yarn type	Core yarn	Cover yarn	Linear density, denier	Tenacity (cN/tex)	Elongation (%)
Cross covered	one metal wire of 34 microns	75 denier textured FR polyester	220	35.71	24.33

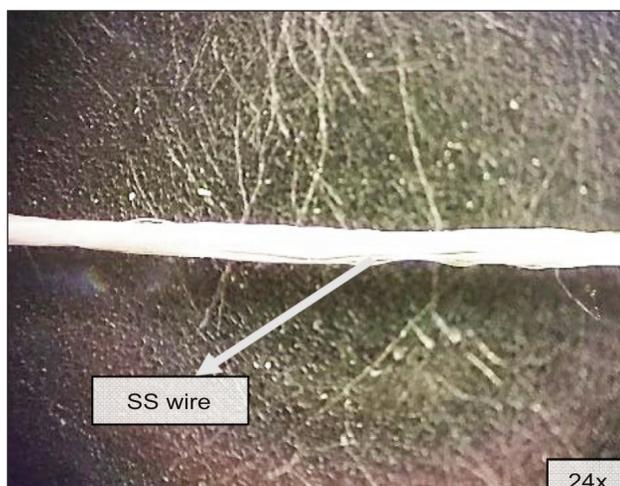Fig. 2. Structure of cross covered composite yarn

Fig. 3. Microscopic photos of cross covered composite yarns

The numbers of the wrapping layers are single layer and double layer. The wrapped count was selected as 12 turns/cm for both layers. Wrapped count is defined as the number of turns of wrapped material in per unit length; the unit is turn/cm.

2. Warp yarn: 75 denier f 72, texturized type polyester. Afterwards, a *Dornier* rapier weaving machine is used on the fabric mentioned above. The type of weave was selected as 5 Shaft Satin. The warp yarn fiber was chosen identical with the cover yarn (to from composite yarn) fiber type to avoid variables. Density of warp direction was 60 ends/cm and weft direction was 26 picks/cm. Structure was selected as woven fabric, they provide more stable conformation, higher density, smoother surface and low shrinkage than the knitted fabric.

Method

EMSE Measurement:

To measure the shielding effectives of textile materials, we have made small-enough pockets for the measurement device (Samsung Galaxy S3 Mini) to fit tightly. The cell-phone software interface is used to measure the signal strength between the cell-tower and the phone continuously. This allowed us to sample the signal strength values between the phone and a cell-tower.

We sampled the signal strength reported by the phone for each second and keep a log of required values for the EMSE measurement test. These values include the strength of the signal in terms of dBm (decibel-milliwatt), the percentage of the signal strength as well as the connected cell-tower id for each of the samples. The last kind of the logged items is especially important for the reliability of such measurements, as the source of the signal, the cell tower which the cell-phones connect to for each instance, cannot be controlled by the examiner. The phones are hard-coded to find the best signal bearing cell-tower to minimize its energy consumption and switches to a better cell-tower if there is a higher-powered cell-tower is available in its proximity. Indeed, during the measurement, the phone switched to different towers. Inclusion of signal measurements from different towers can lead to unreliable measurement results. To mitigate this, we increased the duration of the sampling to 300 minutes for each test, and then filter the strength measurements per a particular cell-tower id; which is placed in a known location. This allowed us to compute the distance between the experiment site and the cell-tower, thus validate the signal strength readings, which can be found in the Validation section. We also skip the first 90 samples (for duration of 90 seconds for each sample) in each measurement to avoid the durations where the experimenter manually exchanges the fabricated pockets.

To analyze the effect of different directions of the steel wires on the measurement, the fabric was cut into two pieces; wherein the first piece fabric the weft yarn is in parallel with the device's short edge and the second one, with weft yarn is in parallel to the device's long edge are labeled with letters, "A" and "B", respectively. Ply directions are illustrated in figure 4.

We began the experiment by putting the device "as it is" on a wooden desk surface allowing for it to receive the GSM signal in an ordinary setting, consisting ground truth (GT) readings. Then the first ply "B" is used to cover the device tightly (B); then a second ply "A" has been fitted on top of ply "B", consisting the vertical and horizontal layers touching each other (BA) and so forth (BAB and BABA in order). Thus, the recorded signal strength levels are labeled as, "GT", "B", "BA", "BAB", "BABA" such that the order of the letters, from left to right, signifies the order of the
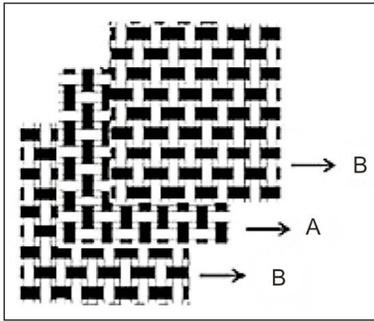
Fig. 4. Ply directions of the fabrics used for EMSE measurement

applied fabrics from inner side to the outer side. The results of the measurement can be found in the next section.

Validation of measurement based on Okumura-Hata Model:

The Okumura-Hata Model is the well-known method, which calculates link loss for mobile communication systems. This model is developed by Hata in [12] based on measurements reported by Okumura et al. [13]. The range of frequency is from 150 to 1500 MHz for this model. In addition to, the distance from the mobile phone to the base-station ranges from 1 to 20 km and the height of the mobile antenna is from 1 to 10 m. Link loss equation can be reduced for frequency as 900 MHz and the mobile antenna height of 1.5 m. For urban areas, it is given by [14]:

$$L_{loss} = 146.8 - 13.82 \log_{10} h +$$
$$+ (44.9 - 6.55 \log_{10} h) \log_{10} R \text{ [dB]} \qquad (1)$$

Where R is the distance from the mobile phone to the base station (km), h – the height of the base-station antenna ranges of from 30 to 200 m.

However, if GSM frequencies are around 1800 MHz, equation (1) is not valid for this case. Therefore, COST 231 Hata Model is developed for urban areas [15]. The model is used in the frequency range 1500 to 2000 MHz. Link loss can be given as:

$$L_{loss} = 157.3 - 13.82 \log_{10} h +$$
$$+ (44.9 - 6.55 \log_{10} h) \log_{10} R \text{ [dB]} \qquad (2)$$

according to COST 231 Hata Model [14]. To analyze the validity of our proposed system, we assume a GSM base-station antenna height such as 30 m and the equation reduced to:

$$L_{loss} = 136.9 + 35.2 \log_{10} R \text{ [dB]} \qquad (3)$$

We will consider equation 3 for the distance, $R = 0.416$ km, the approximate air distance between the cell tower and the cell phone. Hence, link loss is calculated as:

$$L_{loss} = 123.49 \text{ [dB]} \qquad (4)$$

The signal level (SL) can be basically calculated as:

$$SL = TP - L_{loss} \qquad (5)$$

Here, Transmitter Power (TP) is equal to $20 \log_{10} P$ (dB) and power ranges from 1 to 40 W, typically. In

Turkey, typical cell tower transmitter power is around 15.56 dB for 6 W.

Thus, the signal level (SL) is determined as 107.93 dB which is equal to –77.93 dBm from equation 5. Under the same conditions, measurement result with the system was approximately found as –77.62 dBm. These results show that the measurement and the theoretical values are in good agreement for GSM transmitter powers from 1 to 40 W, which validates our approach. We offer an alternative test to evaluate the shielding effectiveness of woven fabrics with SS component.

$SE = 20 \log (E1/E2) = 20 \log (H1/H2) = 10 \log (P1/P2)$ can be used for the evaluations, where the values of power $P1$, the electrical component $E1$ and the magnetic component $H1$ are measured without the shield, whilst the values $P2$, $E2$ and $H2$ are measured with the shield in place.

Statistical Evaluation:

To conduct statistical evaluation, SPSS 17.0 was used. Two-factor analysis of variance (ANOVA) on completely randomized samples was used as a fixed model to understand the statistical importance of fabric wrapping direction and turn numbers of the woven fabrics for the EMSE.

The mean values were compared by Student-Newman-Keuls (SNK) tests. All test results were assessed at a significance level of a £ 0.05. The treatment levels were marked in accordance with the mean values, and any levels marked by different letter (a, b, c) showed that they were significantly different.

RESULTS AND DISCUSSION

The measurement results can be found in table 2 with respect to their mean and standard deviations and box-plot figures.

Box-plot figures show the distribution of measurement results. In these figures, horizontal lines from top to bottom show the maximum; then the third, second (median), first quartiles and the minimum value of the distribution. The signal strength is plotted in figure 5 in dBm units, whereas figure 6 shows the signal strength in Percentage units. The percentage results bring no new information w.r.t. dBm plot in figure 5, they are given solely for reference, as they were used for ANOVA computation.

Table 2 shows the signal strength measurements (starting from "GT" and "B" to "BABA") where B and A represents fabrics positioned to provide perpendicular-located weft directions, as shown in figure 4. Measurement values are given in terms of means and standard deviations of signal strength values (dBm) and signal strength percentages (%).

Table 3 shows the signal strength reductions (from "B" to "BABA") where B and A represents fabrics positioned to provide perpendicular-located weft directions. Reduction values are given in terms of means of signal strength values (dBm) and signal strength percentages (%) w.r.t. to ground truth averages in each given unit.
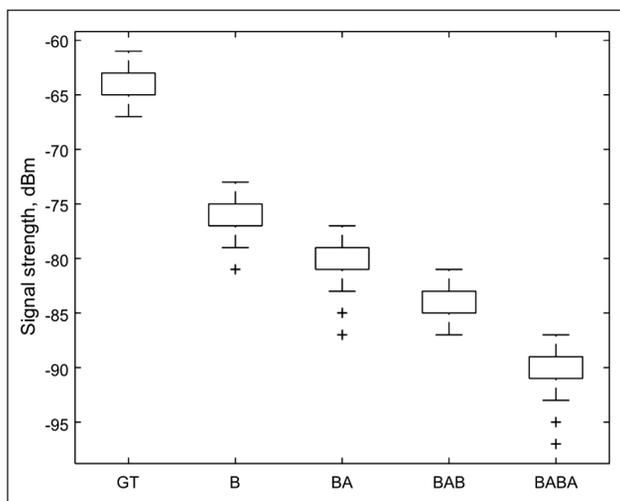
Fig. 5. Signal strength distributions in terms
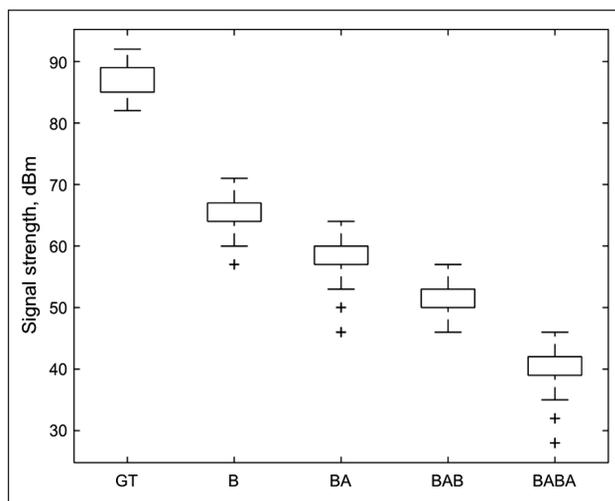of dBm reported by device interface

Fig. 6. Signal strength distributions in terms
of percentage reported by device interface

Table 2

Signal strength	Unit	GT	B	BA	BAB	BABA
Average	dBm	−63.37	−75.94	−80.81	−83.71	−90.63
Standard deviation		1.31	2.23	2.04	1.21	2.13
Average	%	88.16	65.63	57.04	51.96	39.39
Standard deviation		2.37	3.94	3.47	1.98	3.68

Table 3

Reduction from Ground Readings	B	BA	BAB	BABA
[dBm]	−12.58	−17.44	−20.34	−27.27
[%]	−22.53	−31.12	−36.21	−48.77

In table 3, the reduction values for each setting was calculated by subtracting the average of the signal strength reading from the average of a set, such as "B", from the average of Ground Truth ("Ground") readings. The results show that there is a linear relation w.r.t. the number of plies added to the device and is consistent along the experiments. Adding only a single-directed ply caused 12.58 [dBm] decrease in the signal strength; with addition of the second ply (perpendicular to the first one) increased the amount of reduction by 4.9 dBm putting a third layer in the same direction as the first one increased the reduction by 2.9 dBm. Lastly, adding the fourth layer increased the reduction by 6.92 dBm w.r.t. the prior one. As it is expected, increasing the number of layers increased the reduction. However, the most reduction is achieved when plies perpendicular to each other (BA and BABA sets) are applied to the device, which is expected since a mesh-like structure w.r.t. steel wire occurs in these settings.

Statistical analysis of experimental results

The results of the analysis of variance test (ANOVA) for EMSE values are summarized in table 4. The P values in table 4 indicated that there were statistically significant (5% significance level) differences between the EMSE values for different wrapping numbers of woven fabrics.

Table 4

Dependent Variable: EMSE					
Source	Sum of squares	df	Mean square	F	Sig.
Corrected model	1402.785[a]	3	467.595	43.870	.000
Intercept	18504.374	1	18504.374	1736.088	.000
Wrapping number	**1402.785**	**3**	**467.595**	**43.870**	**.000**
Error	85.269	8	10.659		
Total	19992.428	12			
Corrected total	1488.054	11			

[a] R squared = .943 (Adjusted R squared = .921)

Table 5

Student-Newman-Keuls[a,b]				
Wrapping number	**N**	**Subset[*]**		
		1	**2**	**3**
1B	3	25.48		
1BA	3		35.24	
1BAB	3		41.02	
1BABA	3			55.34
Sig.		1.000	.062	1.000

[*] The different subsets indicate that they are significantly different from each other at a significance level of 5 %.

The SNK test results for EMSE values (dB) of the sample fabrics are presented in table 5.

In table 5, SNK results shows that, the different type of wrapping numbers fabrics possessed statistically different EMSE values. The minimum EMSE value was 25.48 dB for the wrapping number 1B while the maximum EMSE value was 55.34 dB for the wrapping number 1BABA. There was statistical difference between the EMSE values for wrapping number 1B and 1BA and between the wrapping number 1BAB and 1BABA. Statistical significant difference was not observed between the EMSE values for wrapping number 1BA and 1BABA.

CONCLUSIONS

The purpose of this study was to present a new mobile based measurement method and evaluate electromagnetic radiation shielding effectiveness of woven fabrics made of composite yarns consisting stainless steel.

The mobile based method is designed for comparative EMSE measurements of fabric samples. To analyze usability of the proposed method the electromagnetic shielding effectiveness of fabric sample set was tested with the proposed method and obtained results were compared.

The effect of wrapping numbers of woven fabrics on EMSE values was found significant.

Another finding about the study was, the measurement and the theoretical values are in good agreement for GSM transmitter powers from 1 to 40 W, which validates our approach.

Lastly, it was proved that the presented new mobile based measurement method can be used safely for the evaluation of the electromagnetic radiation shielding effectiveness of textile fabrics.

BIBLIOGRAPHY

[1] Cifra, M., Fields, J.Z., Farhadi, A. *Electromagnetic cellular interactions*, In: ProgBiophysMol Bio, 2011; 105, pp. 223–246.

[2] Hardell, L., Sage, C. *Biological effects from electromagnetic field exposure and public exposure standards*, In: Biomed Pharmacother, 2008, 62, pp. 104–109.

[3] Hocking, B., Westerman, R. *Neurological effects of radiofrequency radiation*, In: Occup Med (Lond) 2003, 53, pp. 123–127.

[4] Zamanian, A., Hardiman, C. *Electromagnetic radiation and human health: a review of sources and effects*, In: High Frequency Electronics, Summit Technical Media, 2005, pp. 16–26.

[5] Gandhi, O.P. *Electromagnetic fields: human safety issues*, In: Annual Review of Biomedical Engineering, 2002; 4(1), pp. 211–234.

[6] Örtlek, H.G., Gunesoglu, C., Okyay, G., Türkoğlu, Y., *Investigation of electromagnetic shielding and comfort properties of single jersey fabrics knitted from hybrid yarns containing metal wire*, In:TekstilveKonfeksiyon, 2012, vol.22, pp. 90–101.

[7] Grabowska, K.E., Marciniak, K., Ciesielska, W., Izabela L. *The analysis of attenuation of electromagnetic field by woven structures based on hybrid fancy yarns*, In: Textile Research Journal, 2011, 81 (15), pp. 1578–1593.

[8] Bedeloğlu, A. *Electrical, electromagnetic shielding, and some physical properties of hybrid yarn-based knitted fabrics*, In: Journal of The Textile Institute, 2013, vol. 104, no. 11, pp. 1247–1257.

[9] Chen, H.C., Lee, K.C., Lin, J.H. *Electromagnetic and electrostatic shielding properties of co-weaving-knitting fabrics reinforced composites,* In: Applied Science and Manufacturing, 2004, vol. 35, pp. 1249–1256.

[10] Türksoy, E. S., Saritas, Ö.,Üstüntag, S., Saraçoglu, Ö. G. *Simulation of electromagnetic shielding test results based on differential evaluation algorithm*, In: IndustriaTextila, 2015, 66(4), pp.184–191.

[11] Šafářová, V., Tunák, M., Truhlář, M., Militký, J. *A new method and apparatus for evaluating the electromagnetic shielding effectiveness of textiles*, In: Textile Research Journal, 2016, 86(1), pp. 44–56.

[12] Barclay, L. (ed.), *Propagation of radio waves*, 2nd edition (London: IEE), 2003.

[13] Ogbulezie, J.C. et al., *Propagation models for GSM 900 and 1800 MHz for Port Harcourt and Enugu*, In: Nigeria, Network and Communication Technologies, 2013, vol. 2, no. 2.

[14] Christopher Haslett, *Essentials of radio wave propagation*, Ofcom, UK, Cambridge University Press, 2008.

[15] European Commissïon COST Action 231, *Digital mobile radio towards future generation systems'*, (Brussels: European Commission), 1999.

Authors:

ERHAN KENAN ÇEVEN[1]
AHMET KARAKÜÇÜK[2]
AHMET EMİR DİRİK[3]
UĞUR YALÇIN[4]

[1] Uludag University
Faculty of Engineering
Textile Engineering Department
Görükle Campus,16059-Nilüfer-Bursa-Turkey

[2] Uludag University
Faculty of Engineering
Electrical and Electronics Engineering Department
Görükle Campus,16059-Nilüfer-Bursa-Turkey

[3] Uludag University
Faculty of Engineering
Computer Engineering Department
Görükle Campus,16059-Nilüfer-Bursa-Turkey

[4] Uludag University
Faculty of Engineering
Electrical and Electronics Engineering Department
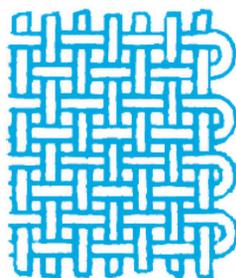Görükle Campus,16059-Nilüfer-Bursa-Turkey

e-mail: rceven@uludag.edu.tr , akarakucuk@uludag.edu.tr,
edirik@uludag.edu.tr, uyalcin@uludag.edu.tr

Corresponding author:

AHMET KARAKÜÇÜK
akarakucuk@uludag.edu.tr

Alternative dressings used for treating major burns

DANA VASILESCU
SABINA IONITA
EMILIA VISILEANU

VICTOR GRAMA
ADRIAN PELINARU
ALEXANDRU-LAUTENȚIU CHIOTOROIU

REZUMAT – ABSTRACT

Pansamente moderne utilizate pentru tratamentul arsurilor majore

Context: Pretutindeni, leziunile de arsură sunt una dintre cele mai importante cauze de morbiditate și mortalitate, cu costuri ridicate pentru sistemul sanitar. Arsurile cu profunzime parțială necesită pansamente care sunt foarte scumpe și care trebuie schimbate foarte des. Dacă aceste tipuri de arsuri nu sunt tratate adecvat, acestea se pot infecta, pot determina cicatrici vicioase și se pot aprofunda și deveni arsuri pe toată grosimea.

Obiectiv: Revizuirea literaturii medicale în ceea ce privește utilizarea diferitelor pansamente pentru managementul arsurilor majore.

Surse de date și selecția studiului: Articolele referitoare la utilizarea biomaterialelor au fost selectate din articole relevante publicate în perioada 1991–2017.

Toate cercetările au folosit termeni precum: pansamente pentru arsuri, managementul arsurilor cu grosime parțială, pansamente moderne pentru arsuri. Au fost cercetate ulterior informații relevante din articole.

Sinteză informații: Optsprezece studii au fost considerate relevante pentru această analiză. Acest articol analizează diferite pansamente utilizate pentru tratamentul leziunilor de arsură. Există numeroase tipuri de pansamente ce pot fi utilizate într-o unitate de arsuri, incluzând: Xeroform, pansamente biologice, pansamente impregnate cu argint, pansamente hidrocoloide, pansamente cu peliculă de poliuretan, pansamente cu hidrogel, pansamente de nylon acoperite cu silicon, substituenți biosintetici de piele și pansamente în cercetare.

Concluzii: Studiile viitoare trebuie să evidențieze tipurile noi de pansamente ce pot fi utilizate pentru a maximiza calitatea epitelizării, pentru a minimiza timpul necesar pentru a crea tegumente noi, pentru a permite scăderea formării de țesut fibros și pentru a minimiza rata complicațiilor, precum riscul de infecții, liza epiteliului nou format și alte afecțiuni ale tegumentului și a complicațiilor generale. Este necesar a fi studiate toate aceste aspecte pentru a se realiza pansamentul cu caracteristici optime, ce va determina rezultate excelente.

Alternative dressings used for treating major burns

Context: Across the globe burn injuries are one of the most important cause of morbidity and mortality, with great costs for health care. Partial-thickness burns require dressings that are very expensive and that must be changed very often. If these types of burns are not treated adequate they can get infected, leave vicious scars and even deepen to become full-thickness burns.

Objective: To review the medical literature regarding the use of different dressings in treated major burn wounds.

Data sources and study selection: The articles regarding the use of dressings were selected from articles published between 1991 and 2017. All searches used the terms dressings for burn wounds, partial thickness burns management, modern burn dressings. Relevant information from the articles was further researched.

Data synthesis: Eighteen studies were considered relevant for this review. This article reviews different dressings used for burn wounds. There are many types of dressings that can be used in a burn unit, including: Xeroform petrolatum gauze, biological dressings, silver-impregnated dressings, hydrocolloid dressings, polyurethane film dressings, hydrogel dressings, silicon coated nylon dressings, biosynthetic skin substitute dressings and newly researched dressings.

Conclusions: Future studies must demonstrate further dressings that can be used to maximize the epitelisation quality, to minimize the time necessary for creating new skin, to permit to form less fibrous tissue and to minimize the complication rate like the infection risk, the lysis of the newly formed epithelium and other skin diseases and general complications. We have to research all these aspects in order to discover the ideal dressing for excellent results.

INTRODUCTION

Across the globe burn injuries are one of the most important causes of morbidity and mortality, with great costs for health care. Most of the burn injuries, according to many demographic studies take place in low or middle income countries (90%) because of the alternative methods of heat and of cooking. Another important fact is that many children suffer from burn injuries that will give them long term disabilities, especially in countries that don't have adequate resources for treatment of burns in an acute setting, few or none burn centers and very expensive treatment options [1–2]. Partial-thickness burns can be divided in superficial and e papillary dermis deep. The superficial partial thickness burns affects the papillary dermis, with moderate oedema and intact blisters, with bright pink or red color and the deep partial-thickness burns affect the papillary and reticular dermis with broken blisters, important oedema and white color [7].

Partial-thickness burns require dressings that are very expensive and that must be changed very often. If these types of burns are not treated adequate they

can get infected, leave vicious scars and even deepen to become full-thickness burns [1].

There are needed efficient, cost effective and easily available dressings for taking care of burn wounds. Dressings have to accelerate wound healing, protect the wound from infection and lower the leakage from the burn wound to minimize the fluids, electrolytes and proteins lost for the burn wound [7]. There are many types of dressings used now for these types of burns: Mepilex, Mepilex Ag, Xeroform petrolatum gauze.

Classic dressings consist of paraffin gauze, and silver sulfadiazine (SSD). Modern dressings consist of hydrocolloid, hydrofibre, silicones, alginates and polyurethane [7]. The gold standard for partial-thickness burns remains the SSD which dries the wound. The advantage of using the modern dressings is that they maintain a wet environment. They can protect the wound form the pathogenic bacteria [7].

The goal of using dressings for burn wounds is to prevent infection, limit pain, and decrease metabolic demand [8]. We can use with good results biological dressings which lower the complication rate, promote healing and minimize the risk for vicious scars [8].It is important to provide healthcare professionals with information about the pathophysiology of burn wound progression and to choose the best types of burn wound dressings and to know the indications for different types of dressings in different burn depths relating to the latest studies [10].

The plastic surgeon must understand the pathophysiology that underlies the wound-healing process to make informed decisions about the best patient management [11–13]. Our article provides an overview of optimal conditions for healing and the assessment of burn wounds dressings. Types of burn wound dressings and their model of action are discussed to provide guidance for use in different clinical settings.

The remaining question is related with the most effective dressing to use for this type of burn injuries, regarding the epithelisation time, minimizing of complications, cost of the product, the availability of it and the long time results.

MAIN PART OF THE REVIEW

The management of partial thickness burns includes general and local treatment, well defined for the depth of the wound and for the surface area burned. The types of burn dressing used for partial thickness burns include:
• Xeroform petrolatum gauze;
• Biological dressings;
• Silver-impregnated dressings;
• Hydrocolloid dressings;
• Polyurethane film dressings;
• Hydrogel dressings;
• Silicon coated nylon dressings;
• Biosynthetic skin substitute dressings;
• Newly researched dressings.

TYPES OF BURN DRESSINGS

Xeroform petrolatum gauze

Xeroform petrolatum gauze is made of a mixture of petroleum and bismuth tribromophenate which is impregnated into fine mesh sterile gauze [1]. Petroleum lets the wound to retain moisture, creating an occlusive dressing and bismuth tribromophenate is an antimicrobial agent [1]. In some studies this gauze is preferred to **DuoDERM, Kaltostat, Biobrane, Aquacel, Mepilex and Jelonat** because it is cheaper, stable, it can be stored at room temperature and it facilitates rapid re-epithelialization [1–5]. Arhana Chattopadhyay et al. studied an alternative for Xeroform that is cheaper and can be easily prepared. This is made by mixing Vaseline (Unilever, Rotterdam, Netherlands) with 3% bismuth tribromophenate powder by weight (Dudley Corp., Lakewood, N.J.) The colloid suspension that resulted was spread onto Kerlix gauze (Covidien, Dublin, and Republic of Ireland). The dressing macroscopically resembles Xeroform concerning color and consistency. This dressing is cheaper that using Xeroform and can be easily done by hand [1]. This type of dressing made by hand is has at least the same bacteriostatic to *E. coli* growth compared with Xeroform and it has the same cytotoxicity level as Xeroform. This type of dressing can be made by hand from raw materials at 34% of the cost of Kendall Xeroform, which is the least expensive brand [1].

It is important to do further research regarding the antimicrobial activity for this type of dressing for *Pseudomonas*, *Acinetobacter*, *Klebsiella*, and *Staphylococcus aureus* [6].

The effect on time to wound closure and burn heal is the same for all the dressing types studied.

As a conclusion to this study, an effective, safe and inexpensive bismuth-petrolatum dressing can be produced by hand [1]. This dressing is antimicrobial, can protect wounds during re-epithelialization and is biocompatible [1].

Biological dressings. Bovine collagen sheets

Collagen is a unique protein with consists of a triple helix, each helix has over 1000 amino acids. There are many types of collagen in the human body, of which the main type in skin is type I collagen. For dressings we can use bovine collagen, which chemically is very similar to the human collagen. Bovine collagen sheets are comprised mostly of type I and III collagens. The granulation of the tissue covered with bovine collagen developed at a normal rate and the cellular events are then same at the events taking place in normal wounds which are healed using classic methods [8].

Collagen sheets are used especially in first- and second-degree burns. The costs and pain related to changing the dressing can be avoided using only a single collagen dressing, especially in children [8].

The biologic characteristics of collagen are: noninflammatory, nontoxic, noncarcinogenetic, has minimal degradation and low antigenicity, collagen facilitates

migration of fibroblasts and microvascular cells, and promotes the synthesis of neodermal collagen matrices, that concludes in minimization of forming of scarring tissue [8].

Collagen bovine sheets are elastic, have good tear strength, are soft, supple, impermeable to bacterial migration, modulate fluid flux from the wound and have no clinical significant immunological or histological responses and are not rejected by the human body. They have a perfect biocompatibility. They lack the threat of infectious diseases as bovine collagen is obtained from countries free of bovine spongiform encephalopathy. This bovine collagen sheets poses long shelf life under normal storage conditions [8].

The action of metalloproteinases is inhibited by the use of bovinecollagen dressing Collagen represents a template for the infiltration of fibroblasts, macrophages, and lymphocytes and attracts monocytes to the wound site, increasing the neovascularisation by increasing the formation of capillaries. As healing progresses, collagen is produced and deposited by the fibroblasts, this newly formed collagen replaces the collagen portion of the collagen sheet [8].

Singh et al. demonstrate that the bovine collagen sheets hastens the wound, lower the need for a skin graft and reduces scar contracture. Biobrane dressing can lower pain related to the changing of the dressing, decrease total healing time, the hospitalization stay and improves the compliance of the patients. The use of bioengineered skin substitutes improves the outcome of partial-thickness facial burns compared to the standard open topical ointment technique [8].

The result of using bovine collagen sheets is very good regarding early recovery and less pain, with no side effects of collagen application [8].

Silver-impregnated dressings

These types of dressings are preferred over silver sulfadiazine cream in management of pediatric burns. They provide a wet and sterile environment, which don't require painful dressing change. There are many types of silver-impregnated dressings, like silver sodium carboxymethyl cellulose dressing (**Aquacel Ag**, ConvaTec, Greensboro, NC), nano-crystalline silver-coated polyethylene dressing (**Acticoat**, Smith & Nephew, London, UK), **Contreet** (Hydrocolloid with silver), **Avance** (foam with silver) [9, 12].

Both types of dressings have the same infection and escalation care rate, which is very rare, Aquacel Ag requires less dressing change than Acticoat. Both dressings are effective, they allow epithelisation and prevent infection. Aquacel may be superior to Acticoat because requires fewer dressing changes and direct manipulation of the wound, which can cause discomfort to the patient and require additional interventions and enhances pain for the patient [9]. Acticoat deliversnano-crystalline silver and Aquacel Ag consists of a fibre dressing with silver [12].

Atrauman Ag (figure 1) is a new silver-containing ointment dressing that has antimicrobial properties with low cellular toxicity. The cytotoxicity for HaCaT keratinocytes was 10%, regarding the slough score, the proportion was reduced from 59.2 to 35.8%, the formation of granulation tissue increased from 27 to 40% and epithelialisation raised from 12.1 to 24%. Atrauman Ag has superior antimicrobial activity compared to cellular toxicity and the low silver ion release rate prevents interference with natural wound-healing mechanisms [11].

The chitosan-based silver dressing has good results in new studies on children regarding the lack of shrinkage of the dressing when is moist form the
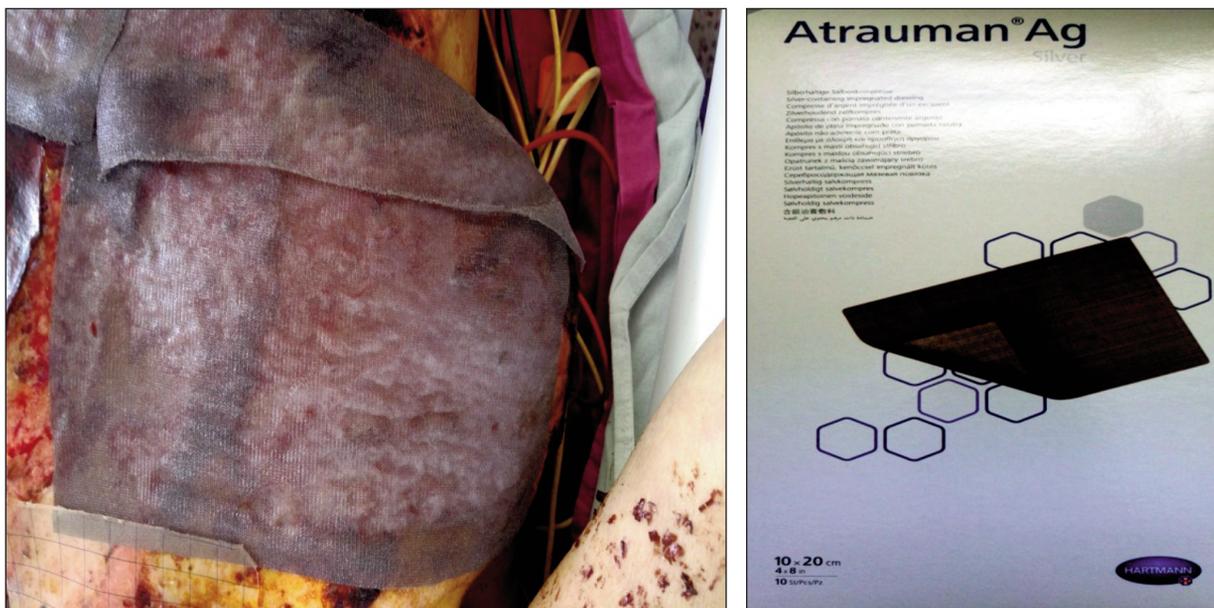

Fig. 1. New silver-containing ointment dressing

Fig. 2. Antimicrobial dressing

Fig. 3. DuoDerm-hydrocolloid dressings

wound exudate, the lack of infection of the wound site and normal time of epithelisation because it offers an optimal environment for moist wound management, and did not demonstrate the shrinkage or disintegration like when using the hydrofibre dressings. The chitosan-based silver dressing is deserving of further study as an alternative to traditional burn dressings [15].

A new, next-generation antimicrobial dressing (**NGAD; AQUACEL Ag+ EXTRA dressing** – figure 2) is widely studied in many countries in managing wound exudate, infection and biofilm, and facilitating progression toward healing. The studies have demonstrated important improvements in wound health, time of healing and size, and in some cases, complete healing [16].

Electrospun mats consisting of polycaprolactone (PCL) and polyvinyl alcohol (PVA) incorporated with silver sulfadiazine (SSD) can be used as antimicrobial wound dressings with the capability of cell seeding. This dressing is coated with fibronectin to enhance the biocompatibility of the scaffold incorporated with SSD particles. Those mats have a hydrophilic surface that can adhere to the wound bed. The electrospun mats that have SSD particles have the property to increase the fiber diameter and have also hydrophilic properties, the SSD particles weaken the mechanical characteristics of the electrospun mats. The best concentration of SSD is demonstrated to consist of 5 weight % SSD/PVA as it has a desirable fiber quality for the mats, also those electrospun mats have good antimicrobial properties and great cell proliferation on the surface [18].

Hydrocolloid dressings

There are many types of hydrocolloid dressings like **Comfeel** (Coloplast) and **DuoDerm** (ConvaTec) – figure 3. These types of burn dressings contain gelatin, pectin and sodium carboxymethylcellulose in an adhesive polymer matrix. When the inner layer of those dressings come in contact with exudates form a gel which many authors demonstrate that facilitates autolytic debridement of the wound [12].

Polyurethane film dressings

The most popular is represented by the polyurethane film dressings that consist of **OpSite** (Smith & Nephew) or **Tegaderm** (3M Company). Those dressings are permeable to water vapour oxygen and carbon dioxide but not to liquid water or bacteria, transparent, adhesive-coated sheets that can be applied directly to the wound. Those types of dressings can be used for lightly exuding wounds [12].

Hydrogel dressings

Hydrogel dressings can be used in amorphous form: **IntraSite** (Smith & Nephew), figure 4, and Solugel or in sheet hydrogels where the gel is presented with a fixed three dimensional macro structure that include **Aqua clear** and **Nu-gel** (Johnson & Johnson), figure 5 [12].

Those dressings are high water content gels containing insoluble polymers, which have an amount of absorptive properties that concludes the use of those dressings for moderate exudative wounds, compared with Polyurethane film dressings which aren't used for exudative wounds [12].

Those polymers include modified carboxymethylcellulose, hemicellulose, agar, glycerol and pectin. Their fluid donating properties assist wound debridement and also in maintaining a moist wound environment [12].

Silicon coated nylon dressings

Silicon coated nylon dressings like **Mepitel** (Mölnlycke) consist of a flexible polyamide net coated

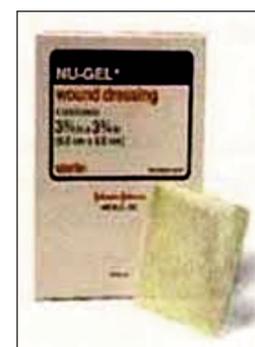Fig. 4. IntraSite-Hydrogel dressings

Fig. 5. Nu-gel-Sheet hydrogels

Fig. 6. Safe^ac-Silicon coated

Fig. 7. Stratatsorb-Silicon coated

gas and fluid exchange which provides both protection from bacterial influx and mechanical coverage [12].

Newly researched dressings

As we all know dermal fibrosis has limited effective therapeutic modalities and the physicians need to create an anti-scarring dressing. Malihe-Sadat Poormasjedi-Meibod et al developed a new antiscarring dressing and investigated its potential as a slow-releasing vehicle for kynurenic acid (KynA), an antifibrotic agent which was incorporated into polymethyl methacrylate (PMMA) nanofibers, with increasing concentration of polyethylene glycol (PEG). *In vivo* application of KynA-incorporated films significantly inhibited collagen (23.89 ± 4.79 vs. 6.99 ± 0.41, collagen-I/β-actin mRNA expression, control vs. treated) and fibronectin expression (7.18 ± 1.09 vs. 2.31 ± 0.05, fibronectin/β-actin mRNA expression, control vs. treated) and enhanced the production of an ECM-degrading enzyme (2.03 ± 0.88 vs. 11.88 ± 1.16 MMP-1/β-actin mRNA expression, control vs. treated). The fabricated KynA-incorporated films can be exploited as antifibrotic wound dressings (© 2016 Wiley Periodicals, Inc. J Biomed Mater Res Part A: 104A: 2334–2344, 2016) [17]. Those new dressings require clinical trials and many other studies to demonstrate the efficacy of the products.

with soft silicone that don't have any biological component. Their mesh structure allows drainage of exudate from the burned surface which is non-adherent and can be changed with no side effects [12]. Some other types of silicon coated: Safet^ac (figure 6) and Stratatsorb (figure 7).

Biosynthetic skin substitute dressings

Biosynthetic skin substitute dressings consist of **Biobrane** (Dow Hickam/Bertek Pharmaceuticals), and **Trans Cyte** (Advanced Tissue Sciences). Those dressings have been developed to mimic the function of skin by recreating the epidermis or dermis, or both (figure 8). Those manufactured epidermal substitutes allow for re-epithelization to occur while permitting a
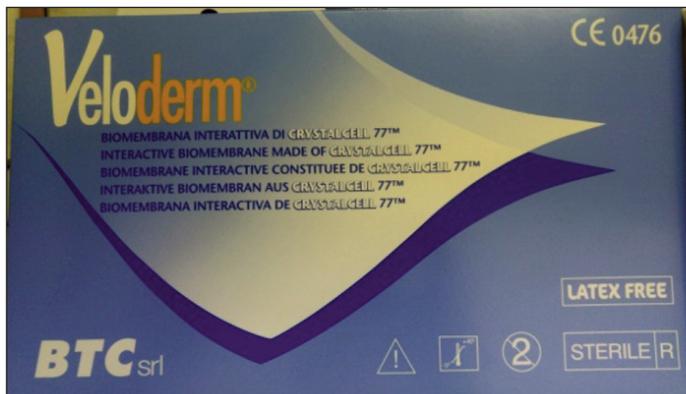

Fig. 8. Biosynthetic skin

CONCLUSIONS

There are many studies and many protocols involving the burn wounds treatment, including special dressings used for enhancing epithelisation and for reducing the infection risk and surgical management. The steps that must be followed in a burn wound are determined regarding the degree and the surface of the burn area.

For first degree burns the treatment is very easy. They can be treated without any dressings. In children they can be treated using low-adherent dressing (e.g. Mepitel™ + Melolin™) because children have a tendency to blister or scratch [14].

Partial thickness burns (second degree) can be treated using different dressings concluded in our study. For small, superficial partial thickness burn wounds, a low adherent dressing (e.g. BactigrasTM + Melolin™ or Mepilex-AgTM). For more extensive or deeper partial thickness burn wound we can use a low-adherent silver dressing (e.g. Acticoat™ or Acticoat 7™) [14].

It is very important to understand that every type of burn wound must be treated accordingly to the international protocols but we have to remember that every patient can have specific medical problems that have to be taken into account in order to accomplish the best results possible.

There are many types of dressings that can be used in a burn unit, including: Xeroform petrolatum gauze, biological dressings, silver-impregnated dressings, hydrocolloid dressings, polyurethane film dressings, hydrogel dressings, silicon coated nylon dressings, biosynthetic skin substitute dressings and newly researched dressings.

In the international literature many studies demonstrate the superiority of expensive dressings and other complementary treatments, but we have to understand that in every country there are ethical, legal and financial problems that must be taken into consideration in order to manage a burn patient. There are many studies from developing countries that explain that some simple dressings like Xeroform petrolatum gauze and its hospital made analogs have very good results that can be compared with those of expensive dressings. Future studies must demonstrate further dressings that can be used to maximize the epitelisation quality, to minimize the time necessary for creating new skin, to permit to form less fibrous tissue and to minimize the complication rate like the infection risk, the lysis of the newly formed epithelium and other skin diseases and general complications. We have to research all these aspects in order to discover the ideal dressing for excellent results.

BIBLIOGRAPHY

[1] Arhana Chattopadhyay, Kathleen Chang, Khoa Nguyen, Michael G. Galvez, Anais Legrand, Christopher Davis, *An inexpensive bismuth-petrolatum dressing for treatment of burns,* In: PRS Global Open, 2016, DOI: 10.1097/GOX.0000000000000741, www.PRSGlobalOpen.com.

[2] Atiyeh, B., Masellis, A., Conte, C. *Optimizing burn treatment in developing low-and middle-income countries with limited health care resources* (Part 2)*,* In: Ann Burns Fire Disasters, 2009:22, pp.189–195.

[3] Malpass, K.G., Snelling, C.F., Tron, V. *Comparison of donorsite healing under Xeroform and Jelonet dressings: unexpected findings,* In: PlastReconstrSurg, 2003; 112, pp. 430–439.

[4] Masella, P.C., Balent, E.M., Carlson, T.L., et al. In: *Evaluation of six split-thickness skin graft donor-site dressing materials in a swine model,* In: PlastReconstrSurg Glob Open, 2013; 1:e84.

[5] Feldman, D.L., Rogers, A., Karpinski, R.H. In: *A prospective trial comparing Biobrane, Duoderm and xeroform for skin graft donor sites,* In: Surg Gynecol Obstet, 1991; 173, pp. 1–5.

[6] Rezaei, E., Safari, H., Naderinasab, M., et al. *Common pathogens in burn wound and changes in their drug sensitivity,* In: Burns, 2011; 37, pp. 805–807.

[7] Jiang, Q., Chen, Z-H., Wang, S-B., et al. In: *Comparative effectiveness of different wound dressings for patients with partial-thickness burns: study protocol of a systematic review and a Bayesian framework network meta-analysis*, In: BMJ Open 2017; 7: e013289, doi:10.1136/bmjopen-2016-013289.

[8] Waghmare, M., Shah, H., Tiwari, C., Makhija, D., Desale, J., Dwivedi, P. *Collagen dressings in the management of partial thickness pediatric burns: Our experience*, In*:* Indian J Burns 2016; 24:53-7.

[9] Brown, Matthew MBChB; Dalziel, Stuart R. FRACP, PhD; Herd, Eleanor RGON, BA, MN (Child and Family); Johnson, Kathryn BSc, MN, NP; Wong She*,, A randomized controlled study of silver-based burns dressing in a pediatric emergency department,* In: Journal of Burn Care & Research: July/August 2016, Volume 37, Issue 4, p e340–e347, doi: 10.1097/BCR.0000000000000273.

[10] Douglas, Helen E. and Wood, Fiona, *Burns dressings [online],* In: Australian Family Physician, vol. 46, no. 3, Mar 2017, pp. 94–97. Availability:<http://search.informit.com.au/documentSummary;dn=673300860640654;res= IELHEA, ISSN: 0300-8495.

[11] Ziegler, K., Görl, R., Effing, J., Ellermann, J., Mappes, M., Otten, S., Kapp, H. *Reduced cellular toxicity of a new silver-containing antimicrobial dressing and clinical performance in non-healing wounds,* In: Skin Pharmacol Appl Skin Physiol 2006; 19, pp. 140–146, https://doi.org/10.1159/000092594.

[12] Wasiak, J., Cleland, H., Campbell, F. *Dressings for superficial and partial thickness burns,* In: Cochrane Database of Systematic Reviews 2008, Issue 4. Art. No.: CD002106. DOI: 10.1002/14651858.CD002106.pub3.

[13] Tarig Abdelrahman, Heather Newton, *Wound dressings: principles and practice,* In: DOI: http://dx.doi.org/10.1016/j.mpsur.2011.06.007, October 2011 Volume 29, Issue 10, pp. 491–495.

[14] The Royal Childrens Hospital Melbourne Clinical Practice Guidelines, *Burns / management of burn wounds*, In: http://www.rch.org.au/clinicalguide/guideline_index/Burns/

[15] Massand, S., Cheema, F., Davis, J., USB. Burkey, USP.M. Glat, *The use of a chitosan dressing with silver in the management of paediatric burn wounds: a pilot study,* In: DOI: http://dx.doi.org/10.12968/jowc.2017.26.Sup4.S26, Published Online: April 05, 2017

[16] D. Metcalf, PhD, Associate Director, Research & Development; D. Parsons, PhD, Director, Science & Technology; P. Bowler, MPhil, Vice President, Science & Technology; *A next-generation antimicrobial wound dressing: a real-life clinical evaluation in the UK and Ireland*, In: Journal of Wound Care, vol. 25, nr. 3, march 2016.

[17] Malihe-Sadat Poormasjedi-Meibod, Mohammadreza Pakyari, John K. Jackson, Sanam Salimi Elizei, Aziz Ghahary, *Development of a nanofibrous wound dressing with an antifibrogenicproperties* in vitro *and* in vivo*model*, In: Volume 104, Issue 9, September 2016, pp. 2334–2344.

[18] Mina Mohseni, Amir Shamloo, Zahra Aghababaei, Manouchehr Vossoughi, Hamideh Moravvej, *Antimicrobial wound dressing containing silver sulfadiazine with high biocompatibility: in vitro study, artificial organs,* In: Journal, Volume 40, Issue 8, August 2016, pp. 765–773, First published: 20 April 2016,DOI: 10.1111/aor.12682

Authors:

DANA VASILESCU[1]
SABINA IONITA[1]
ALEXANDRU CHIOTOROIU[1]
EMILIA VISILEANU [3]
VICTOR GRAMA[2]
ADRIAN PELINARU[1]

[1] Plastic and Reconstructive Surgery – Floreasca Hospital Emergency Bucharest Romania

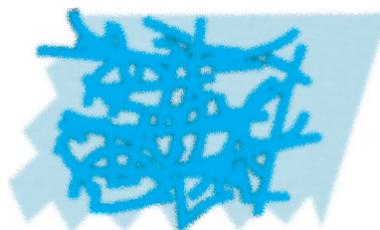[2] General Surgery – Floreasca Hospital Emergency Bucharest Romania

All authors had equal contribution to this article

[3] The National Research and Development Institute for Textile and Leather

Corresponding author:

Dr. DANA VASILESCU
dr.danavasilescu@hotmail.com

Hydrothermal route to (Fe, N) codoped titania photocatalysts with increased visible light activity

L. DIAMANDESCU
M. FEDER
F. VASILIU

L. TANASE
ARCADII SOBETKII

I. DUMITRESCU
M. TEODORESCU
T. POPESCU

REZUMAT – ABSTRACT

Ruta hidrotermală a fotocatalizatorilor de dioxid de titan codopaţi cu Fe şi N cu activitate sporită în lumina vizibilă

Nanoparticulele de TiO_2 dopate cu fier şi azot au fost sintetizate şi investigate cu scopul de a obţine sisteme fotocatalitice cu o eficienţă sporită în lumina vizibilă. În prima etapă, Degussa P25, disponibilă pe piaţă, a fost impregnată cu fier (0.3, 0.5 şi 1 at. %) şi azot în condiţii hidrotermale. În cea de-a doua etapă, TiO_2 dopat cu Fe-N a fost sintetizat prin ruta hidrotermală pornind de la $TiCl_3$, $FeCl_3 \cdot 6H_2O$ şi uree, la 200°C timp de 2 ore. Toate probele au fost tratate la 400°C timp de 2 ore. Difracţia de raze X (XRD) a evidenţiat o compoziţie pe scară nano în două faze (Anatase and Rutile) a Degussa P25 şi un conţinut Anatase monofazat pe scară nano a probei de TiO_2 dopat cu Fe-N (1at.%) sintetizat hidrotermal. Prezenţa fierului şi a azotului în probe a fost confirmată de măsurătorile Mössbauer şi spectroscopia fotoelectronica de raze X (XPS). Microscopia electronică de transmisie (TEM) a evidenţiat structura, dimensiunea şi morfologia particulelor. Măsurătorile fotocatalitice (bazate pe degradarea albastrului de metilen) au evidenţiat cea mai eficientă compoziţie din seria TiO_2 Degussa P25 ca fiind corespunzătoare la 1 at.% Fe, atât în spectrul UV, cât şi în cel vizibil. În acelaşi timp, proba de TiO_2 dopat cu Fe-N (1at.%) sintetizată hidrotermal a prezentat cea mai bună activitate în spectrul vizibil. Sistemele pe scară nano au fost sintetizate în scopul testării pe material textil.

Cuvinte-cheie: hidrotermal, dioxid de titan, fotocataliză, lumină vizibilă

Hydrothermal route to (FE, N) codoped titania photocatalysts with increased visible light activity

Iron and nitrogen doped TiO_2 nanoparticles were synthesized and investigated with the aim to obtain photocatalytic systems with enhanced visible light efficiency. In a first step, commercially available Degussa P25 was impregnated with iron (0.3, 0.5, and 1 at. %) and nitrogen under hydrothermal conditions. In the second step, Fe-N doped TiO_2 was synthesized by a hydrothermal route starting with $TiCl_3$, $FeCl_3 \cdot 6H_2O$ and Urea, at 200°C for 2 h. All samples were post annealed at 400°C for 2h. The X-ray diffraction (XRD) revealed a two phase nanoscaled composition (Anatase and Rutile) of Degussa P25 and a single phase-nanoscaled Anatase content of the hydrothermally synthesized (1at.%) Fe-N doped TiO_2 sample. The presence of Fe and nitrogen in samples was confirmed by Mössbauer and X-ray photoelectron spectroscopy measurements (XPS). Transmission electron microscopy (TEM) revealed the structure, particle dimension and morphology. The photocatalytic measurements (based on degradation of Methylene Blue) evidenced the most efficient composition in TiO_2 Degussa P25 series as corresponding to 1 at.% Fe, in both UV and visible spectrum. At the same time, the hydrothermal synthesized sample (1at.%) Fe-N doped TiO_2 exhibits the best activity in visible spectral region. The nanoscaled systems were synthesized in view of tests on textile materials.

Keywords: hydrothermal, titania, photocatalysis, visible light

INTRODUCTION

Titania (TiO_2) is the most important photocatalyst. The principal drawback of TiO_2 is caused by its characteristic band gap of about 3.2 eV which allows only the use of UV radiation (~5% from the solar spectrum). Many efforts were focused to extend the absorption range to visible region of solar spectrum, maintaining photocatalytic activity [1]. One route was the doping or codoping of TiO_2 with different cation or anions [2–3]. Owing to its unique half-filled electronic configuration, which could narrow the band gap energy through the appearance of intermediate energy levels, Fe^{3+} was frequently used [2]. Fe^{3+} dopant proved to be better than Ru^{3+}, V^{4+}, Mo^{5+}, Os^{3+}, and Re^{5+} [3]. It is accepted that the Fe^{3+} substituting Ti^{4+} within TiO_2 lattice can reduce the electron–hole recombination rate and improve the photocatalytic efficiency. The photocatalytic performance of cation doped TiO_2 is still modest. Theoretical calculations showed that essential improvements could be expected by anion (C, S, N, F, B) doping [1]. There are a lot of experimental papers reporting relevant red shift and photocatalytic efficiency increase [4–6]. Synergistic effects are expected by cation-anion codoping [1].

It is well known the materials properties are strongly dependent on raw materials and synthesis procedure. In order to study the effect of Fe and N codoping on TiO_2 efficiency we impregnated Degussa P25 photocatalyst under hydrothermal conditions – in a first step; in a second one we synthesized Fe-N doped TiO_2 by a hydrothermal route. In both cases

the samples were postannealed at 400 °C. The structural and photocatalytic properties of the obtained samples are presented.

EXPERIMENTAL

Preparation

The (Fe, N) impregnation of TiO_2 Degussa P25 powder, was performed as follows: adequate amounts of TiO_2 (Aeroxide®P25), $FeCl_3 \cdot 6H_2O$ and Urea (Reagent) were dispersed/dissolved under mechanical and ultrasonically stirring in distilled water. The resulted mixture was hydrothermally treated at 200 °C for 2 h in a Teflon lined autoclave. The resulted powder was washed with distilled water to remove salts until pH ~ 6.5, then was dried and calcined at 400 °C for 2 h, in air. Three iron concentrations have been considered in preparation: 0.3; 0.5 and at.1%. For the synthesis of 1 at.% Fe and N codoped TiO_2, adequate amounts of $TiCl_3$ and $FeCl_3 \cdot 6H_2O$ were introduced under vigorous stirring in distilled water. The pH was adjusted at 8.5 with 25 % NH_4OH solution. The precipitate of Ti (III) hydroxide was oxidized at room temperature with oxygen (air) until the colour changes from blue-violet to white. The coprecipitated of Ti(IV) and Fe(III) hydroxides was washed with distilled water in order to remove salts and then dried in air at 105 °C. For the nitrogen doping, the as resulted coprecipitate was hydrothermally treated at 200 °C for 2 h in presence of Urea. Finally, the dried powder was calcined at 400°C for 2 h in air.

Characterization

The phase content was examined using a both DRON X-ray powder diffractometer linked to data acquisition and processing facilities and a Bruker Advance D8 equipment, using CuK_α radiation (λ = 1.5406 Å). A JEOL 200 CX transmission electron microscope operating at an accelerating voltage of 200 kV was utilized to obtain information about the structure and morphology of the obtained photocatalytic samples. X-Ray Photoelectron Spectroscopy measurements have been carried out in an analysis chamber (Specs) by using a monochromatized Al $K_{\alpha 1}$ X-ray source (1486.74 eV), in normal emission regime. The electrons are collected and analyzed by a 150 mm radius Phoibos electron analyzer operating in large area mode with pass energy of 30 eV. The overall resolution is estimated to be in the range of 0.9 eV – total full width at half maximum (FWHM). During the analysis, the base pressure in the analysis chamber was in the range of 3×10^{-7} Pa. Room temperature transmission ^{57}Fe Mössbauer spectra were recorded using a WissEL-ICE Oxford Mössbauer cryomagnetic system, in order to evidence the presence of Iron in the doped samples.

Thin films on Quartz buffer were obtained by dip coating technique with Xdip_SV1 apparatus. For the photocatalytic tests (on Methylene Blue), PCC-2 Photocatalysis Evaluation Checker was used in both UV and Visible spectral regions. The wave length

was 368 nm for UV and 610 nm for visible light experiments.

RESULTS AND DISCUSSION

In figure 1 the X-ray diffractograms of representative (Fe-N) impregnated TiO_2 Degussa P25, named (1 at.%) Fe-N-P25 and hydrothermally synthesized (1at.%)-Fe-N-TiO_2 samples are shown. The X-ray diffractogram of the impregnated sample TiO_2 Degussa P25 (figure 1, *a*) exhibits two phases: Anatase (~ 83 wt. %) and Rutile (~17 wt. %), no other phases were evidenced in the refinements cycles. The mean crystallite dimensions are close to 30 nm for Anatase and 50 nm for Rutile. The (1at.%) Fe-N-TiO_2 sample synthesized under coprecipitated/hydrothermal conditions exhibit a XRD typical for nanoscaled Anatase phase (figure 1, *b*). The mean crystallite size calculated with Scherrer equation is ~15 nm. TEM images on representative Fe-N-P25 and Fe-N-TiO_2 samples are shown in figures 2, *a* and 2, *b*.
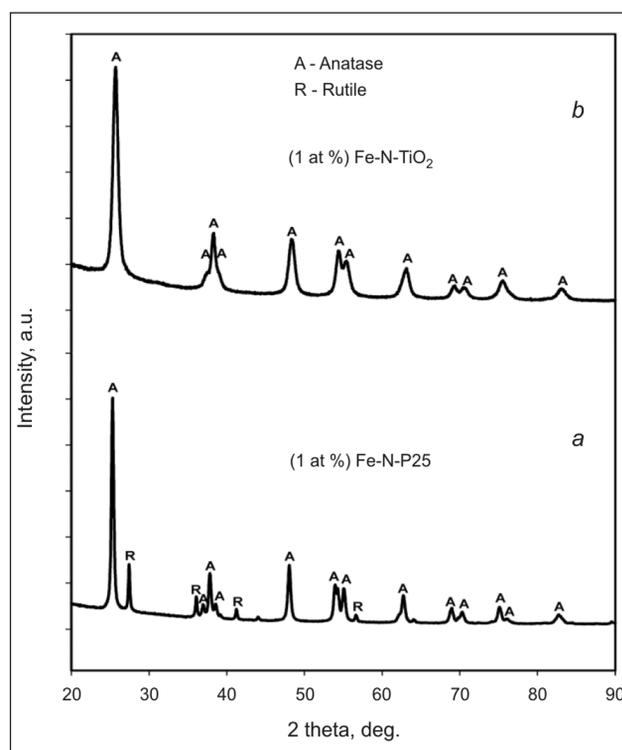

Fig. 1. X-ray diffractograms of the (1 at.%)-Fe-N-P25 and (1at.%)-Fe-N-TiO_2

In the case of Fe-N impregnated Degussa P25 samples the mean particle size is about 29 nm with large extension from ~ 5 to 65 nm (figure 2, *a*). The sample (1at.%)-Fe-N-TiO_2 shows particles with mean diameter of about 28 nm, from 10 to 85 nm (figure 2, *b*).

The presence of Iron in samples was firstly revealed by Mössbauer spectroscopy. All spectra consist in a quadrupole doublet. A representative spectrum is shown in figure 3 together with the computer fit (continuous line). The Isomer shift of ~ 0.29 mm/s and the quadrupole splitting (~ 0.62 mm/s) are characteristic for Fe^{3+} ions in octahedral symmetry.
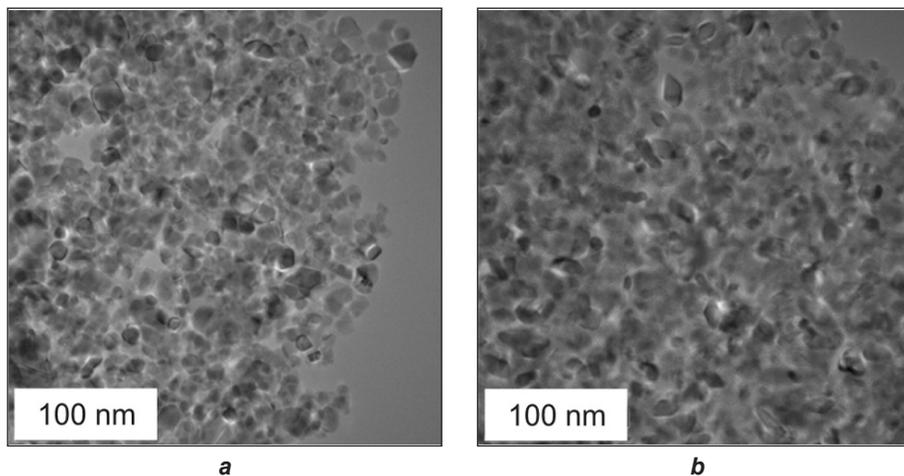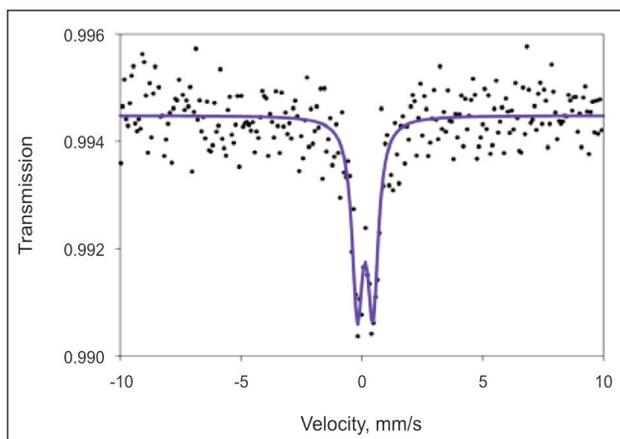
Fig. 2. *a* – (1 at.%)-Fe-N-P25; *b* – (1at.%)-Fe-N-TiO$_2$

Fig. 3. Mössbauer Spectrum of (1at.%)-Fe-N-TiO$_2$

binding energies and the integral amplitudes, divided by the Wagner Atomic Sensitivity Factors of every sub-component determined by deconvoluting the spectra using Voigt profiles, according to the method described in [7–8]. All the data has been calibrated to the standard binding energy of the contamination C 1s peak, 284.6 eV. Figure 4, *c*, *d* reveals the presence of Fe and Nitrogen into the doped samples. The main components of Ti 2p$_{3/2}$ (458.65 eV) and O 1s (529.98 eV) in the standard Degussa P25 sample reveal a stoichiometric TiO$_2$, with a ratio O/Ti of 2.02. Introducing the doping atoms into the structure of TiO$_2$ leads to a shift towards lower binding energies for both Ti 2p$_{3/2}$ and O 1s, also reported in, due to an Oxygen deficit, as consequence of the Nitrogen doping [9]. The same paper offers an interpretation concerning the chemical bonding of Nitrogen. The N 1s peak at ~399.6 eV may be assigned to Ti-O-N or Ti-N-O bonds, in the (1at.%)-Fe-N-P25, or to NH$_3$, more possible in the (1at.%)-Fe-N-TiO$_2$ sample, because of the lower binding energy (~ 398.6 eV) [9–10]. The peak at ~ 400.5-401.2 is usually attributed to interstitial Nitrogen [11]. A determination of the total nitrogen ratio detected by XPS related to the total TiO$_2$ reveals the presence of 0.5 at.% N in the (1at.%)-Fe-N-P25 sample, and of 0.6 at.% N in (1at.%)-Fe-N-TiO$_2$ sample. In contrast, computing the ratio Fe/(Ti+O), the (1at.%)-Fe-N-P25 sample shows a value of 2.1 at.%, much higher than the other doped sample, where the amount of Fe is of ~0.02 at.%. This result can be explained by taking into account the distinct genesis of the sample (impregnation versus hydrothermal synthesis) correlated with the XPS method that gives

The presence of Nitrogen and Fe in the studied samples was revealed by XPS measurements. Some examples are presented in figure 4.

XPS measurements were performed on three samples: TiO$_2$ Degussa P25 (without doping), (1at.%)-Fe-N-P25 and (1at.%)-Fe-N-TiO$_2$. The characteristic spectra of Ti 2p, O 1s, Fe 2p and N 1s are represented in figure 4, *a, b* while table 1 contains the
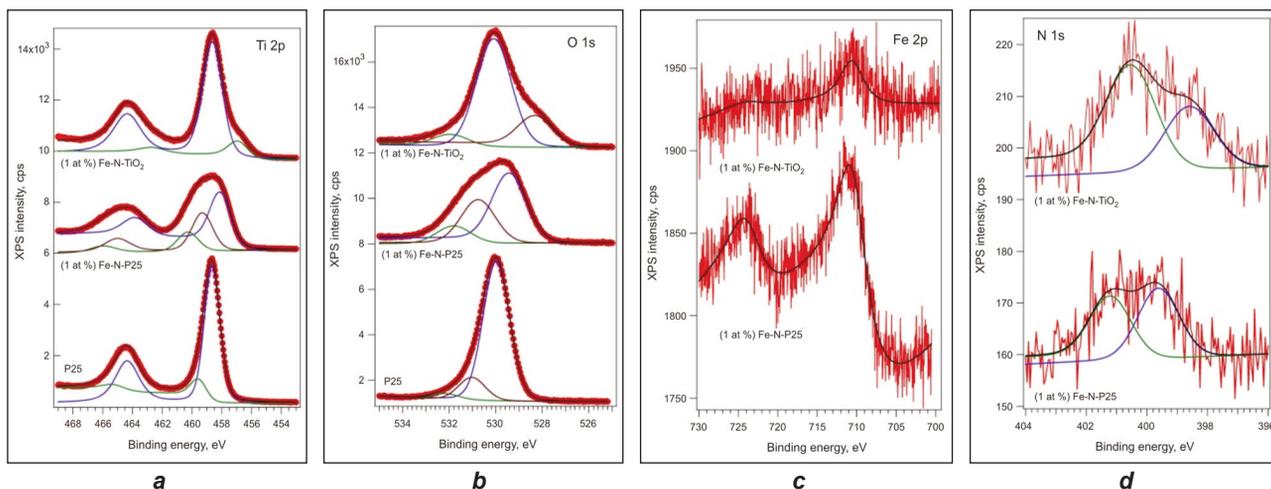
Fig. 4. The XPS spectra recorded on the P25, (1at.%)Fe-N-P25 and (1at.%)Fe-N-TiO$_2$ samples

Table 1

Sample	P25		(1at.%)Fe-N-P25		(1at.%)Fe-N-TiO$_2$	
	Binding energy (eV)	Integral amplitude (eV × kcps)	Binding energy (eV)	Integral amplitude (eV × kcps)	Binding energy (eV)	Integral amplitude (eV × kcps)
Ti 2p$_{3/2}$	458.65	6.87	458.08	3.25	456.88	7.61
	459.63	0.96	459.30	2.4	458.62	1.07
	-	-	460.27	1.23	-	-
O 1s	529.98	13.91	529.42	8.61	528.29	3.88
	531.03	2.27	530.75	5.53	530.09	14.08
	532.16	0.57	531.81	2.24	531.92	1.48
Fe 2p$_{3/2}$	-	-	710.40	0.45	710.55	0.064
N 1s	-	-	399.62	0.058	398.60	0.063
	-	-	401.19	0.05	400.50	0.096

XPS DATA OBTAINED BY THE DECONVOLUTIONS OF THE XPS SPECTRA OF THE P25, (1at.%)-Fe-N-P25 AND (1at.%)-Fe-N-TiO$_2$
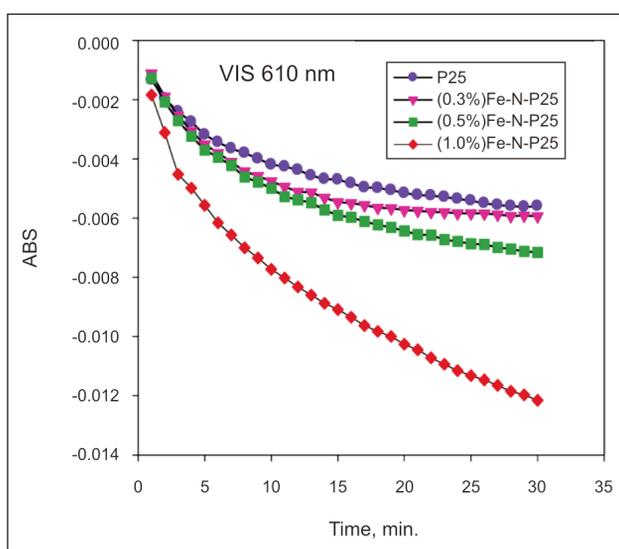

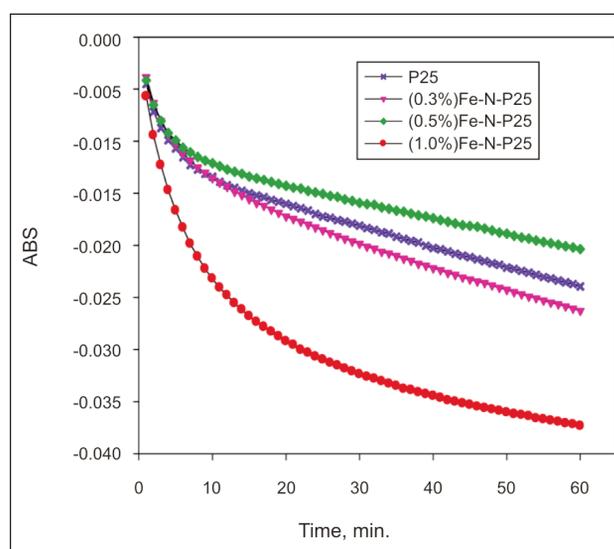Fig. 5. VIS Absorbance for the P25 series

Fig. 6. UV Absorbance for the P25 series

information only about surface phenomena. The Fe 2p$_{3/2}$ signal is around 710.45±0.1 eV, pretty close to the value reported in, assigning this to the presence of Fe^{3+} ions [12]. Comparing this with the emergence of an extra component at ~460.37 eV in the Ti 2p spectrum of the (1at.%)-Fe-N-P25 sample, one may assume the formation of Fe-O-Ti type bonding [13]. Suspensions containing the prepared doped powders were used to obtain films (on Quartz support). Polyethylene glycol (PEG 600) was used in order to ensure the best adherence of Titania nanoparticles to the quartz surface. Before photocatalytic test, the samples were calcined to remove PEG then cleaned under 30 W UV lamp (λ = 365 nm), for 2 hours. After cleaning, the films were immersed for 2h in MB and finally dried at room temperature. In figures 5 and 6, the Absorbances (ABS) as given by PCC-2 tester are shown in Visible and UV radiation respectively, for

TiO$_2$ Degussa P25 impregnated samples. ABS is defined as ln(V_0/V_n) where V_0 is voltage with sensor oriented in medium (Reflection 0) and V_n is the voltage at the moment t during measurement.

The sample (1%) Fe-N-P25 (fig. 5, 6) is as far the best to be used in both UV and visible spectral region. In figure 7 the ABS are presented for the hydrothermally synthesized sample TiO$_2$ doped with 1% Fe and Nitrogen. One can remark that the photocatalytic activity in visible is twice higher than in UV radiation. Therefore, the performance of the hydrothermal (1at.%) Fe-N doped TiO$_2$ sample in visible light spectrum is superior to those of Degussa P25 doped or undoped powders. It is generally accepted that the degradation rate depends on the formation of HO• radicals at the photocatalyst surface and on the probability to interact with pollutant molecules. In the case of iron, there is a probability to be incorporated
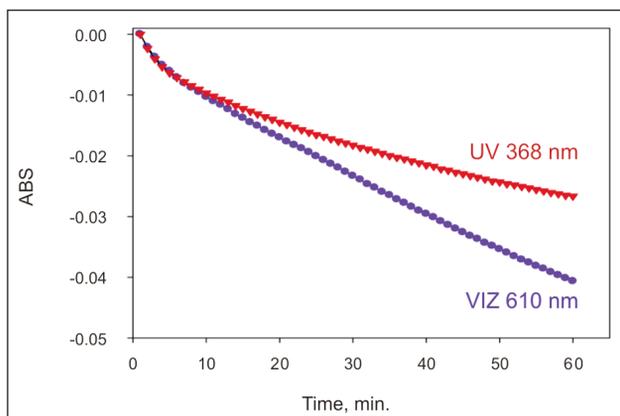
Fig. 7. Absorbance for (1at.%)-Fe-N-TiO$_2$-sample

into the TiO$_2$ lattice, acting as electrons and holes traps and leading to an improvement of photocatalytic efficiency. A read shift toward the visible light spectrum was reported for iron doped titania [1, 14]. This behaviour is concentration dependent. At higher concentrations, the ions Fe^{3+} became recombination centres of holes and electrons implying a decrease in the photocatalytic activity [15]. It was found that the presence of nitrogen in the TiO$_2$ structure can have positive effects; by reducing the band gap energy and creation of localized energy levels in the gap, remarkable visible light efficiency was reported [16–17]. A synergistic effect appears by metal-anion codoping leading to a more efficient photocatalytic activity [1,15]. This behaviour is also confirmed by our experiments showing that the codoped TiO$_2$ Degussa P25 and the hydrothermal synthesised (Fe, N) codoped TiO$_2$ are more efficient than the undoped TiO$_2$ powders.

CONCLUSION

(Fe, N) codoped Degussa P25 and hydrothermally synthesised TiO$_2$ samples were investigated with aim to design photocatalysts with increased visible light efficiency. The hydrothermal procedures were performed at moderate temperatures (~ 200 °C/2 h) followed by postannealing at 400 °C. XRD, TEM, XPS and Mössbauer spectroscopy revealed the formation of nanoscaled (Fe, N) codoped TiO$_2$ structures. The photocatalytic tests were performed on Methylene Blue. In the P25 series with different iron content (0.3, 0.5 and 1 at.%) and nitrogen, the most efficient photocatalyst in both UV and visible spectral range was (1at.%) Fe-N-P25.

The hydrothermal sample (1at.%) Fe-N-TiO$_2$ was found to have good activity especially in visible light spectrum. A tentative explanation of this behaviour was presented. Furthermore, the photocatalytic systems synthesized will be tested on textiles materials to study the selfcleaning and antibacterial effects as well.

BIBLIOGRAPHY

[1] Kubacka, A., Fernandez-García, M., Colon, G. *Advanced nanoarchitectures for solar photocatalytic applications,* In: Chemical Reviews 2012, vol. 112, pp. 1555–1614.

[2] Zhu, J., Ren, J., Huo, Y., Bian, Z., Li, H. *Nanocrystalline Fe/TiO visible photocatalyst with a mesoporous structure prepared via a nonhydrolytic Sol-Gel route,* In: J. Phys. Chem. C 2007, vol. 111, pp. 18965–69.

[3] Xiangxin Yang, Chundi Cao, Larry Erickson, Keith Hohn, Ronaldo Maghirang, Kenneth Klabunde, *Photo-catalytic degradation of Rhodamine B on C-, S-, N-, and Fe-doped TiO$_2$ under visible-light irradiation,* In: Applied Catalysis B: Environmental 2009 vol. 91, pp. 657–662.

[4] Asahi, R., Morikawa, T., Ohwaki, T., Aoki, K., Taga, Y. *Visible-light photocatalysis in nitrogen-doped titanium oxides,* In: Science 2001, vol. 293, pp. 269–271.

[5] Gang Liu, Xuewen Wang, Zhigang Chen, Hui-Ming Cheng, Gao Qing (Max) Lu, *The role of crystal phase in determining photocatalytic activity of nitrogen doped TiO$_2$,* In: Journal of Colloid and Interface Science 2009, vol. 329, pp. 331–338.

[6] Beata Wawrzyniak, Antoni Waldemar Morawski, and Beata Tryba, *Preparation of TiO$_2$-nitrogen-doped photocatalyst active under visible light,* In: International Journal of Photoenergy 2006, Article ID 68248, pp. 1–8.

[7] Wagner, C.D., Davis, L.E., Zeller, M.V., Taylor, J.A., Raymond, R.M., Gale, L.H. *Empirical atomic sensitivity factors for quantitative analysis by electron spectroscopy for chemical analysis,* In: Surf. Interface Anal., 1981, vol. 3, pp. 211–225.

[8] Teodorescu, C.M., Esteva, J.M., Karnatak, R.C., El Afif, A. *An approximation of the Voigt I profile for the fitting of experimental x-ray absorption data*, In: Nucl. Instrum. Meth. A 1994, vol. 34, pp. 141–147.

[9] Wang, J., Tafen, D.N., Lewis, J.P., Hong, Z., Manivannan, A., Zhi, M., Li, M., Wu, N. *Origin of photocatalytic activity of Nitrogen-Doped TiO$_2$ Nanobelts,* In: J. Am. Chem. Soc. 2009, vol.131, pp. 12290–12297.

[10] Moulder, J.F., Stickle, W.F., Sobol, P.E., Bomben, K.D. *Handbook of X-ray photoelectron Spectroscopy*; In: Eden Prairie (1992).

[11] Fujishima, A., Zhang, X., Tryk, D.A. *TiO₂ photocatalysis and related surface phenomena,* In: Surf. Sci. Rep*.,* 2008, vol. *63*, p. 515.

[12] Dolat, D., Mozia, S., Wrobel, R.J., Moszynski, D., Ohtani, B., Guskos, N., Morawski, A.W. *Nitrogen-doped, metal-modified rutile titanium dioxide as photocatalysts for water remediation*, In: Applied Catalysis B: Environmental, 2015, vol. 162, pp. 310–318.

[13] Hung, W.C., Chen, Y.C., Chu, H., Tseng, T.K. *Synthesis and characterization of TiO₂ and Fe/TiO₂ nanoparticles and their performance for photocatalytic degradation of 1,2-dichloroethane*, In: Applied Surface Science, 2008, vol. 255, pp. 2205–2213.

[14] Diamandescu, L., Vasiliu, F., Tarabasanu-Mihaila, D., Feder, M., Vlaicu, A.M., Teodorescu, C.M., Macovei, D., Enculescu, I., Parvulescu, V., Vasile, E. *Structural and photocatalytic properties of iron- and europium-doped TiO₂ nanoparticles obtained under hydrothermal conditions,* In: Mater. Chem. Phys., 2008, vol. 112, pp. 146–153.

[15] Chen, X., Mao, S.S. *Titanium dioxide nanomaterials: synthesis, properties, modifications and applications*, In: Chem. Rev., 2007, vol. 107, p. 2891.

[16] Di Valentin, C., Finazzi, E., Pacchioni, G., Selloni, A., Livraghi, S., Paganini, M.C., Giamello, E. *N-doped TiO*, In: Chem. Phys., 2007, vol. 339, p. 44.

[17] Finazzi, E., Di Valentin, C., Selloni, A., Pacchioni, G. *First principles study of nitro-gen doping at the anatase TiO*, In: J. Phys. Chem. C, 2007, vol. 111, p. 9275.

Authors:

L. DIAMANDESCU[1]

M. FEDER[1]

F. VASILIU[1]

L. TANASE[1]

C. M. TEODORESCU[1]

T. POPESCU[1]

I. DUMITRESCU[2]

ARCADII SOBETKII[3]

[1] National Institute of Materials Physics
Atomistilor 105 bis, P.O. Box MG 7, Bucharest Magurele 077125, Romania
e-mail: director@infim.ro, webpage: http://www.infim.ro

[2] National R&D Institute for Textiles and Leather Bucharest (INCDTP)
16 Lucretiu Patrascanu, 030508 Bucharest, Romania

[3] National Research and Development Institute for Non Ferrous and Rare Metals

Corresponding author:

L. DIAMANDESCU
director@infim.ro
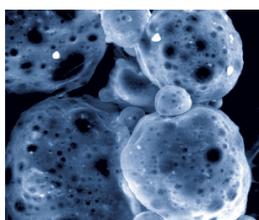
Voltage response of piezoelectric woven fabric, made of tourmaline containing polypropylene filaments

VATANSEVER BAYRAMOL DERMAN

REZUMAT – ABSTRACT

Răspunsul la tensiune al țesăturii piezoelectrice din turmalină cu conținut de filamente de polipropilenă

În această lucrare au fost adăugate trei raporturi diferite de greutate (1%, 3% și 5%) a turmalinei (TM) în polimerul de polipropilena (PP), polimer folosind un compounder twin screw. Amestecurile preliminare de PP cu polipropilenă pură și pulbere TM au fost utilizate pentru a produce filament de PP/TM printr-un procedeu de filare din topitură cu o unitate de polarizare aplicată în zona de etirare. Filamente piezoelectrice au fost utilizate pentru a produce țesături piezoelectrice realizate pe o mașină de țesut manuală. Foile de aluminiu au fost atașate pe ambele părți ale probelor de țesătură piezoelectrică în calitate de electrozi. Au fost obținute caracteristicile mecanice, termogramele DSC, spectrele de absorbanță FTIR și micrografiile SEM ale probelor de țesătură piezoelectrică. Pentru a investiga efectul raportului TM asupra răspunsului la tensiune al mostrelor de țesătură piezoelectrică, un sistem de rezistență la impact a fost folosit pentru a permite greutăților să cadă liber pe probe. Tensiunile de ieșire ale probelor au fost înregistrate cu ajutorul unui osciloscop digital. Conform rezultatelor colectate de osciloscopul digital, adiția de TM a contribuit la tensiunea de ieșire a probelor. Tensiunea de vârf înregistrată, generată de proba de țesătură din PP pură (PPP-0TM), a fost de 1,20 V, iar proba de țesătură piezoelectrică cu un conținut de 5% TM (PPP-5TM) a prezentat o tensiune de vârf de 3,92 V.

Cuvinte-cheie: răspuns la tensiune, turmalină, polipropilenă, piezoelectric, țesătură

Voltage response of piezoelectric woven fabric, made of tourmaline containing polypropylene filaments

In this work, three different weight ratios (1%, 3% and 5%) of tourmaline (TM) were added to polypropylene (PP) polymer using a twin screw compounder. Pristine PP and TM powder added PP master batches were used to produce PP/TM filaments via a melt-spinning process with a polarization unit affixed in the drawing zone. Piezoelectric filaments were then used to produce piezoelectric woven fabrics on a handloom. Aluminium sheets were attached on both sides of piezoelectric woven fabric samples as electrodes. Mechanical characteristics, DSC thermograms, FTIR absorbance spectra and SEM micrographs of piezoelectric woven fabric samples were obtained. To investigate the effect of TM ratio on the voltage response of piezoelectric woven fabric samples, an impact rig was used which allowed the weights to drop freely onto the samples. Voltage outputs of the samples were recorded via a digital oscilloscope. According to the results collected from the digital oscilloscope, addition of TM contributed to the voltage output of the samples. Recorded peak voltage generated by the woven fabric sample made of pristine PP (PPP-0TM) was 1.20 V while the piezoelectric woven fabric sample containing 5% TM (PPP-5TM) showed a peak voltage of 3.92 V.

Keywords: voltage response, tourmaline, polypropylene, piezoelectric, fabric

INTRODUCTION

Smart materials have received a significant interest in recent years. The members of smart materials family included but not limited to shape memory polymers and alloys, photovoltaic structures, electro/magneto-rheological fluids, piezoelectric materials etc. Each of these materials shows an extraordinary response as a result of applied stimuli. Piezoelectric materials, for instance, generate an electrical potential when mechanically deformed and conversely undergo a shape change when an electrical potential is applied. From the materials point of view, polymeric materials seem to be more convenient and promising for the applications where the flexibility and lightweight are crucial. In the literature a number of comparative works have been conducted on ceramic and polymer based piezoelectric materials [1–2].

The first piezoelectric polymer reported was poly(vinylidene) fluoride (PVDF) [3]. Cellular polypropylene is one of the other polymers which were reported to exhibit piezoelectric behaviour [4–8]. Polypropylene (PP) provides a number of advantages upon other polymers which makes it preferable for technical applications. However, piezoelectric strain coefficient of polymer-based materials is much lower than that of ceramic-based piezoelectric materials. Therefore, there is a number of works to test the power generation characteristics, the durability and stability and the enhancement on piezoelectric behaviour of polymeric materials [9–15]. There is limited number of works on the effect of tourmaline when used as an additive to a polymer matrix. Tourmaline (TM) is a complex borosilicate and it is naturally piezoelectric with spontaneous and permanent poles [16–17]. These poles create dipoles which induce an electric field on the surface of the tourmaline when subjected to a mechanical strain [18]. Furthermore, TM is very sensitive to uniformly applied pressure in all directions that makes it suitable for pressure sensor applications [19].

In this work, TM powder has been blended with PP polymer and the effect of the addition of TM powder in PP polymer was investigated. First of all, PP monofilaments were successfully produced and polarized simultaneously. Filaments underwent thermal, mechanical and electrical conditions in the draw area on a laboratory scale melt extruder. To investigate the effects of tourmaline on the voltage output of PP, the produced filaments were woven in a handloom. The woven piezoelectric samples with an active area of 50 mm × 75 mm were produced and then subjected to an impact. The voltage response of the samples was recorded via a digital oscilloscope and the result was comparatively evaluated.

MATERIALS AND METHODs

Materials

Isotactic polypropylene pellets with a melting temperature of ~165°C and a melt flow index of 25 g/10 min at 230°C under an applied load of 2.16 kg were obtained from Lyondellbasell Polymers. Tourmaline powder was obtained from Shanghai HuZhengNano Technology Company (China).

Masterbatch and filament production method

Pristine isotactic PP polymer and TM powder were compounded by using a ThermoFisher Scientific Prism EuroLab16 twin-screw compounder to produce masterbatches having 1%, 3% and 5% TM in PP. The temperature parameters were 170°C, 190°C, 200°C, 200°C, 210°C and 210°C from the feeding barrel to the die. Molten PP polymer and TM powder were mixed in the heating zone via the twin-screw with a rotation speed of 250 rpm. A thick PP/TM monofilament was produced, cooled in a water bath, dried and cut into small pallets to produce masterbatches. Then the produced PP/TM masterbatches were dried at 80°C in the oven for at least 2 hours.

A laboratory scale melt extruder having a single screw (⌀ 22 mm) was used for PP/TM filament production. The extruder screw was operated at a speed of 2 rpm. The temperature of the five heating zones was maintained at 100°C, 170°C, 180°C, 190°C and 200°C, respectively. In an ordinary PP filament production process, the temperature of Barrel 1 is kept just above the melting point of the polymer. The detailed information on melt extrusion can be found in the literature [14, 21, 22]. A portable polarization unit was inserted between temperature controlled slow rollers and the fast roller where the filament is mechanically stretched. The speed of the slow rollers was 15 rpm while the fast rollers rotated with a speed of 37.5 rpm. A Spellman SL300 series high voltage power supply was used to apply 15 kV high voltage to the filaments. The produced filaments were named as PPP-0TM, PPP-1TM, PPP-3TM and PPP-5TM. The first letter "P" stands for polarized monofilaments. "PP" presents the main polymeric material which is isotactic polypropylene and the numbers 0-1-3-5 together with "TM" show the weight ratio of tourmaline in the produced monofilaments.

Weaving of the piezoelectric PP/TM filaments

A handloom was used for the purpose of producing woven piezoelectric textile structures. Piezoelectric monofilaments were used as weft and warp threads to produce plain woven textile structures. The produced woven textile structures were sandwiched between two aluminium sheets which were used as electrodes as seen in figure 1. The whole sample was wrapped by a non-conductive transparent tape to keep the electrodes in place. The size of the woven textile structures was 70 mm × 100 mm while the size of the electrodes was 50 mm × 75 mm.
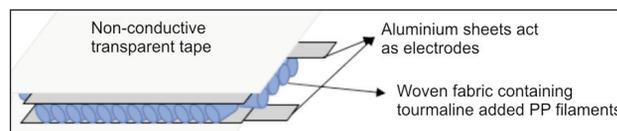

Fig. 1. Example of the composite structures having piezoelectric woven textile layer sandwiched between two aluminium sheets which are also sandwiched between non-conductive transparent tape

Characterisation

It should be noted that filament count, mechanical properties, thermal and infrared investigations and also microstructural evaluations of the PP/TM blend structures were carried out in filament form. The voltage response of PP/TM blends was studied after the filaments were woven to form a textile structure. For the measurement of the count of the filaments precision scales were used. 10 measurements were carried out for each set of filament sample and average value was recorded. The mechanical properties of the filaments were measured by using a Textechno Statimat M Test Equipment. Testing parameters were set to 100 mm for gauge length, 10 N for the load cell and 300 mm/min. for test speed. 10 measurements were carried out for each type of filament sample. Individual results and total evaluation was obtained from the equipment. Morphology of the samples were studied by using a Hitachi S-3400N Scanning Electron Microscope (SEM). Microstructural images of PP/TM filaments were captured at an accelerating voltage of 5 kV and various magnifications. Thermal characteristics of the PP/TM monofilaments were studied by using a TA Instruments DSC Q2000 equipment. The samples were scanned from −50°C to 200°C under nitrogen atmosphere with a heating rate of 10°C/min. Absorbance spectra of the filaments as a function of wave numbers were investigated by using a Thermo Scientific's IS10 Nicolet FT-IR Spectrometer with smart iTR accessory.

Voltage response of the produced PP/TM filaments were studied under an InstronDynatup® Mini Tower®, using ASTM D 3763 standard impact test method. The prepared samples were located in the test equipment one by one. An impact caused by a weight of 2.25 lbs was free-fallen from a height of 5 cm onto the samples. A digital oscilloscope was used for investigation of the voltage response of the woven piezoelectric structures and the results were directly recorded to an external data storage device.

RESULTS AND DISCUSSIONS

Mechanical properties of the produced filaments were investigated. 10 measurements were carried out for each type of filament for the determination of their count, tenacity, elongation and work to rupture values. The count of each filament was the main input for the TextechnoStatimat M Test Equipment. The values provided from the tensile test equipment are given in table 1.

COUNTS AND TEXTECHNOSTATIMAT M TEST RESULTS FOR PRODUCED PP/TM FILAMENTS			
	PPP-0TM	**PPP-1TM**	**PPP-3TM**	**PPP-5TM**
Count (tex)	16.91	17.28	17.61	17.41
Tenacity (cN/tex)	14.55	15.63	13.67	13.43
Elongation (%)	150.04	105.28	75.49	111.86
Work to rupture (cN*cm)	2571.14	2124.96	1484.07	2039.55

Since the production parameters were the same for each sample, the count of the filaments were found to be in a range of 16.91–17.61 tex. This variation may have caused by the melt extruder which was a laboratory scale unit. On the other hand, if the number of count measurements is increased, the count values would be expected to converge. The tenacity of the filaments containing 1 wt% TM got higher values as compared to the pristine PP filaments and the filaments containing 3 wt% and 5 wt% TM. Due to good dispersion of TM nanoparticles in the polymer matrix, tenacity of the filament improved from 14.55 cN/tex to 15.63 cN/tex when 1 wt% TM was added in polymer matrix. However, the tensile properties of filaments containing higher than 1 wt% TM in the structure were slightly reduced, which could be due the agglomeration of TM particles in filament structure. The energy or work required to break the filaments decreased when TM particles were added to the polymer matrix. However, there was no clear trend in the change of the work to rupture values.

The surface and the cross-sectional characteristics of the produced filaments were investigated by using SEM images illustrated in figure 2. Images coded with "L" shows surface morphology of the filaments while images coded with "C" shows cross-sectional view of the filaments. The numbers from 0 to 5 present the weight ratio of TM in the polymer matrix. As seen in figure 2, L0 and C0, pristine PP filaments have a smoother surface and cross-section as compared to TM added PP filaments due to having no TM in the structure. An increasing unevenness is seen with an increase in TM ratio in the filaments. Holes and pits can be seen in the cross-sectional images of C1, C3 and C5 and it is seen that these holes and pits tend to grow larger with the increase in the TM ratio, which may be due to the increase in the agglomeration of the TM nano particles.

Figure 3 shows DSC thermograms of the produced filaments while table 2 gives the melting temperature [Tm (°C)], melting enthalpy [ΔHm (J/g)] and degree of crystallinity [Xc (%)] of the filaments. Tm and ΔHm were directly taken from the DSC thermograms while Xc was calculated via the standard heat of crystallinity for 100% crystalline PP taken as 209 J/g [14, 22–25]. The results given in table 2 show that addition of TM powder resulted an increase in the crystallinity of the PP/TM filaments. The calculated crystallinity of PPP-1TM filament is 41.8% while the crystallinity values of the filaments containing higher ratios of TM, namely PPP-3TM and PPP-5TM, were found higher than that of pristine but lower than that of PPP-1TM. This can be interpreted as that the addition of TM powder up to 1wt% contributed crystallisation of PP however beyond this point TM nano powder may act as impurity and result in the observed decrease in crystallinity of the filaments. An XRD analysis can be carried out for further investigation on the crystalline structure of the pristine and PP/TM filaments.

Chemical compositions of the produced pristine PP and PP/TM filaments were evaluated by using
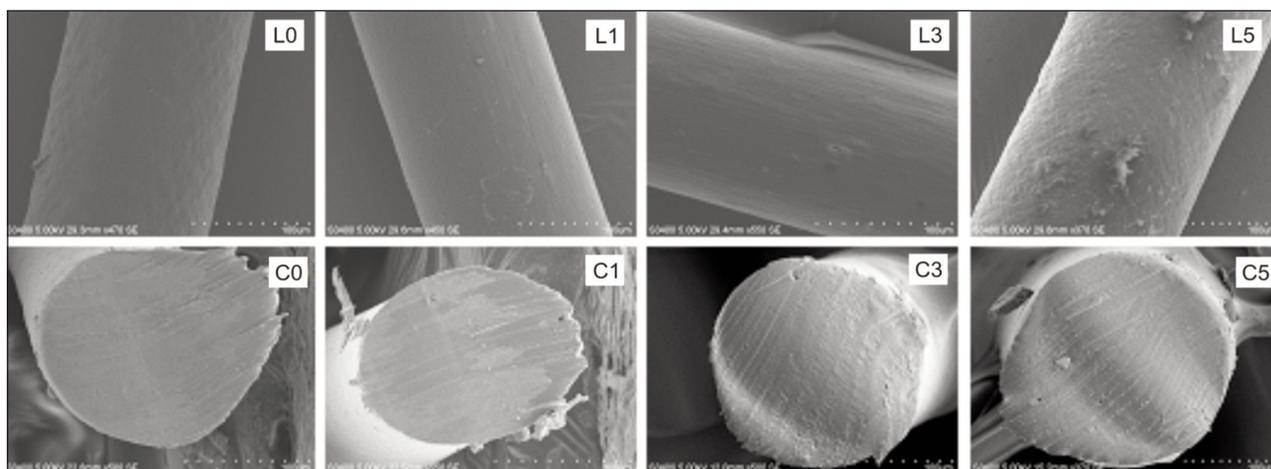

Fig. 2. Longitudinal (L) and cross-sectional (C) SEM images of pristine PP and PP/TM filaments; numbers following the letters present the amount of TM in filament structure
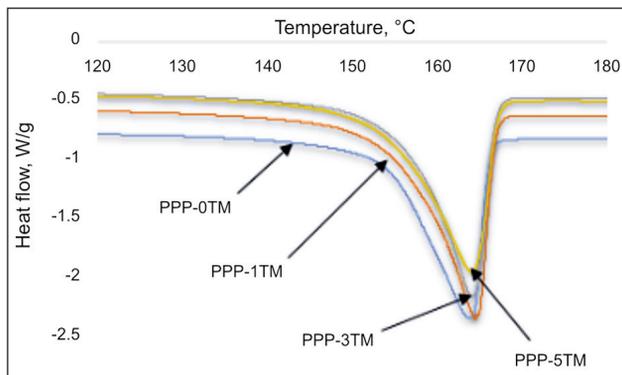
Fig. 3. Melting characteristics of produced PP/TM filaments taken from DSC thermograms
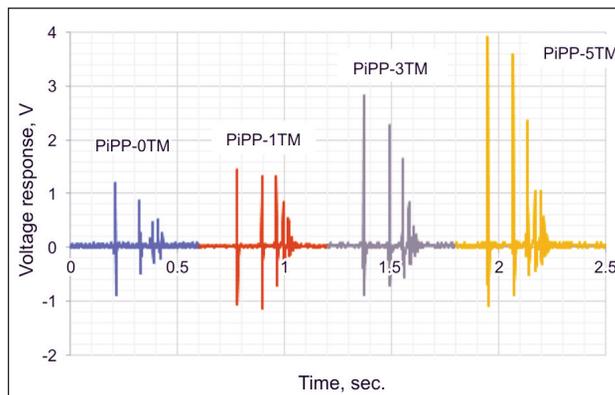

Fig. 4. Comparable graph for voltage responses of the produced piezoelectric woven fabric samples under applied impact

Table 2

	Melting temperature Tm ($°C$)	**Melting enthalpy ΔHm** (J/g)	**Degree of crystallinity Xc** (%)
THERMAL CHARACTERISTICS OF THE FILAMENTS; MELTING TEMPERATURE AND MELTING ENTHALPY VALUES WERE OBTAINED FROM DSC, DEGREE OF CRYSTALLINITY			
Sample ID			
PPP-0TM	163.69	77.39	37.0
PPP-1TM	164.53	87.30	41.8
PPP-3TM	164.07	84.11	40.2
PPP-5TM	164.16	83.05	39.7

Thermo Scientific's IS10 Nicolet FT-IR Spectrometer. There were no new peaks or peak shifts observed in the spectra obtained for the various filaments. However, the intensities of some peaks increased when TM was added to the polymer structure. This can be explained in two ways; a change in the polarity of the molecule or increased number of functional groups for that specific wave number.

Typical voltage generation characteristics of the prepared woven fabric samples are given in figure 4. Five measurements were carried out for each sample. Sample without TM addition showed a voltage response of 1.20 V while samples produced from TM added PP filaments showed higher voltage outputs. Sample named as PPP-1TM produced 1.46 V while voltage outputs of PPP-3TM and PPP-5TM were 2.84 V and 3.92 V, respectively. In figures 4, it is clearly seen that an increase in voltage generation was observed with an increase in the weight ratio of TM in the filament structure. This can be attributed to the addition of TM, which is a naturally occurring piezoelectric material [19, 25–26], and contributed to enhanced voltage generation of the filament structure. Since the samples were located on a non-conductive paper type covered metal plate, free falling impact weight bounced and impacted on to the sample few more times before it came to a stop. Therefore, piezoelectric samples showed a voltage output smaller than the one caused by the first impact. The reason was that the gravity and the mass of the rig were constant while the falling height of the rig was lower than 5 cm which caused a decrease in the voltage generated by the second fall.

CONCLUSIONS

Pristine PP and TM added PP filaments were successfully melt-spun and poled via a polarization unit fixed in the drawing area of the extruder. The produced filaments were first examined for their mechanical, thermal, infrared characteristics and morphology. An increase in tenacity of the filament was observed when 1 %wt TM was added to the polymer. However, the tenacity was decreased further addition of TM. This is because of the tendency of TM particles to agglomerate at higher concentration and act as impurity in the polymer, which results in the observed decrease in the tensile property. Similar results were also observed for degree of crystallinity. The produced filaments were then used to produce piezoelectric woven fabrics by using a handloom. Aluminium sheets were used as electrodes and attached on both sides of piezoelectric woven fabric samples.

The peak voltage generation of the woven samples were investigated. It was observed that PPP-0TM sample showed a peak voltage of 1.20 V while TM containing PP filaments showed higher voltage generation. The recorded peak voltage values were 1.46 V, 2.84 V and 3.92 V for PPP-1TM, PPP-3TM and PPP-5TM, respectively. Therefore, it can be concluded that the addition of natural piezoelectric TM particles in PP polymer contributed the enhanced voltage output of the material. The results of the study show that the TM containing polymer filaments are very promising for green technical textile applications.

BIBLIOGRAPHY

[1] Patel, I., Siores, E., Shah, T. *Utilisation of smart polymers and ceramic based piezoelectric materials for scavenging wasted energy*, In: Sensors and Actuators A: Physical, 2010, vol. 159, pp. 213–218.

[2] Vatansever, D., Hadimani, R.L., Shah, T., Siores, E. *An investigation of energy harvesting from renewable sources with PVDF and PZT*, In: Smart Materials and Structures, 2011, vol. 20, 055019.

[3] Kawai, H. *The piezoelectricity of poly(vinylidene fluoride)*, In: Japanese Journal of Applied Physics, 1969, vol. 8, pp. 975–976.

[4] Zhang, X., Sessler, G.M., Hillenbrand, J. *Improvement of piezoelectric coefficient of cellular polypropylene films by repeated expansions*, In: Journal of Electrostatics, 2007, vol. 65, pp. 94–100.

[5] Qaiss, A., Saidi, H., Fassi-Fehri, O., Bousmina, M. *Cellular polypropylene-based piezoelectric films*, In: Polymer Engineering & Science, 2012, vol. 52, pp. 2637–2644.

[6] Gilbert-Tremblay, H., Mighri, F., Rodrigue, D. *Morphology development of polypropylene cellular films for piezoelectric applications*, In: Journal of Cellular Plastics, 2012, vol. 48, pp. 341–354.

[7] Mellinger, A., Wegener, M., Wirges, W., Mallepally, R.R., Gerhard-Multhaupt, R. *Thermal and temporal stability of ferroelectret films made from cellular polypropylene/air composites*, In: Ferroelectrics, 2006, vol. 331, pp. 189–199.

[8] Klimiec, E., Krolikowski, B., Machnik, M., Zaraska, W., Dzwonkowski, J. *Increase of piezoelectric constant and thermal durability of polypropylene electret by introducing SiO_2 and kaolin filler and creating a cellular structure*, In: Journal of Electronic Materials, 2015, vol.44, pp. 2283–2291.

[9] Matsouka, D., Vassiliadis, S., Prekas, K., Vatansever Bayramol, D., Soin, N., Siores, E. *On the measurement of the electrical power produced by melt spun piezoelectric textile fibres*, In: Journal of Electronic Materials, 2016, vol. 45, no. 10, pp. 5112–5126.

[10] Matsouka, D., Vassiliadis, S., Vatansever Bayramol, D., Soin, N., Siores, E. *Investigation of the durability and stability of piezoelectric textile fibres*, In: Journal of Intelligent Material Systems and Structures, 2017, vol. 28, no. 5, pp. 663–670.

[11] Baur, C., DiMaio, J.R., McAllister, E., Hossini, R., Wagener, E., Ballato, J., Priya, S., Ballato, A., Smith Jr., D.W. *Enhanced piezoelectric performance from carbon fluoropolymer nanocomposites*, In: Journal of Applied Physics, 2012, vol. 112, 124104.

[12] Zhao, X.L., Wang, J.L., Tia, B.B., Liu, B.L., Wang, X.D., Sun, S., Zou, Y.H., Lin, T., Sun, J.L., Meng, X.J., Chu, J.H., *Enhanced piezoelectric response in the artificial ferroelectric polymer multilayers*, In: Applied Physics Letters, 2014, vol. 105, 222907

[13] Ouyang, Z-W., Chen, E-C., Wu, T-M. *Enhanced piezoelectric responses and crystalline arrangement of electroactive polyvinylidene fluoride/magnetite nanocomposites*, In: Journal of Applied Polymer Science, 2014, vol. 131, 40941.

[14] Vatansever Bayramol, D., Soin, N., Hadimani, R.L., Shah, T., Siores, E. *Effect of addition of multiwalled carbon anotubes on the piezoelectric properties of polypropylene filaments*, In: Journal of Nanoscience and Nanotechnology, 2015, vol. 15, pp. 7130–7135.

[15] Bhavanasi, V., Kumar, V., Parida, K., Wang, J., Lee, P.S. *Enhanced piezoelectric energy harvesting performance of flexible PVDF-TrFE bilayer films with graphene oxide*, In: ACS Applied Materials & Interfaces, 2016, vol. 8, pp. 521–529.

[16] Nakamura, T., Kubo, T. *The tourmaline group crystals reaction with water*, In: Ferroelectrics, 1992, vol. 137, pp. 13–31.

[17] Ji, Z.J., Jin, Z.Z., Liang, J.S., Wang, J., Yan, X.W. *Observation of electric dipole on polar crystalline tourmaline granules*, In: Journal of Synthetic Crystals, 2002, vol. 31, p. 503.

[18] Yamaguchi, S. *Surface electric fields of tourmaline*, In: Applied Physics A, 1983, vol. 31, pp. 183–185.

[19] Pandey, C.S., Schreuer, J. *Elastic and piezoelectric constants of tourmaline single crystals at non-ambient temperatures determined by resonant ultrasound spectroscopy*, In: Journal of Applied Physics, 2012, vol. 111, 013516.

[20] Hadimani, R.L., Vatansever Bayramol, D., Sion, N., Shah, T., Qian, L., Shi, S., Siores, E. *Continuous production of piezoelectric PVDF fibre for e-textile applications*, In: Smart Materials and Structures, 2013, vol. 22, 075017.

[21] Vatansever Bayramol, D. *Effects of tourmaline on the voltage response of PVDF filaments*, In: IndustriaTextila, 2017, vol. 68, no. 1, pp. 47–53.

[22] Yeo, S.Y., Jeong, S.H. *Preparation and characterization of polypropylene/silver nanocomposite fibers*, In: Polymer International, 2003, vol. 52, pp. 1053–1057.

[23] Selvakumar, V., Manoharan, N. *Thermal properties of polypropylene/montmorillonite nanocomposites*, In: Indian Journal of Science and Technology, 2014, vol. 7, pp. 136–139.

[24] Pan, W., Ding, X., Gu, H., Hu, G. *Effect of talc on crystallization and properties of polypropylene*, In: American Journal of Materials Research, 2015, vol. 24, pp. 35–43.

[25] Buchanan, J.P. *Physical characteristics of piezoelectric crystals*, In: Handbook of Piezoelectric Crystals for Radio Equipment Designers WADC TR-56-156 Philco Corporation, Ohio, USA (1956).

[26] Yazıcı, E.Y., Alp, I., Yılmaz, A.O., Celep, O., *Piezoelektrik teknolojive piezo-malzemeolarakturmalin* 5. Endüstriyel Hammaddeler Sempozyumu, 13–14 May 2004, Izmir-Turkey 279–285.

Authors:

VATANSEVER BAYRAMOL DERMAN

Namık Kemal University, CorluFaculty of Engineering
Department of Textile Engineering, 59860, Tekirdag, Turkey
dvbayramol@nku.edu.tr

Corresponding author:

VATANSEVER BAYRAMOL DERMAN
dvbayramol@nku.edu.tr

The study of the solar radiation in the context of industrial restructuring and the need to reduce environmental pollution

NICOLAE DIACONU   MARIN SILVIU NAN   OLIMPIU STOICUTA

REZUMAT – ABSTRACT

Studiul radiaţiei solare în contextul restructurării industriale şi a necesităţii reducerii poluării mediului înconjurător

În cadrul acestui articol se prezentă o analiză comparativă a celor mai cunoscute modele matematice ale radiaţiei solare globale ce cade pe un plan orizontal, în condiţii de cer senin. Modelele matematice sunt particularizate pentru municipiul Petroşani. Validarea modelelor se realizează prin intermediul datelor obţinute cu ajutorul piranometrului Voltcraft PL-110SM.

Cuvinte-cheie: modelare şi simulare matematică, radiaţie solară globală, panou fotovoltaic, timp solar

The study of the solar radiation in the context of industrial restructuring and the need to reduce environmental pollution

This article presents a comparative analysis of the most famous mathematical models of global solar radiation falling on a horizontal plane, under a clear sky. The mathematical models are customized for the city of Petrosani. Validation of the models is achieved through data obtained using Voltcraft PL-110SM pyranometer.

Keywords: modelling and mathematical simulation, global solar radiation, photovoltaic panel, solar time

INTRODUCTION

Designing a photovoltaic system involves conducting several steps. An essential step in the correct sizing of a photovoltaic system, is to estimate the solar radiation. In this context, the paper aims to highlight the main mathematical models used to estimate the direct sunlight radiation that falls on a horizontal plan, under a clear sky. The mathematical models of sunshine are customized for the city of Petrosani. The validation of these models shall be based on data provided by Voltcraft PL-110SM Pyranometer.

At the end of the article the program Matlab-Simulink simulation of solar radiation is presented, estimated by using the Haurwitz model.

MATHEMATICAL MODELLING OF SOLAR RADIATION

For the mathematical modelling of solar radiation, we will define the following angles:

a) the angle of declination (δ [grade]) is the angle between the plane of the Equator and the Earth-Sun line. The angle of declination varies between $-23.45°$ at the winter solstice and $23.45°$ at the summer solstice and at equinox, the angle of declination is $0°$.

The declination angle is determined by the following formula (1):

$$\delta = 23.45° \cdot \sin\left(\frac{360° \, (n - 81)}{365}\right) \qquad (1)$$

where n represents the number of days in a year.

b) the hour angle (ω [grade]) is the angle between the meridian of the observer and the meridian of

longitude whose plan contains the Sun. This angle is used to define the rotation of Earth on its axis. The upper and lower limit of the variation of the angle of the beach zone, is: $(-180, 180)°$. The hour angle is calculated by the following formula (2):

$$\omega = 15° \cdot (T_s - 12) \qquad (2)$$

where T_s is the local solar time.

c) the altitudinal angle (α [grade]) is the angle between the direction of the sunlight and its projection in the horizontal plane. The calculation formula of the altitudinal angle is (3):

$$\sin(\alpha) = \sin(\delta) \sin(\varphi) + \cos(\delta) \cos(\varphi) \cos(\omega) \qquad (3)$$

where φ [grade] is the latitude (the angle between the Equator and the geographical location of interest), δ [grade] is the angle of declination and ω [grade] – the angle of the zone.

Based on the altitudinal angle, **the zenith angle** can be calculated: $\zeta = 90° - \alpha$.

The linking relation between the local solar time and local time is based on the equation of time (EOT). The equation of time is defined by the following (4–5):

$$EOT(n) = 9.87 \cdot \sin(2 \cdot b(n)) -$$
$$- 7.53 \cdot \cos(b(n)) - 1.5 \cdot \sin(b(n)) \qquad (4)$$

where

$$b(n) = \frac{360° \, (n - 81)}{365} \qquad (5)$$

where n represents the number of days in a year. Figure 1 represents the equation of time versus the number of days in 2015.
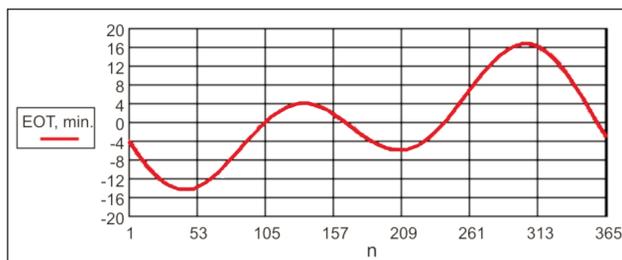
Fig. 1. Changes in relation to the number of days in a year (2015), the equation of time

In this context, the linking relationship between the local solar time (T_s) and the local (T_L) is (6):

$$T_s = T_L + \frac{T_C}{60} \quad (6)$$

where:
• local time (T_L) is calculated by the following formula (7):

$$T_L = \frac{\text{hour} \cdot 3600 + \text{min} \cdot 60 + \text{s}}{3600} \quad (7)$$

where the "hour", "min" and "s" are hour, minute and second that define the local time.
• the time correction factor (T_C) is calculated by the following formula (8):

$$T_C = 4 \cdot (L_o - L_m) + EOT(n) \quad (8)$$

where L_o[grade] is the longitude of the place and $L_m = 15° \cdot \Delta_{GMT}$ is standard local time based on the first meridian, where Δ_{GMT} is the difference between local and GMT (Greenwich Mean Time), in hours (for Romania is $\Delta_{GMT} = +3$ for summer time, respectively $\Delta_{GMT} = +2$ for winter time).
In Romania, the summer time is applied each year on the last Sunday of March (3.00 becomes 4.00) and winter time applies in the last Sunday of October (4.00 becomes 3.00).
The moments at which the sunrise and the sunset are calculated using the following relation (9–10):

$$T_R = 12 - \frac{1}{15°} \cdot \arccos\left(-tg(\varphi) \cdot tg(\delta)\right) - \frac{T_C}{60} \quad (9)$$

$$T_A = 12 + \frac{1}{15°} \cdot \arccos\left(-tg(\varphi) \cdot tg(\delta)\right) - \frac{T_C}{60} \quad (10)$$

where φ[grade] is the latitude, δ[grade] – the angle of declination, T_C – the factor of time correction, T_R – the time the Sun rises, and T_A – the time the Sun sets.
Considering these, we will present below the most known mathematical models for estimating the solar radiation of the globe, valid under a clear sky [1]–[3]:
1. **The mathematical model Kasten–Czeplak** is defined by the following relation (11):

$$Q = 910 \cdot \sin(\alpha) - 30 \quad (11)$$

where α is the altitudinal angle.
2. **The mathematical model Adnot** is defined by the following relationship (12):

$$Q = 915.39 \cdot [\sin(\alpha)]^{1.15} \quad (12)$$

where α is the altitudinal angle.
3. **Haurwitz mathematical model** is given by the following equation (13):

$$Q = 1098 \cdot e^{-\frac{0.057}{\sin(\alpha)}} \cdot \sin(\alpha) \quad (13)$$

where α is the altitudinal angle.
4. **The EIM model** (Empirical Irradiance Model) is defined by the following relation (14):

$$Q = Q_0 \cdot \left(1 - 0.4645 \cdot e^{-0.69 \cdot \sin(\alpha)}\right) \cdot e^{-\frac{0.05211}{\sin(\alpha)}} \sin(\alpha) \quad (14)$$

where α is altitudinal angle and Q_0 is given by the following relation(15):

$$Q_0 = I_{s0} \cdot \left(1 + 0.033412 \cdot \cos\frac{2 \cdot \pi \cdot (n - a)}{365}\right) \quad (15)$$

where:
$I_{s0} = 1361$ [W/m^2] is the sun constant, n – the number of days in a year, and a – the day in which the perihelion takes place ($a = 4$; January 4, 2015).
The model given by relation, was developed by Paulescu and Schett (2004), and is based on the data obtained from the meteorological station in Timişoara, under a clear sky [3, 15].
5. **The Kasten model** is defined by the following relation (16):

$$Q = 0.84 \cdot I_{s0} \cdot \cos(\zeta) \cdot e^{-0.027 \cdot AM \cdot (f_1 + f_2(T_L - 1))} \quad (16)$$

where:
$I_{s0} = 1361$ [W/m^2] is the solar constant, ζ – the zenith angle, AM – the air mass ratio, $f_1 = e^{-\frac{\alpha}{8000}}$, $f_2 = e^{-\frac{\alpha}{1250}}$, α – the altitudinal angle, and T_L is Linke turbidity factor.
Linke turbidity factor for the towns of Petrosani depression has the value of 3.03 for October, November and December and 3.6 for the other months of the year.
6. **The Perez model** is defined by the following relation (17):

$$Q = g_1 \cdot I_{s0} \cdot \cos(\zeta) \cdot e^{-g_2 \cdot AM \cdot (f_1 + f_2 \cdot (T_L - 1))} \cdot e^{-0.01 \cdot AM^{1.8}} \quad (17)$$

where:
$g_1 = 5.09 \cdot 10^{-5} \alpha + 0.868$, $g_2 = 3.92 \cdot 10^{-5} \alpha + 0.0387$.
The most popular formulas of the air mass coefficient (AM), which intervenes the relations (16) and (17) are [4]–[14]:
• **the classic formula that defines the air mass factor:**

$$AM = \frac{1}{\cos(\zeta)} = \sec(\zeta) \quad (18)$$

• **Hardie formula** (1962):

$$AM = \sec(\zeta) - h_1 \cdot (\sec(\zeta) - 1) - h_2 \cdot (\sec(\zeta) - 1)^2 - h_3 (\sec(\zeta) - 1)^3 \quad (19)$$

where
$h_1 = 0.0018167$; $h_2 = 0.002875$; $h_3 = 0.0008083$.

- **Rozenberg formula** (1966):

$$AM = \left[\cos(\zeta) + 0.025 \cdot e^{-11 \cdot \cos(\zeta)}\right]^{-1} \quad (20)$$

- **Young and Irvine formula** (1967):

$$AM = \frac{1}{\cos(\zeta)}\left[1 - 0.0012 \cdot (\sec^2(\zeta) - 1)\right] \quad (21)$$

- **Rodgers formula** (1967):

$$AM = \frac{35}{\sqrt{1 + 1224 \cdot \cos^2(\zeta)}} \quad (22)$$

- **Badescu formula** (1987):

$$AM = \frac{-\cos(\zeta) + \sqrt{\cos^2(\zeta) + f^2 - 1}}{f - 1} \quad (23)$$

- **Kasten and Young formula** (1989):

$$AM = \left[\cos(\zeta) + a \cdot (96.07995 - \zeta)^{-1.6364}\right]^{-1} \quad (24)$$

where $a = 0.50572$.

- **Gueymard formula** (1993):

$$AM = \frac{1}{\cos(\zeta) + b \cdot \zeta \cdot (94.37515 - \zeta)^{-1.21563}} \quad (25)$$

where $b = 0.00176759$

- **Young formula** (1994):

$$AM = \frac{n_1 \cdot \cos^2(\zeta) + n_2 \cdot \cos(\zeta) + n_3}{\cos^3(\zeta) + m_1 \cdot \cos^2(\zeta) + m_2 \cdot \cos(\zeta) + m_3} \quad (26)$$

where:
$n_1 = 1.002432$; $n_2 = 0.148386$; $n_3 = 0.0096467$;
$m_1 = 0.149864$; $m_2 = 0.0102963$; $m_3 = 0.000303978$.

- **Pickering formula** (2002):

$$AM = \frac{1}{\sin\left(\alpha + \dfrac{244}{165 + 47 \cdot \alpha^{1.1}}\right)} \quad (27)$$

where α is the altitudinal angle, ζ – the zenith angle; $f = 1 + h_a/R$; $R = 6372.797$ [km] is the average radius of the Earth, and $h_a = 11$ [km].

The variation of the air mass coefficient depending on the zenith angle, is shown in figure 2.

From figure 2, it is observed that for a zenith angle of range $\zeta \in [0, 80]$ [grade], the variations of the air mass coefficient are identical, the differences emerging in the range $\zeta \in (80, 90]$ [grade].

The classic formula for determining the air mass coefficient is very useful in the range $\zeta \in [0, 80]$ [grade], but when the zenith angle goes to 90 [grade], the air mass coefficient can't be estimated correctly, this converging to infinity.

Hardie formula (19) and Yrvine and Young formula (21) returns the correct values of the air mass coefficient when the range is in the zenith angle $\zeta \in [0, 87]$ [grade].

For zenith angle values $\zeta \in (87, 90]$ [grade] formulas (19) and (21) did not correctly estimate the air mass coefficient, it converges to minus infinity.

In the relations (16) and (17), the air mass coefficient is calculated using the formula of Kasten and Young (24). This formula is one of the most used in the literature to determine the air mass coefficient.

In the following lines we will customize the shown above mathematical models, for Petrosani depression.

Petrosani depression is an intermountain unit of the Meridional Carpathians, whose physical features designate a first order individuality.

The depression is located in the SE Hunedoara county, between Retezat mountains to the N, Sureanu mountains to NE and Vâlcan and Parâng mountains to the S.

The length of Petrosani depression length is about 45 km, measured between Cimpa settlement to the E and Campul lui Neag settlement to the V.

The width of the depression is approximately 9 km and 1.5 km on the west side, which gives it a triangular shape [15–16].

The main localities of Petrosani depression are: Petrila, Petrosani, Aninoasa, Vulcan, Lupeni and Uricani. The latitude and longitude of the Jiu Valley cities are shown in table 1. From table 1 it is noted that the latitude of the Jiu Valley localities are not very different.
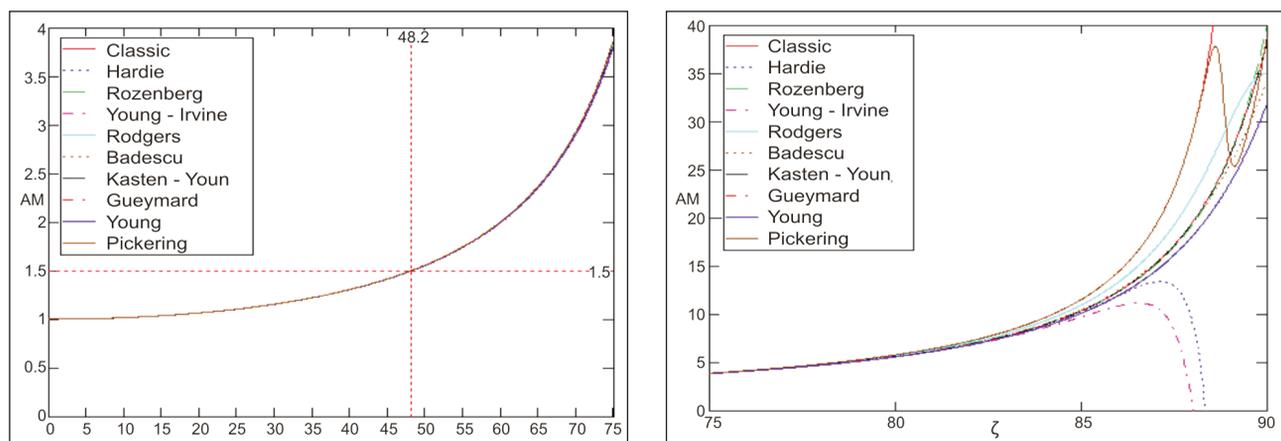

Fig. 2. The variation of the air mass coefficient depending on the zenith angle

Nr. crt.	City	Latitude [degrees]	Longitude [degree]
1.	Petrila	45.45	23.4167
2.	Petroşani	45.41	23.38
3.	Aninoasa	44.75	23.4833
4.	Vulcan	45.38	23.29
5.	Lupeni	45.35	23.2333
6.	Uricani	45.33	23.15

For this reason, in the following we will present the estimation of the global solar radiation for the city of Petrosani. To validate the mathematical models presented above, using Voltcraft PL-110SM pyranometer, the global solar radiation intensity in Petrosani city was measured in April 16, 2015, July 20, 2015 and October 15, 2015.

Fig. 3. Voltcraft PL-110SM Pyranometer [17]

The measurement of global solar radiation was carried out in a horizontal plane (the tilt angle is zero degrees) over the three days as described above.

Based on the measured values, the figures 4–6 presents global solar radiation intensity, measured and estimated for all the data above.

Similarly, the variation during the year 2015, of the global solar radiation, for the city of Petroşani and for $T_s = 12$ is shown in the figure 7.
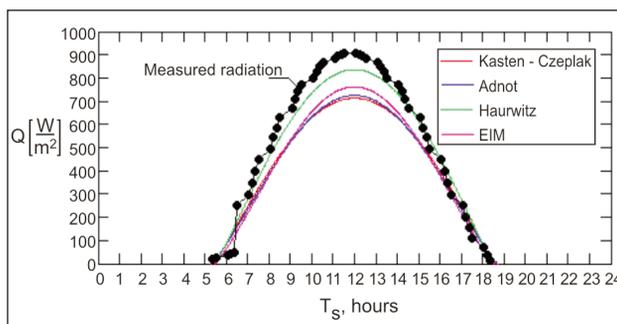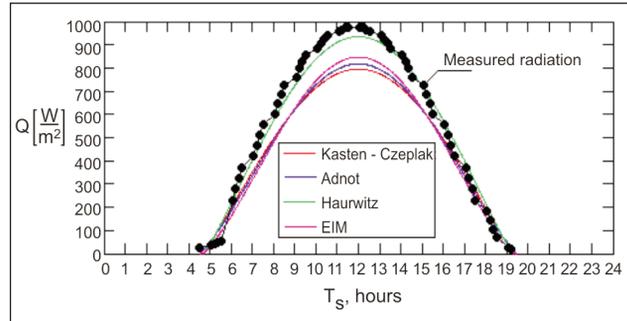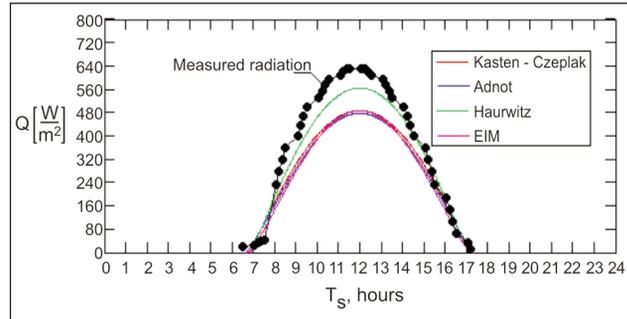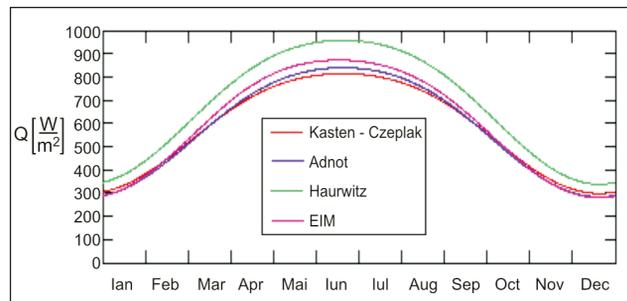

Fig. 4. Solar radiation estimated/measured in relation to the solar time, April, 16th, 2015

Fig. 5. Solar radiation estimated/measured in relation to solar time, July 20th, 2015

Fig. 6. Solar radiation estimated/measured to solar time, October 15th, 2015

Fig. 7. Changes in the global solar radiation during the year 2015 in the city of Petrosani

Following the comparative analysis between the values of solar radiation, obtained using mathematical models, and the values of solar radiation obtained experimentally using Voltcraft PL-110SM pyranometer, it was observed that the Haurwitz model provides values closest to the measured solar radiation.

On the other hand, it appears that the biggest differences between measured and estimated values are recorded when solar time is in the range $T_s \in [11...13]$ [h].

To highlight the performance of the Kasten and Perez model, below is presented in tandem the global solar radiation, under a clear sky, obtained with the Haurwitz (13), Kasten (16) and Perez (17) models.

Thus, in figures 8 and 9 is shown the estimated global solar radiation for the city of Petrosani, for the days of July 20, 2015 and 15 October 2015.

From the above figures, it is noted that both Kasten and Haurwitz models estimate the same global solar radiation. On the other hand, we observe that the
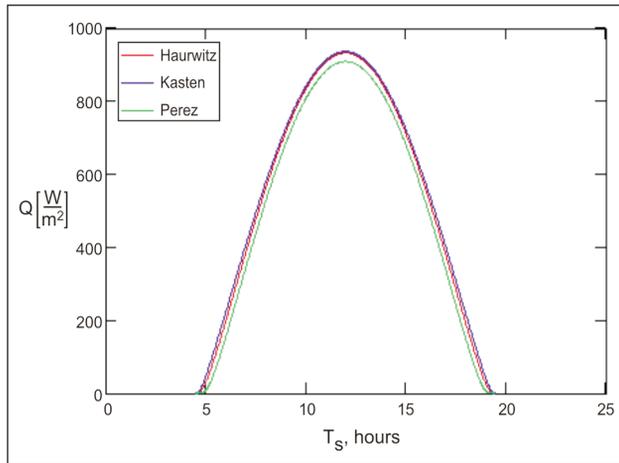
Fig. 8. Solar radiation estimated/measured in relation to solar time, July 20th, 2015
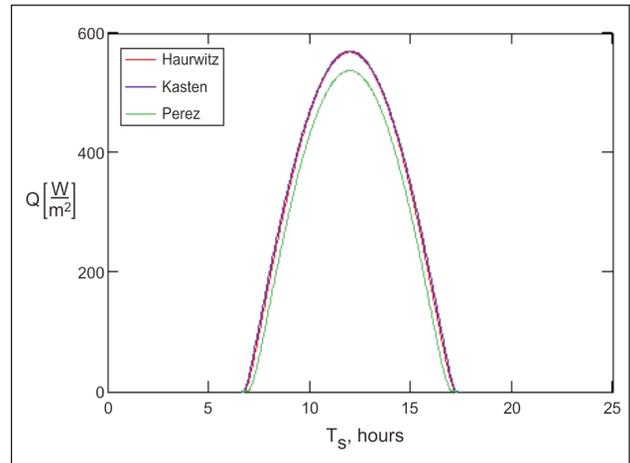

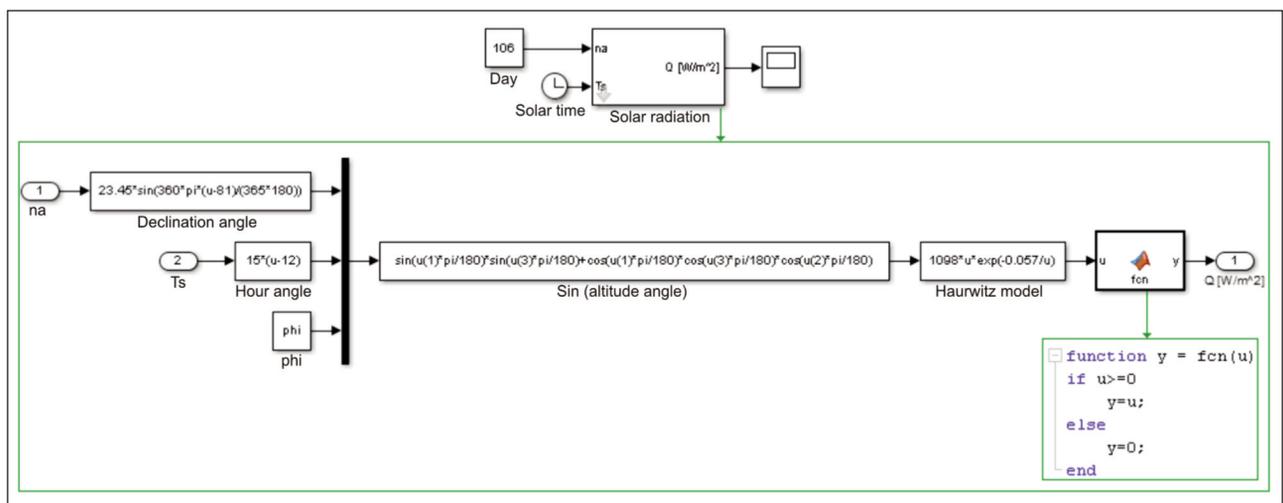Fig. 9. Solar radiation estimated/measured to solar time, October 15th, 2015

Fig. 10. Matlab–Simulink program of global solar radiation – Haurwitz model

Perez model underestimates the global solar radiation from the city of Petrosani.

The graphs from the figures presented above were obtained in Mathcad 13.1 [18].

Haurwitz model shown above, was implemented in Matlab–Simulink [19] as well, based on the program from the figure 10.

In order to implement the program in figure 10, the Matlab–Simulink program, the following settings are made:

- the simulation range is $t \in [t_0 \ t_f] = [0 \ 24]$;
- the integration method is Dorman–Prince of the order 4/5;
- the relative error of the integration method: $\varepsilon_r = 10^{-7}$;
- the absolute error method of integration: $\varepsilon_a = 10^{-7}$;
- the latitude is set up: phi = 45.41 [grade].

The program can easily be customized to other places in the Petrosani depression.

In these circumstances, after the completion of the program described above, on 16 April 2015 in the city of Petrosani, we get the result shown in figure 11.

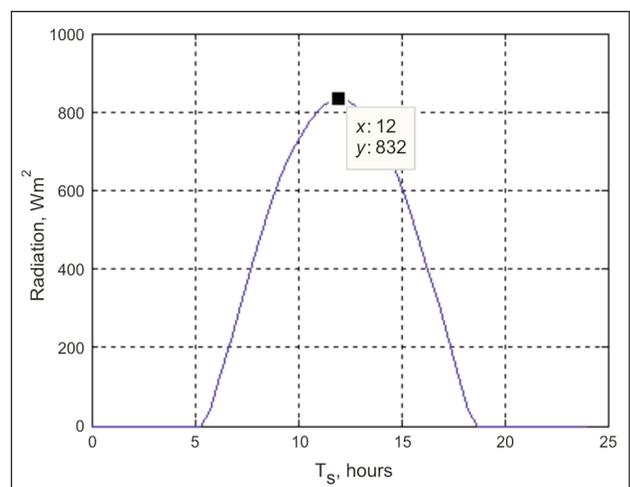Fig. 11. Solar radiation in relation to solar time, based on Matlab–Simulink program

CONCLUSIONS

Following the comparative analysis between solar radiation values estimated using a mathematical model, shown above, and the solar radiation values

obtained experimentally using Voltcraft PL-110SM pyranometer, it was observed that Haurwitz model, estimates the best global solar radiation, in the city of Petrosani, that falls on a horizontal plane, under a clear sky.

With help of the software simulation presented in this article, photovoltaic systems designers, can obtain with an accuracy quite good, the global solar radiation falling on a horizontal plane, under a clear sky, in the city of Petrosani.

BIBLIOGRAPHY

 [1] Iziomon, M.G., Mayer, H. *Assessment of some global solar radiation parameterizations*, In: Journal of Atmospheric and Solar – Terrestrial Physics, no. 64, pp. 1361–1643, 2002.
 [2] Wong, L.T., Chow, W.K. *Solar radiation model*, In: Journal of Applied Energy, no. 69, pp. 191–224, 2001.
 [3] Paulescu, M., Schlett, Z. *Performance assessment of global solar irradiation models under Romanian climate*, In: Journal of Renewable Energy, vol. 29, pp. 767–777, 2004.
 [4] Hardie, R.H. *In astronomical techniques*, University of Chicago Press, 1962.
 [5] Rozenberg, G.V. *Twilight: A study in atmospheric optics*, In: New York Plenum Press, translated from the Russian by R.B. Rodman, 1966.
 [6] Young, A.T., Irvine, W.M. *Multicolor photoelectric photometry of the brighter planets*, In: The Astronomical Journal, vol. 72, pp. 945–950, 1967.
 [7] Rodgers, C.D. *The radiative heat budget of the troposphere and lower stratosphere*, M.I.T. Department of Meteorology, 1967.
 [8] Badescu,V. *Can the model proposed by barbaro et al. be used to compute global solar radiation on the Romanian territory*, In: Solar Energy, vol. 38, pp. 247–254, 1987.
 [9] Kasten, F., Young, A.T. *Revised optical air mass tables and approximation formula*, In: Applied Optics, vol. 28, pp. 4735–4738, 1989.
[10] Gueymard, C.A. *Critical analysis and performance assessment of clear sky solar irradiance models using theoretical and measured data*, In: Solar Energy, vol. 51, pp. 121–138, 1993.
[11] Young, A.T. *Air-mass and refraction*, In: Applied Optics, vol. 33, pp. 1108–1110, 1994.
[12] Pickering, K.A. *The southern limits, of the ancient star*, In: Catalog, 2002.
[13] Kasten, F.A. *Simple parameterization of the pyrheliometric formula for determining the linke turbidity factor*, In: Meteorologische Rundschau, vol. 33, pp. 124–127, 1980.
[14] Ineichen P., Perez, R. *A new airmass independent formulation for the Linke turbidity coefficient*, In: Solar Energy, vol. 73, pp. 151–157, 2002.
[15] Petrilean, D.C., Irimie, S.I. *Solutions for the capitalization of the energetic potential of sludge collected in Danutoni Wastewater Treatment Plant,* In: Journal of environmental protection and ecology, ISSN 1311-5065, vol. 16, no. 3, pp. 1203–1211, 2015.
[16] Petrilean D.C., Popescu F.D. *Temperature determination in hydrotechnical works as a variable of the energy change between air and environment*, In: WSEAS TRANSACTIONS on HEAT and MASS TRANSFER, ISSN: 1790-5044, Issue 4, Volume 3, pp. 209–218, 2008.
[17] *** *Technical documentation of Voltcraft PL-110SM pyranometer, www.conrad.com*.
[18] *** *Mathcad 13.1 User's Guide*, www.mathsoft.com.
[19] Ghinea, M., Fireteanu, V. *Matlab Numerical calculus. Graphics. Applications*, In: Teora Publisher, 2004.

Authors:

NICOLAE DIACONU[1]
NAN MARIN SILVIU[2]
STOICUTA OLIMPIU[3]

[1]e-mail: diaconu_primarie@yahoo.com

[2]University of Petrosani, Faculty of Mechanical and Electrical Engineering
Department of Mechanical Engineering, Industrial Engineering and Transportation
e-mail: nan.marins@gmail.com

[3]University of Petrosani, Faculty of Mechanical and Electrical Engineering
Department of Control Engineering, Computers, Electrical Engineering and Power and Power Engineering
e-mail: stoicutaolimpiu@yahoo.com

Petrosani – 332006
Str. Universitatii, No. 20, jud. Hunedoara, Romania

Corresponding author:

NICOLAE DIACONU
e-mail: diaconu_primarie@yahoo.com

INFORMATION FOR AUTHORS

Industria Textila magazine is an international peer-reviewed journal published by the National Research & Development Institute for Textiles and Leather – Bucharest, in print editions.

Aims and Scope: *Industria Textila* magazine welcomes papers concerning research and innovation, reflecting the professional interests of the Textile Institute in science, engineering, economics, management and design related to the textile industry and use of fibres in consumer and engineering applications. Papers may encompass anything in the range of textile activities, from fibre production through textile processes and machines, to the design, marketing and use of products. Papers may also report fundamental theoretical or experimental investigations, practical or commercial industrial studies and may relate to technical, economic, aesthetic, social or historical aspects of textiles and the textile industry.

Submission of Manuscripts
The paper submitted for publication shall concern problems associated with production and application of fibers and textiles.

Please include full postal address as well as telephone/fax/e-mail details for the corresponding author, and ensure that all correspondence addresses are included. Also include the scientific title of the authors.

Industria Textila magazine considers all manuscripts on the strict condition that they have been submitted only to the *Industria Textila* journal, on this occasion, and that they have not been published already, nor are they under consideration for publication or in press elsewhere. Authors who fail to adhere to this condition will be charged with all costs which *Industria Textila* magazine incurs and their papers will not be published.

Manuscripts
Manuscripts of the following types are accepted:
Research Papers – An original research document which reports results of major value to the Textile Community
Notes – see below
Book Reviews – A brief critical and unbiased evaluation of the current book, normally invited by the Editor
Correspondence – Communications based on previously published manuscripts

Manuscripts shall be submitted in English in double-spaced typing, A4 paper, size font 10, Arial, margins 2 cm on all sides, under electronic version in Word for Windows format.

The volume of the submitted papers shall not exceed 10 pages (including the bibliography, abstract and key words), typescript pages including tables, figures and photographs.

All articles received are reviewed by a reviewer, renowned scientist and considered expert in the subject the article concerns, which is appointed by the editorial board. After the article has been accepted, with the completions and the modifications required by the reviewer or by the editorial staff, it will be published.

The submission of the above-mentioned papers is by all means the proof that the manuscript has not been published previously and is not currently under consideration for publication elsewhere in the country or abroad.

There may also be published papers that have been presented at national or international scientific events, which have not been published in volume, including the specification related to the respective event.

The articles assessed as inappropriate by the reviewer or by the editorial staff, concerning the subject matter or level, shall not be published.

The manuscript shall be headed by a concise title, which should represent in an exact, definite and complete way the paper content. Authors should also supply a shortened version of the title, suitable for the running head, not exceeding 50 character spaces.

The manuscript shall also be headed by complete information about the author(s): titles, name and forename(s), the full name of their affiliation (university, institute, company), department, city and state, as well as the complete mailing address (street, number, postal code, city, country, e-mail, fax, telephone).

Tables and figures (diagrams, schemes, and photographs) shall be clear and color, where possible.

The photographs shall be sent in original format (their soft), or in JPEG or TIF format, having a resolution of at least **300 dpi**.

All tables and figures shall have a title and shall be numbered with Arabic numerals, consecutively and separately throughout the paper, and referred to by the number in the text.

Generally, symbols and abbreviations shall be used according to ISO 31: specifications for quantities, units and symbols. SI units must be used, or at least given comprehensive explanations or their equivalent.

Cited references shall be listed at the end of the paper in order of quotation and contain: **for a paper in a periodical** – the initials and surname of the author(s), title of journal and of the article, year and number of issue, number of volume and page numbers; **for a book** – the initial and surname of the author(s), full name of the book, publisher, issue, place and year of publishing, and the pages cited; **for patents** – the initial and surname of the author(s), the title, the country, patent number and year.

[1] Popescu, D., Popa, I., Cicea, C., Iordănescu, M. *The expansion potential of using sales promotion techniques in the Romanian garments industry*. In: Industria Textilă, 2013, vol. 64, issue 5, pp. 293-300

Authors are requested to send an abstract of the paper, preferably no longer than 100 words and a list of 5-6 key words (preferably simple, not compound words, in alphabetical order). Avoid abbreviations, diagrams and direct reference to the text.

All manuscripts with the material proposed for publication, shall be sent to:

 certex@certex.ro

Complimentary issue – The corresponding author will receive a complimentary print copy of the issue in which his/her article appears. It will be up to the corresponding author if he/she decides to share or route his/her copy to his/her co-author(s).